THE STATE UNIVERSITY OF NEW JERSEY
RUTGERS
CAMPUS at NEW BRUNSWICK

College of Engineering, Department of Mechanical and Aerospace Engineering
P.O. Box 909, Piscataway, New Jersey 08855-0909

(908) 445-4408 FAX (908) 445-5313 e-mail: benaroya@zodiac.rutgers.edu

Haym Benaroya, Associate Professor
Mechanical and Aerospace Engineering

3 August 1994

Dr. Thomas F. Swean
CODE 3212
Office of Naval Research
Ballston Tower One
800 North Quincy Street
Arlington, Virginia 22217-5660

Dear Tom:

Attached to this letter is the report of our first year's efforts under Grant No: N00014-93-1-0763, entitled: "Stochastic Nonlinear Dynamics of Floating Structures". This work was carried out by me and ONR Grant-supported Graduate Assistant, Patrick Bar-Avi. In addition, related work was carried out by Ed Weinstein and me on the issue of solving for the moments of a system governed by the Fokker-Planck equation.

Attached are the following documents:

1. *Nonlinear Dynamics of an Articulated Tower in the Ocean*, submitted for review and publication to the **Journal of Sound and Vibration**
2. *Nonlinear Dynamics of an Articulated Tower in the Ocean*, submitted for review, presentation and publication at the ASME **Winter Annual Meeting**
3. *The van Kampen Expansion for the Fokker-Planck Equation of a Duffing Oscillator*, accepted for publication in **Journal of Statistical Physics**
4. *The van Kampen Expansion for the Fokker-Planck Equation of a Duffing Oscillator Excited by Colored Noise*, accepted for publication in **Journal of Statistical Physics**
5. *The van Kampen Expansion for a Linked Fokker-Planck Equation of a Duffing Oscillator Excited by Colored Noise*, submitted for review and publication in **Journal of Statistical Physics.**

The essence of our work on the offshore problem is embodied in document 1 above. Our approach to the problem has been, and continues to be, based on an examination of the physics of the environment and its interaction with the structure. This allows us to proceed along a research path that best examines the importance of each force component, each nonlinearity, and helps us decide which terms in our analytical model can be ignored or must be retained. In addition, by going back and forth between analytical model and simulation, we are able to estimate the loss in accuracy resulting from any particular approximation.

It is in this manner that we have proceeded with the work you see before you on the articulated tower. We have explored various behavior regimes, including a chaotic one and a friction damping effect. Our main conclusion during this phase is that a simplified, classical nonlinear oscillator model, such as the Duffing or the van der Pol, will not be representative of the highly complex and nonlinear offshore fluid-structure interaction problem. Thus, the need to make a connection between the physical world and the mathematics we choose to model it. We prefer a top-down approach. It is always easier to *a posteriori* drop terms shown to be negligible than to add terms required to better fit the behavior.

On the articulated tower, in the current, second, year of the grant, we are generalizing the model to include effects such as current, and allowing the structure to move freely about its base support hinge. Thus, transverse forces due to vortex shedding can be incorporated.

Our work on the van Kampen expansion of the Fokker-Planck also continues. The above three manuscripts (3,4,5) focused on unforced motion about an equilibrium due to noise. This permitted us to examine the method, and extend it to include colored noise models, and also to consider coupled oscillator models, which have broad applicability in the physical sciences and engineering. Our coupled model was of a Duffing coupled to a linear harmonic oscillator, with colored noise forcing. These are being published in J. Stat. Phys., where the original papers by van Kampen were published. Our next step is to consider particular forced cases for the above. As for all nonlinear oscillations, each loading case requires specific considerations.

As usual, I would be pleased to visit you to provide you with more details, and you are welcome here for a working visit.

Thank you for your interest in our work. Your support is appreciated. Best regards.

Sincerely yours,

Haym Benaroya

cc: Administrative Grants Officer
Director, Naval Research Laboratory
DTIC

Nonlinear Dynamics of an Articulated Tower in the Ocean

P. Bar-Avi and H. Benaroya

Department of Mechanical and Aerospace Engineering, Rutgers University

Piscataway, N.J. 08855

June 1, 1994

Abstract

This paper presents studies on the response of an articulated tower in the ocean subjected to deterministic and random wave loading. The tower is modeled as an upright rigid pendulum with a concentrated mass at the top and having one angular degree of freedom about a hinge with coulomb damping. In the derivation of the differential equation of motion, nonlinear terms due to geometric (large angle) and fluid forces (drag and inertia) are included. The wave loading is derived using Morison's equation in which the velocity and acceleration of the fluid are determined along the instantaneous position of the tower, causing the equation of motion to be highly nonlinear. Furthermore, since the differential equation's coefficients are time-dependent (periodic), parametric instability can occur depending on system parameters such as wave height and frequency, buoyancy, and drag coefficient. The nonlinear differential equation is then solved numerically using 'ACSL' software. The response of the tower to deterministic wave loading is investigated and a stability analysis is performed (resonance and parametric instability). To solve the equation for random loading, the Pierson-Moskowitz power spectrum, describing the wave height, is first transformed into an approximate time history using Borgman's method with slight modification. The equation of motion is then solved, and the influence on the tower response of different parameter values such as buoyancy, initial conditions and wave height and frequency, is investigated.

Key words : Articulated, Dynamics, Random, Stability, Chaos

1 Review and Proble)efinition

Compliant platforms such as articulated towers are economically attractive for deep water conditions because of their reduced structural weight compared to conventional platforms. The foundation of the tower does not resist lateral forces due to wind, waves and currents; instead, restoring moments are provided by a large buoyancy force, a set of guylines or a combination of both. These structures have a fundamental frequency well below the wa ... r frequency. As a result of the relatively large displacements, geometric nonlinearity is an impc ...nt consideration in the analysis of such a structure. The analysis and investigation of these kind of problems can be divided into two major groups; deterministic and random wave and/or current loading. We briefly review work in this area in the next two subsections.

1.1 Deterministic loading

Chakrabarti and Cotter (1979) [3] analyzed the motion of articulated tower. The tower is articulated by a universal joint having single degree of freedom. They assumed, linear waves, small perturbations about an equilibrium position, linear drag force and that the wind current and wave are colinear. Their resulting equation of motion is,

$$I\ddot{\psi} + B(\dot{\psi}) + D\dot{\psi} + C\psi = M_0 e^{i(\alpha - \beta t)}, \tag{1}$$

where I is the total moment of inertia including added mass, $B(\dot{\psi})$ is the nonlinear drag term, $D\dot{\psi}$ is the structural damping, $C\psi$ is the restoring moment due to buoyancy and M_0 is the wave moment. An analytical solution is then compared to experimental results to show good agreement as long as the system is inertia predominant, and not drag predominant.

In a later paper, Chakrabarti and Cotter (1980) [4] investigated transverse motion, the motion

perpendicular to the horizontal velocity. The tower pivot is assumed to have two angular degrees of freedom and is taken to be frictionless. It is also assumed that the motion is not coupled, so the inline solution is obtained (the same as in the previous paper) from which the relative velocity between the tower and the wave is obtained. The lift force (in the transverse direction) can then be obtained and the linear equation of motion is solved analytically and compared to experimental results. The comparison shows good agreement, especially when the drag terms are small.

Jain and Kirk (1981) [9] investigated the dynamic response of a double articulated offshore structure to waves and current loading. They assumed four degrees of freedom, two angular for each link. The equations of motion were derived using Lagrange equations. In deriving the equations of motion the following assumptions were made: drag and inertia forces tangent to the tower are negligible, and the wave and current velocities are evaluated at the upright position (small angles assumption). The linearized equations were solved to find the natural frequencies of the system and then numerically solved to find the response due to colinear and non-colinear current and wave velocities. They found that when the wave and the current velocities are colinear, the response of the top is sinusoidal, while for noncolinear velocities the response is a complex three dimensional whirling oscillation.

Thompson et al. (1984) [16] investigated the motions of an articulated mooring tower. They modeled the structure as a bilinear oscillator which consists of two linear oscillators having different stiffnesses for each half cycle,

$$m\ddot{x} + c\dot{x} + (k_1, k_2)x = F_0 \sin \omega t, \tag{2}$$

where k_1, k_2 are the stiffnesses for $x > 0$ and $x < 0$ respectively. The equation is solved numerically for different spring ratios and, as expected, harmonic and subharmonic resonances appeared in the

response. A comparison between the response and experimental results of a reduced-scale model showed good agreement in the main phenomenon.

Choi and Lou (1991) [5] have investigated the behaviour of an articulated offshore platform. They modeled it as an upright pendulum having one degree of freedom, with linear springs at the top having different stiffnesses for positive and negative displacements (bilinear oscillator). The equation of motion is simplified by expanding nonlinear terms into a power series and retaining only the first two terms. They assumed that the combined drag and inertia moment is a harmonic function. The discontinuity in the stiffness is assumed to be small, and thus replaced by an equivalent continuous function using a least-squares method to get the following Duffing equation

$$I\ddot{\theta} + c\dot{\theta} + k_1\theta + k_2\theta^2 + k_3\theta^3 = M_0 \cos \omega t, \tag{3}$$

where k_1, k_2, k_3 are spring constants depending on buoyancy, gravity and the mooring lines. The equation of motion is solved analytically and numerically, and stability analysis is performed. The analytical solution agrees very well with the numerical solution. The main results of their analysis are that as damping decreases, jump phenomena and higher subharmonics occur, and chaotic motion occurs only for large waves and near the first subharmonic (excitation frequency equals twice the fundamental frequency); the system is very sensitive to initial conditions.

Seller and Niedzwecki (1992) [14] investigated the response of a multi-articulated tower in planner motion (upright multi-pendulum) to account for the tower flexibility. The restoring moments (buoyancy and gravity) were taken as linear rotational springs between each link, although the authors say that nonlinear springs are more adequate for this model. Each link is assumed to have a different cross section and density. The equations of motion are derived using Lagrange's equations, in which the generalized coordinates are the angular deflections of each link. The equations

in matrix form are

$$[M]\{\ddot{\theta}\} + [K]\{\theta\} = [Q], \tag{4}$$

where $[M]$ is a mass matrix that includes the actual mass of the link and added mass terms, while the stiffness matrix $[K]$ includes buoyancy and gravity effects. Damping and drag forces are not included in the model. The homogeneous equations for a tri-articulated tower are numerically solved to study the effects of different parameters, such as link length, material density and spring stiffness, on the natural frequency of the system.

Gotlib et al. (1992) [7] analyzed the nonlinear response of a single degree of freedom articulated tower. In the derivation of the equation, the expressions for the buoyancy moment arm, added mass term, and drag and inertia moments are evaluated along the stationary upright tower position and not at the instantaneous position of the tower. The governing equation is of the form

$$\ddot{\theta} + \gamma\dot{\theta} + R(\theta) = M(\dot{\theta}, t), \tag{5}$$

where $R(\theta) = \alpha \sin\theta$ and α is linear function of buoyancy and gravity, $M(\dot{\theta}, t)$ is the drag moment. Approximated harmonic and subharmonic solutions are derived using a finite Fourier series expansion, and stability analysis is performed by a Lyapunov function approach. The solution shows a jump phenomenon in primary and the secondary resonances.

1.2 Random loading

Muhuri and Gupta (1983) [12] investigated the stochastic stability of a buoyant platform. They used a linear single degree of freedom model as follows

$$\ddot{x} + 2c\dot{x} + (1 + G(t))x = 0, \tag{6}$$

where x is the displacement, c is the damping coefficient and $G(t)$ is a stochastic time-dependent function due to buoyancy. It is assumed that $G(t)$ is a narrow-band random process with zero-mean. A criterion for the mean square stability is obtained from which the following results are found: for $c > 1$ the system is always stable, and for $0 < c < 1$ there are regions of stability and instability.

Datta and Jain (1990) [6] investigated the response of an articulated tower to random wave and wind forces. In the derivation of the single degree of freedom equation of motion the tower is discretized into n elements having appropriate masses, volumes and areas lumped at the nodes, and there is viscous damping. The equation of motion is,

$$I(1 + \beta(t))\ddot{\theta} + c\dot{\theta} + R(1 + \nu(t))\theta = F(t), \tag{7}$$

where $I\beta(t)$ is the time varying added mass term, $R\nu(t)$ is time varying buoyancy moment and $F(t)$ is the random force due to wave and wind. The Pierson-Moskowitz spectrum is assumed for the wave height and Davenport's spectrum assumed for the wind velocity. The equation is solved in the frequency domain using an iterative method, which requires that the deflection angle $\theta(t)$ and the forcing function $F(t)$ be decomposed into Fourier series: The coefficient of the *sin* and *cos* are then found iteratively. From their parametric study, they concluded the following:

1. Nonlinearities such as large displacements and drag force do not influence the response when only wind force is considered.

2. The random wind forces result in higher responses than do wave forces.

3. The r.m.s. response due only to wind forces varies in a linear fashion with the mean wind velocity.

In a later paper, Jain and Datta (1991) [8] used the same equation and the same method of solution to investigate the response due to random wave and current loading. The wave loadings

(drag, inertia and buoyancy) are evaluated via numerical integration. The following results were obtained from the parametric study,

1. The dynamic response is very small since its fundamental frequency is well below the wave's fundamental frequency.

2. Nonlinear effects (drag force, variable buoyancy) have considerable influence on the response.

3. Current velocity has a large influence on the response.

Hanna et al. (1983) [15] analyzed the nonlinear dynamics of a guyed tower platform. The tower is represented by a lumped parameter model consisting of discrete masses. Each mass has three degrees of freedom, two translations and one rotation about the vertical axis. The external forces on the structure are approximated by concentrated forces and torques at the nodal points. The equation of motion is

$$[M]\{\ddot{u}\} + [C]\{\dot{u}\} + [K(u)]\{u\} = \{P(t, u, \dot{u})\}, \tag{8}$$

where $[M]$ is the total mass matrix including added mass terms, $[C]$ is the structural damping matrix assumed to be proportional to the mass matrix and $[K(u)]$ is the total nonlinear stiffness matrix that includes mooring lines effects, soil stiffness and geometric stiffness. $\{P(t, u, \dot{u})\}$ is the nonlinear dynamic load vector due to wave, current and wind. The equation is then solved using normal mode superposition and the response is calculated at each time step. This method is good only if the nonlinearities are not large. Deterministic and random loading are considered. The solution shows insignificant flexure modes while the torsional one has a noticeable effect on the deck rotational response.

Kanegaonkar and Haldar (1988) [10] investigated the nonlinear random vibration of a guyed tower. They included nonlinearities due to guylines stiffnesses, geometry, load and material. The

simplified planner equation of motion is

$$I\ddot{\theta} + c\dot{\theta} + K\theta + k_1\theta^3 = M(t), \tag{9}$$

where K is a spring constant depending on buoyancy, gravity and guyline horizontal stiffness, and k_1 is a constant depending on the guyline vertical stiffness. $M(t)$ is the random wave loading. The equation is then solved numerically where the wave height is defined by the Pierson-Moskowitz spectrum. It was seen that the response is non-Gaussian for significant wave heights greater than 5 m.

Gerber and Engelbrecht (1993) investigated the response of an articulated mooring tower to irregular seas. It is an extension of earlier work done by Thompson et al. (1984) [16]. The tower is modeled as a bilinear oscillator, that is, a linear oscillator with different stiffnesses for positive and negative deflections,

$$m\ddot{x} + c\dot{x} + (k_1, k_2)x = F(t). \tag{10}$$

The random forcing function $F(t)$ is assumed to be the sum of a large number of harmonic components, each in different frequency, a procedure similar to that proposed by Borgman (1969) [2]. The equation is then solved analytically since it is linear for each half cycle. The solution is obtained for different cases; linear oscillator (both stiffnesses are the same), bilinear oscillator, and for the case of impact oscillator (a rigid cable) in which oscillation can occur only in one half of the cycle. For future study they suggest to include nonlinear stiffness and/or using a different spectrum to describe the wave height.

1.3 Problem Definition

In this paper, the response of an articulated tower submerged in the ocean is investigated. The nonlinear differential equation of motion is derived, including nonlinearities due to geometry, coulomb damping, drag force, added mass buoyancy. All forces/moments are evaluated analytically and explicitly at the instantaneous position of the tower and, therefore, they are time-dependent and highly nonlinear. The equation is then numerically solved using 'ACSL' - Advanced Continuous Simulation Language [1], a powerful software language for deterministic and random wave loading using the Pierson-Moskowitz wave height spectrum. A harmonic and subharmonic solutions for deterministic wave heights are obtained. The response to random wave heights for different significant wave heights is investigated, the influence of coulomb damping on the response is analyzed, and chaotic regimes of behavior are identified.

The distinctions between this study and the literature with which we are aware are that,

1. A sound and exact derivation of the nonlinear equation of motion is provided.

2. All terms in the equation of motion are analytically derived.

3. Coulomb friction in the tower hinge is added.

4. Usage of 'ACSL' for the numerical solution provides an easy way to modify parameters and sensitivity studies.

2 Problem Description

A schematic of the structure is shown in Fig. 1. It consists of a tower submerged in a fluid having a concentrated mass at the top and one degree of freedom θ about the z axis. The tower is subjected to wave loading. Two coordinate systems are used; one fixed (x,y,z) and the second attached to the tower (x',y',z'). All forces/moment are derived in the fixed coordinate system, which means that the tower rectilinear velocity is resolved into x, y coordinates. The motion of the tower is assumed to be only in plane.

This problem has similarities to that of an inverted pendulum, but due to the presence of gravity waves, additional considerations are made :

1. Forces due to buoyancy and vertical wave velocity are summed and denoted as T_0.
2. Drag forces proportional to the square of the relative velocity between the fluid and the tower need to be considered.
3. Fluid inertia forces due to fluid acceleration are part of the loading environment.
4. Fluid added mass is directly included in the inertia forces.

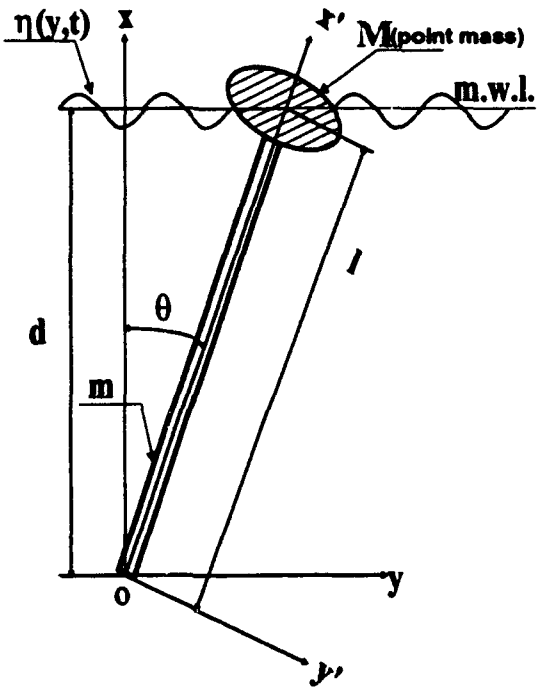

Figure 1: Model and Coordinate Frames

3 Equation of Motion

The equation of motion is derived using Newton's second law, setting all applied moments acting on the tower about hinge equal to the dynamic moment. We will find the equation of motion to be of the form,

$$J[g(\theta)]\ddot{\theta} = \sum M\left[t, \omega, f(\theta), \dot{\theta} sgn(\dot{\theta})\right], \tag{11}$$

where $J[g(\theta)]$ is the effective position-dependent moment of inertia, $g(\theta)$ and $f(\theta)$ are nonlinear functions of θ (trigonometric functions), ω is the wave frequency, and $\sum M$ is the sum of all external moments that act on the tower. Certain assumptions have been made in deriving the nonlinear equation of motion. These are listed below.

3.1 Assumptions

1. The tower stiffness is infinite: $EI = \infty$.
2. The hinge has coulomb damping.
3. The tower has a uniform mass per unit length, m, and is of length l and diameter D.
4. The tower is a smooth slender structure with uniform cross section.
5. The end mass M is considered to be concentrated at the end of the tower. (It has no volume.)
6. The tower length is greater than the fluid depth, but the dynamics is not limited to the case of the mass always being above the mean water level.
7. The structure is statically stable due to the buoyancy force.
8. The waves are linear having random height.
9. Morison's fluid force coefficients C_D and C_M are constant.
10. The center of mass (c.g.) of the tower is at its geometric center.
11. Currents, wind and wave slamming forces are not included.

3.2 Forces/Moments acting on the tower

Fig. 2 describes the external forces acting on the tower. These are :

1. T_0 is a vertical buoyancy force.
2. F_v, F_h are the vertical and horizontal fluid forces due to fluid drag and inertia.
3. Mg, mlg are the forces due gravity.

We next describe these forces and moments.

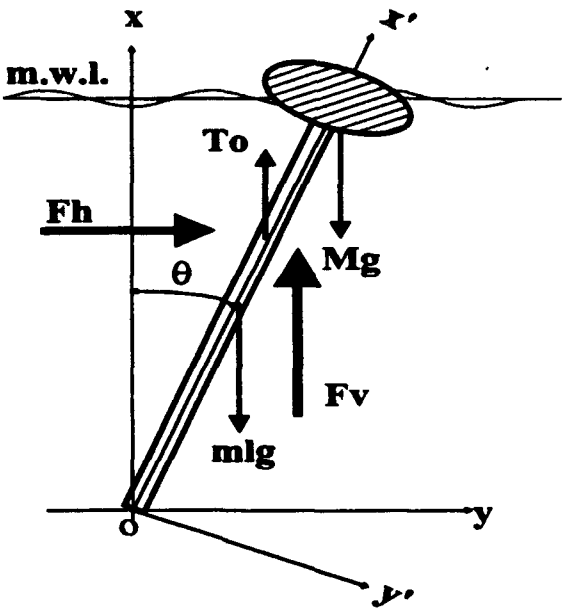

Figure 2: External Forces on the Tower

3.2.1 Inertia Moment

The inertia moment equals the total moment of inertia of the tower multiplied by the angular acceleration of the tower plus the fluid added mass term,

$$M_I = (J_0 + Ml^2)\ddot{\theta} + M_{fl}, \tag{12}$$

where J_0 is the moment of inertia of the tower about point 'o' and M_{fl} is the fluid added mass moment. The tower moment of inertia is

$$J_0 = \frac{1}{3}ml^3. \tag{13}$$

The added mass force per unit length is

$$F_{fl} = C_A \rho \pi \frac{D^2}{4}\dot{\mathbf{V}}, \tag{14}$$

where C_A is the added mass coefficient which equals $C_A = C_M - 1$, C_M is the inertia coefficient and $\dot{\mathbf{V}}$ is the tower acceleration. In order to find the added mass term the tower's acceleration is

derived by taking the second time-derivative of the tower radius vector in the x, y coordinate,

$$\begin{aligned}
\mathbf{R} &= x' \cos\theta \hat{x} + x' \sin\theta \hat{y} \\
\frac{d\mathbf{R}}{dt} &= \mathbf{V} = -x'\dot{\theta}\sin\theta\hat{x} + x'\dot{\theta}\cos\theta\hat{y} \\
\frac{d\mathbf{V}}{dt} &= \dot{\mathbf{V}} = -x'(\ddot{\theta}\sin\theta + \dot{\theta}^2\cos\theta)\hat{x} + x'(\ddot{\theta}\cos\theta - \dot{\theta}^2\sin\theta)\hat{y}. \qquad (15)
\end{aligned}$$

Replacing $x' = \frac{x}{\cos\theta}$ we find

$$\begin{aligned}
\mathbf{R} &= x\hat{x} + x\tan\theta\hat{y} \\
\mathbf{V} &= -x\dot{\theta}\tan\theta\hat{x} + x\dot{\theta}\hat{y} \\
\dot{\mathbf{V}} &= -x(\ddot{\theta}\tan\theta + \dot{\theta}^2)\hat{x} + x(\ddot{\theta} - \dot{\theta}^2\tan\theta)\hat{y} \qquad (16)
\end{aligned}$$

and the fluid added mass moment is

$$M_{fl} = \int_0^L \mathbf{R} \times F_{fl} dx. \qquad (17)$$

Substituting the expression for $\dot{\mathbf{V}}$ in F_{fl} and evaluating the cross product yields,

$$M_{fl} = \left[C_A \rho\pi \frac{D^2}{4} \int_0^L x^2(1 + \tan^2\theta)dx\right]\ddot{\theta}, \qquad (18)$$

where L is the projection, in the x direction, of the submerged part of the tower, and is quantified later. Thus, the fluid added mass moment is

$$M_{fl} = \frac{1}{3} C_A \rho\pi \frac{D^2}{4} L^3(1 + \tan^2\theta)\ddot{\theta}, \qquad (19)$$

and, assuming that the fluid added mass due to the end mass is negligible, the total inertia moment is

$$M_I = J_{eff}\ddot{\theta}, \qquad (20)$$

where J_{eff}, the total moment of inertia, is

$$J_{fl} = \frac{1}{3}(ml + M)l^2 + \frac{1}{3} C_A \rho\pi \frac{D^2}{4} L^3(1 + tan^2\theta). \qquad (21)$$

3.2.2 Moments due to Gravity and Buoyancy

The following moment is due to terms that do not depend on the fluid velocity, such as gravity and buoyancy forces,

$$M_g = T_0 l_b - (M + m\frac{l}{2})gl\sin\theta, \tag{22}$$

where g is the gravitational constant, T_0 is the time dependent buoyancy force and l_b is its m arm;

$$T_0 = \rho g V_o \tag{23}$$

where V_o is the volume of the submerged part of the tower. Assuming that $D << d$ we find

$$T_0 = \rho g \pi \frac{D^2}{4} L_s, \tag{24}$$

and L_s, which is the length of the submerged part of the tower, is

$$L_s = \frac{d + \eta(y,t)}{\cos\theta} \tag{25}$$

d is the mean water level, ρ is the fluid density, $\eta(y,t)$ is the wave height elevation given by

$$\eta(x,t) = \frac{1}{2} H\cos(ky - \omega t + \varepsilon), \tag{26}$$

where

$$\omega^2 = gk\tanh(kd) \tag{27}$$

H is the wave height, ω is the wave frequency, and k is the wave number. Since we are interested in η at the instantaneous position of the tower and at $x = d$ with $y = d\tan\theta$,

$$\eta(\theta,t) = \frac{1}{2} H\cos(kd\tan\theta - \omega t + \varepsilon). \tag{28}$$

The buoyant force acts at the center of mass of the submerged part of the tower. If we consider the tower to be of cylindrical cross-section then the center of mass in x', y' coordinates is

$$\begin{aligned} l_b^{y'} &= \frac{D^2}{16L_s}\tan^2\theta \\ l_b^{x'} &= \frac{1}{2}L_s + \frac{D^2}{32L_s}\tan^2\theta. \end{aligned} \tag{29}$$

Transforming to x, y coordinates we find

$$\begin{aligned} l_b &= l_b^{y'}\cos\theta + l_b^{x'}\sin\theta \\ l_b &= \frac{D^2}{16L_s}\tan^2\theta\cos\theta + \frac{1}{2}L_s + \frac{D^2}{32L_s}\tan^2\theta\sin\theta. \end{aligned} \tag{30}$$

3.2.3 Morison's Equation for Wave Force

In general, the fluid forces acting on a slender tower are of two types: drag and inertia. The drag force is proportional to the square of the relative velocity between the fluid and the tower, and the inertia force is proportional to the fluid acceleration. The drag and inertia forces per unit length are approximated by Morison's equation,

$$\mathbf{F}_{fl} = C_D\rho\frac{D}{2} \mid \mathbf{U}-\mathbf{V} \mid (\mathbf{U}-\mathbf{V}) + C_M\rho\pi\frac{D^2}{4}\dot{\mathbf{U}}, \tag{31}$$

where $\mathbf{F}_{fl}$ is the fluid force per unit length, and $\mathbf{U}$, $\mathbf{V}$ are the fluid and tower absolute velocities, respectively. In order to find the moments due to the fluid forces, the fluid and tower absolute velocities are divided into two components: u in the x direction, w in the y direction. Then the horizontal and vertical forces are evaluated.

Assuming a linear deterministic wave field initially, the horizontal and vertical fluid velocities are respectively (Wilson [17] pp. 84) :

$$u = \frac{1}{2}H\omega\frac{\cosh kx}{\sinh kd}\cos(ky-\omega t)$$

$$w = \frac{1}{2} H\omega \frac{\sinh kx}{\sinh kd} \sin(ky - \omega t), \tag{32}$$

and the respective accelerations:

$$\begin{aligned} \dot{u} &= \frac{1}{2} H\omega^2 \frac{\cosh kx}{\sinh kd} \sin(ky - \omega t) \\ \dot{w} &= -\frac{1}{2} H\omega^2 \frac{\sinh kx}{\sinh kd} \cos(ky - \omega t). \end{aligned} \tag{33}$$

To evaluate the fluid forces, the velocities and accelerations have to be defined along the tower. Substituting this expression for $y = x \tan\theta$ in equation (32) yields the fluid horizontal and vertical velocities along the tower,

$$\begin{aligned} u &= \frac{1}{2} H\omega \frac{\cosh kx}{\sinh kd} \cos(kx \tan\theta - \omega t) \\ w &= \frac{1}{2} H\omega \frac{\sinh kx}{\sinh kd} \sin(kx \tan\theta - \omega t). \end{aligned} \tag{34}$$

Fig. 3 depicts sample velocity profiles of the fluid and the tower (equation (16)) along the tower length. The velocities are time dependent and in the figure they are shown at a particular instant of time.

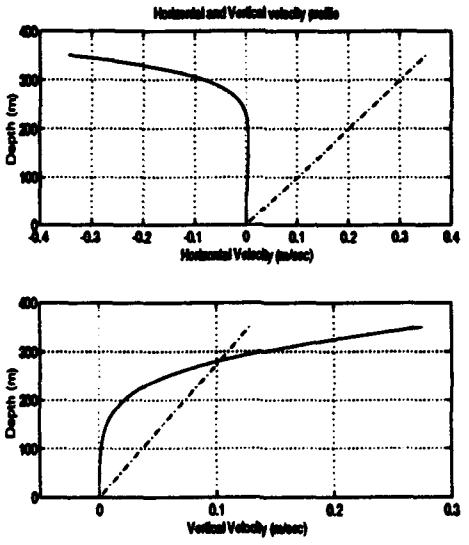

Figure 3: Tower and Fluid Velocity Profiles (Solid Line = Fluid, Dashed Line= Tower)

Taking the derivative of the velocities with respect to time, noticing that θ is time dependent, leads to the accelerations

$$\begin{aligned}
\dot{u} &= -\frac{1}{2}H\omega\left(-\omega+\dot{\theta}\frac{kx}{\cos^2\theta}\right)\frac{\cosh kx}{\sinh kd}\sin(kx\tan\theta-\omega t)\\
\dot{w} &= \frac{1}{2}H\omega\left(-\omega+\dot{\theta}\frac{kx}{\cos^2\theta}\right)\frac{\sinh kx}{\sinh kd}\cos(kx\tan\theta-\omega t).
\end{aligned} \tag{35}$$

The moments due to the fluid velocity and acceleration are as follows. The inertia moments are

$$\begin{aligned}
M_{Ih} &= C_M\rho\pi\frac{D^2}{4}\int_0^L \dot{u}x dx\\
M_{Iv} &= C_M\rho\pi\frac{D^2}{4}\int_0^L \dot{w}x\tan\theta dx,
\end{aligned} \tag{36}$$

and the drag moments are given by

$$\begin{aligned}
M_{Dh} &= C_D\rho\frac{D}{2}\int_0^L \mid u-v_y\mid (u-v_y)x dx\\
M_{Dv} &= C_D\rho\frac{D}{2}\int_0^L \mid w-v_x\mid (w-v_x)x\tan\theta dx.
\end{aligned} \tag{37}$$

where M_{Ih}, M_{Iv} are the inertia moments and M_{Dh}, M_{Dv} are the drag moments due to horizontal and vertical accelerations, respectively. The moment arm for the vertical force is $y = x\tan\theta$. L, which is the upper limit of the integral, depends on the angle θ as follows :

$$L = \begin{cases} l\cos\theta & \text{if } d > l\cos\theta \\ d & \text{if } d < l\cos\theta. \end{cases} \tag{38}$$

This means that the moments are calculated only for the submerged part of the tower.

Substituting the velocities (34) and accelerations (35) into the moment equations yields the inertia moments

$$\begin{aligned}
M_{Ih} &= C_M\rho\pi\frac{D^2}{4}\int_0^L \left[-\frac{1}{2}H\omega\left(-\omega+\dot{\theta}\frac{kx}{\cos^2\theta}\right)\frac{\cosh kx}{\sinh kd}\sin(kx\tan\theta-\omega t)\right]x dx\\
M_{Iv} &= C_M\rho\pi\frac{D^2}{4}\int_0^L \left[\frac{1}{2}H\omega\left(-\omega+\dot{\theta}\frac{kx}{\cos^2\theta}\right)\frac{\sinh kx}{\sinh kd}\cos(kx\tan\theta-\omega t)\right]x\tan\theta dx,
\end{aligned} \tag{39}$$

and the drag moments

$$
\begin{aligned}
M_{Dh} &= C_D\rho\frac{D}{2}\int_0^L\left(\frac{1}{2}H\omega\frac{\cosh kx}{\sinh kd}\cos(kx\tan\theta-\omega t)-x\dot{\theta}\right)^2 x dx \\
M_{Dv} &= C_D\rho\frac{D}{2}\int_0^L\left(\frac{1}{2}H\omega\frac{\sinh kx}{\sinh kd}\sin(kx\tan\theta-\omega t)+x\dot{\theta}\tan\theta\right)^2 x\tan\theta dx.
\end{aligned}
\tag{40}
$$

The direction of the drag moment depends on the sign of the relative velocity between the fluid and the tower. In equation (40), it is assumed that this velocity is positive. When solving the governing nonlinear differential equation numerically, the relative velocity must be evaluated for each time step to determine that sign.

The integrals in equations (39) and (40) are very complicated to evaluate analytically. Although this work is concerned with large angles, we are interested in examining the limitations of the 'small angle' assumption. To do this, analytic expressions for the above integrals are evaluated using 'MAPLE' about $y = 0$, and compared with numerical integrations. This exercise shows that this assumption is very good and the error for $\theta \leq 30^0$ is less the 1 %. Thus, we have at our disposal accurate analytical approximations.

Substituting (34), (35) into the moment formulas and integrating leads to the inertia and drag moments, respectively,

$$
\begin{aligned}
M_{Ih} &= C_M\rho\pi\frac{D^2}{4}\frac{B_2}{2e^{kL}k^2}\left\{(-kLe^{kL^2}+kL+e^{kL^2}+1-2e^{kL})\omega\right. \\
&\left.+\frac{\left(2\,e^{kL^2}-2-2\,kLe^{kL^2}-2\,kL+k^2L^2e^{kL^2}-k^2L^2\right)\dot{\theta}}{\cos^2\theta}\right\},
\end{aligned}
\tag{41}
$$

$$
\begin{aligned}
M_{Iv} &= C_M\rho\pi\frac{D^2}{4}\frac{B_1\tan\theta}{2e^{kL}k^2}\left\{\left(-kLe^{kL^2}-kL+e^{kL^2}-1\right)\omega\right. \\
&\left.+\frac{\left(2\,e^{kL^2}+2-2\,kLe^{kL^2}+2\,kL+k^2L^2e^{kL^2}+k^2L^2-4\,e^{kL}\right)\dot{\theta}}{\cos^2\theta}\right\},
\end{aligned}
$$

$$
\begin{aligned}
M_{Dh} &= C_D\rho\frac{D}{2}\left\{\frac{\dot\theta^2 L^4}{4}+\left(\frac{(-k+2\,k^2L)\,e^{kL^2}}{16\,k^3}+\frac{2\,k+4\,k^3L^2}{16\,k^3}+\frac{-2\,k^2L-k}{16\,k^3e^{kL^2}}\right){B_1}^2\right.\\
&\left.+\left(\frac{(32\,kL-32-16\,k^2L^2)\,e^{kL}}{16\,k^3}+\frac{32\,kL+32+16\,k^2L^2}{16\,k^3e^{kL}}\right)\dot\theta\,B_1\right\},
\end{aligned}
\tag{42}
$$

$$
\begin{aligned}
M_{Dv} &= C_D\rho\frac{D}{2}\left\{\frac{\dot\theta^2\tan^3\theta L^4}{4}-\left(\frac{(-k+2\,k^2L)\,e^{kL^2}}{16\,k^3}+\frac{2\,k-4\,k^3L^2}{16\,k^3}+\frac{-2\,k^2L-k}{16\,k^3e^{kL^2}}\right){B_2}^2\tan\theta\right.\\
&\left.+\left(\frac{(32\,kL-32-16\,k^2L^2)\,e^{kL}}{16\,k^3}+\frac{4}{k^3}+\frac{-16\,k^2L^2-32\,kL-32}{16\,k^3e^{kL}}\right)\dot\theta\tan^2\theta\,B_2,\right.
\end{aligned}
$$

where B_1, B_2 are defined as :

$$
\begin{aligned}
B_1 &= \frac{1}{2}H\omega\frac{\cos(\omega t)}{\sinh(kd)}\\
B_2 &= \frac{1}{2}H\omega\frac{\sin(\omega t)}{\sinh(kd)}.
\end{aligned}
\tag{43}
$$

The drag moment's direction is opposite to the relative velocity between the fluid and the tower. Since this velocity depends on depth (x axis) and may have different signs along the length, we will find its average, and the sign of the average relative velocity will determine the direction of the resultant drag moment.

The general expression for the average relative velocity is given by :

$$
\overline{\mathbf{V}}_{rel}=\frac{1}{L}\int_0^L(\mathbf{U}-\mathbf{V})dx. \tag{44}
$$

We have to evaluate the horizontal $\overline{V}^x_{rel}$ and vertical $\overline{V}^y_{rel}$ relative velocities. Thus, we have

$$
\overline{V}^y_{rel}=\frac{1}{L}\int_0^L\left(\frac{1}{2}H\omega\frac{\cosh kx}{\sinh kd}\cos(kx\tan\theta-\omega t)-x\dot\theta\right)dx, \tag{45}
$$

and after integrating we get

$$
\begin{aligned}
\overline{V}^y_{rel} &= -\frac{\dot\theta\,L}{2}+\frac{\frac{1}{2}H\omega\cos^2\theta}{kL\sinh(kd)}\{\sinh(kL)\cos(kL\tan\theta-\omega t)\\
&+\cosh(kL)\tan\theta\sin(kL\tan\theta-\omega\,t)+2\tan\theta\,\sin(\omega\,t)\}\,.
\end{aligned}
$$

Similarly

$$\overline{V}^x_{rel} = \frac{1}{L}\int_0^L \left(\frac{1}{2}H\omega\frac{\sinh kx}{\sinh kd}\sin(kx\tan\theta - \omega t) + x\dot{\theta}\tan\theta\right)dx, \tag{46}$$

and after integrating

$$\begin{aligned}\overline{V}^x_{rel} &= \frac{\dot{\theta}\,L\tan\theta}{2} + \frac{\frac{1}{2}H\omega\cos^2\theta}{kL\sinh(kd)}\{-\sinh(kL)\tan\theta\,\cos(kL\tan\theta - \omega t)\\ &\quad + \cosh(kL)\sin(kL\tan\theta - \omega t) + 2\,\sin(\omega t)\}.\end{aligned}$$

When we subsequently solve the equation of motion numerically, we will check the sign of the relative velocities to set the correct direction of the drag moments and also to check the sign of $(d - l\cos\theta)$ to set the limits of integration.

3.2.4 Damping Moment

The tower hinge is assumed to dissipate energy via coulomb friction. In this section, this friction/damping moment is evaluated. The damping force is equal to the product of the normal force N and the coefficient of friction μ. It is assumed to be independent of the velocity, once the motion is initiated. Since the sign of the damping force is always opposite to that of the velocity, the differential equation of motion for each sign is valid only for a half cycle interval. The friction force is

$$F_{fr} = N\mu[sgn(\dot{\theta})]. \tag{47}$$

The normal force is

$$N = \sum F_x\cos\theta + \sum F_y\sin\theta, \tag{48}$$

where $\sum F_x$, $\sum F_y$ are the total forces in the x, y directions, respectively. These forces are due to gravity, buoyancy and fluid drag and inertia,

$$\sum F_x = T_0 - F_g + F_{Iv} + F_{Dv}$$

$$\sum F_y = F_{Ih} + F_{Dh}, \tag{49}$$

where T_0 is the buoyancy force given in equation (24), F_g is the gravitational force,

$$F_g = (ml + M)g, \tag{50}$$

and F_{Dh}, F_{Dv}, F_{Ih}, F_{Iv} are the fluid drag and inertia forces in the horizontal (y) and vertical (x) directions, respectively. These forces are calculated using Morison's equation in a similar way as the moments and are given by,

$$\begin{aligned}
F_{Dh} &= C_D\rho\frac{D}{2}\left\{\frac{L^3\dot{\theta}^2}{3} + \left(\frac{(-kL+1)\,e^{kL}}{k^2} - \frac{2}{k^2} + \frac{1+kL}{k^2e^{kL}}\right)B_1\,\dot{\theta} + \left(\frac{e^{kL^2}}{8\,k} + \frac{L}{2} - \frac{1}{8\,ke^{kL^2}}\right){B_1}^2\right\} \\
F_{Dv} &= C_D\rho\frac{D}{2}\left\{\frac{L^3\dot{\theta}^2\tan^2\theta}{3} + \left(\frac{(\,kL-1\,)\,e^{kL}}{k^2} + \frac{kL+1}{k^2e^{kL}}\right)B_2\,\dot{\theta}\tan\theta + \left(\frac{e^{kL^2}}{8\,k} - \frac{L}{2} - \frac{1}{8\,ke^{kL^2}}\right){B_2}^2\right\} \\
F_{Ih} &= C_M\rho\pi\frac{D^2}{4}\left\{\left(\left(\frac{e^{kL^2}kL - kL - e^{kL^2} - 1}{2\,k^2e^{kL}} + k^{-2}\right)\frac{\dot{\theta}k}{\cos^2\theta} - \frac{\left(e^{kL^2}-1\right)\omega}{2\,e^{kL}k}\right)B_2\right\} \\
F_{Iv} &= C_M\rho\pi\frac{D^2}{4}\left\{\left(\frac{\left(e^{kL^2}kL + kL - e^{kL^2} + 1\right)}{2\,k^2e^{kL}}\frac{\dot{\theta}k}{\cos^2\theta} - \frac{\left(e^{kL^2}+1\right)\omega}{2\,e^{kL}k} + \frac{\omega}{k}\right)B_1\right\}.
\end{aligned} \tag{51}$$

If we assume a hinge radius R_h, then the damping moment is

$$M_{fr} = R_h\left(\sum F_x\cos\theta + \sum F_y\sin\theta\right)\mu[sgn(\dot{\theta})]. \tag{52}$$

Finally, adding all the external moments, equations (22), (41), (42), (52), and setting them equal to the total inertia moment, equation (20), yields the governing nonlinear differential equation of motion,

$$J_{eff}\ddot{\theta} = -M_{fr} - M_g + M_{Ih} - M_{Iv} + M_{Dh} - M_{Dv}. \tag{53}$$

Both sides of this equation are nonlinear functions of θ, $\dot{\theta}$, t and ω :

$$\begin{aligned}
J_{eff}(\theta)\ddot{\theta} &= -M_{fr}(\theta,\omega,t,sgn(\dot{\theta})) - M_g(\theta,\omega,t) + M_{Ih}(\theta,\dot{\theta},\omega,t) - \\
&\quad M_{Iv}(\theta,\dot{\theta},\omega,t) + M_{Dh}(\dot{\theta},\omega,t) - M_{Dv}(\theta,\dot{\theta},\omega,t),
\end{aligned} \tag{54}$$

which agrees with the general form of equation (11).

4 Numerical Solution

The numerical solution for the nonlinear differential equation (53) was performed using 'ACSL' and the analyses of the results was performed using 'MATLAB'. The 'ACSL' code written for this application is available upon request. In order to build confidence in the solution, some test cases have been solved using the following physical parameters :

Tower properties

1. l - Length of the tower = 400 (m)
2. D - Tower diameter = 15 (m)
3. M - End mass = $2.5 * 10^5$ (Kg)
4. m - Tower mass per unit length = $2 * 10^3$ $(\frac{Kg}{m})$
5. μ - Friction coefficient = 0.1-0.4
6. R_h - Hinge radius = 1.5 (m)

Fluid properties

1. d - Mean water level = 350 (m)
2. C_D - Drag coefficient =0.6 - 1.0
3. C_M - Inertia Coefficient =1.5
4. ρ - Water density = 1025 $(\frac{Kg}{m^3})$
5. ω - Wave frequency = 0.2 - 1.0 $(\frac{rad}{sec})$

4.1 Response for Deterministic Wave Heights

In this section the response of the tower to deterministic wave heights is established. Free vibration and stability analyses are performed.

First, the natural frequency of the tower is found as if it was an upright pendulum subjected to a constant tension force T_0 and gravitational force M_g. Fig. 4 shows the tower response to an impulse for $C_D = 0$ and $H = 0$ in the time and frequency domain. The response is harmonic in the tower natural frequency $\Omega_n = 0.026\ (Hz)$, and it agrees with the calculation for the natural frequency of a pendulum :

$$\Omega_n = \frac{1}{2\pi}\sqrt{\frac{T_0 l_b - (0.5ml + M)gl}{J_{eff}}}. \tag{55}$$

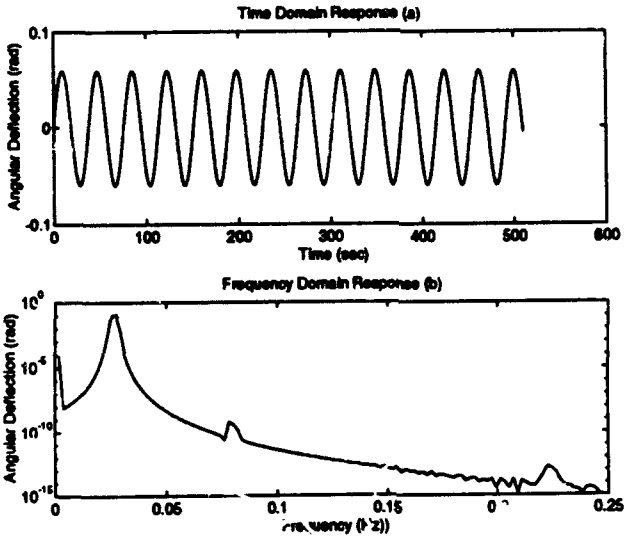

Figure 4: Tower Natural Frequency, $C_D = 0$

Fig 5 (a,b) shows the same but for $\mu = 0$ and $C_D = 1$, the decay here is not linear since the drag force is propotional to the velocity squared. Fig 5 (c,d) shows the free vibration with frictional damping, $\mu = 0.1$, in the time and frequency domain. Here the amplitude decays linearly with time as expected when coulomb damping is present. From the figure we can evaluate the equivalent damping ratio for $C_D = 0$ to be $\xi = 0.02$. Since the damping is nonlinear, the 'natural frequency' and its multipliers are seen in the figure.

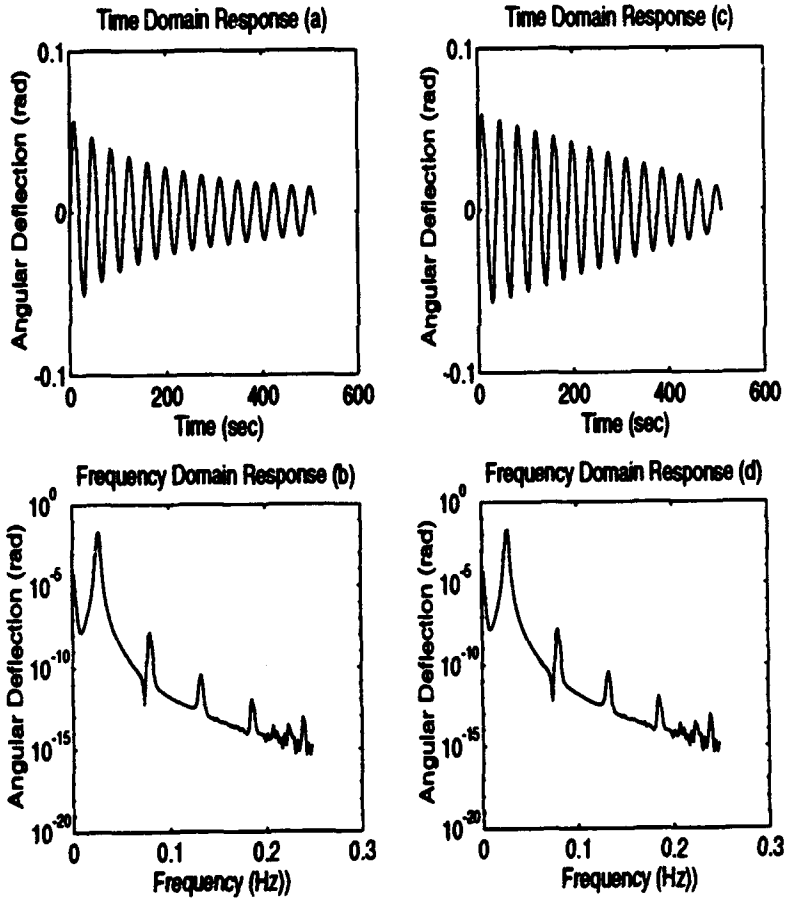

Figure 5: Tower Free Vibration with Damping, (a, b) $\mu = 0.1$, (c, d) $C_D = 1$

Fig. 6 shows the response in the time domain and frequency domain for $H = 1\ (m)$ and wave loading frequency $\omega = 0.064\ (Hz)$. Figures (a, b) are with $\mu = 0$ and (c, d) are with $\mu = 0.4$. In the frequency domain, the tower 'natural frequency' and the wave natural frequency are clearly seen. It can be seen that the friction has a damping and stabilizing effect on the system.

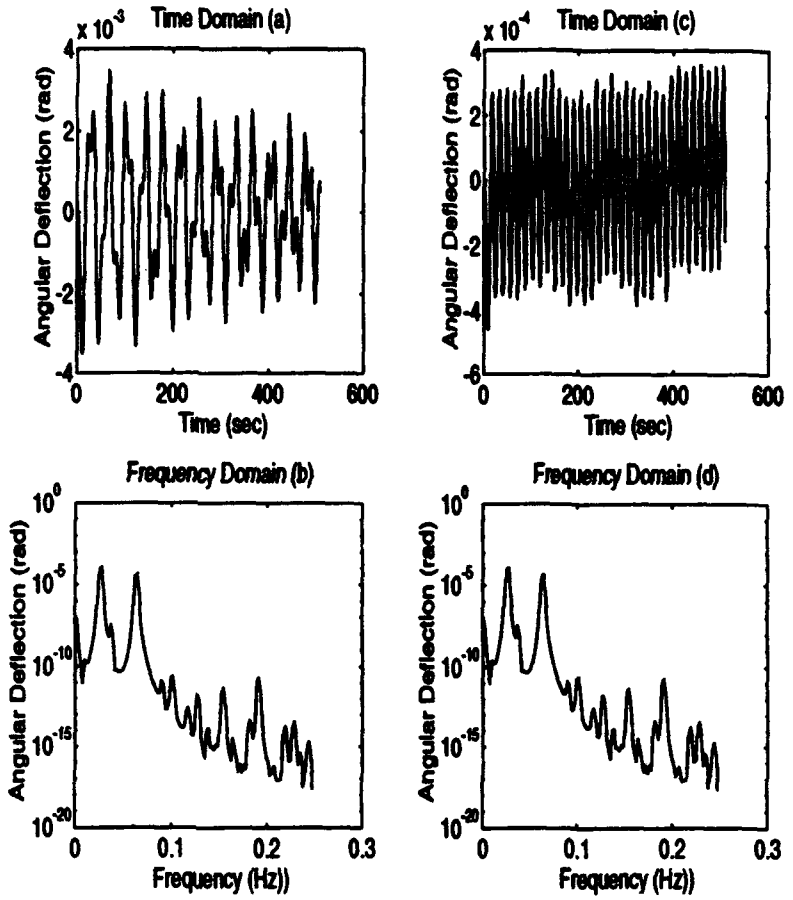

Figure 6: Tower response to wave excitation, Time and Frequency Domain, $H = 1\ (m)$

Since this is a nonlinear system, its response to harmonic excitation at the system's 'natural frequency' or its multipliers can be multivalued, indicating the occurrence of a 'jump'. Fig. 7 shows the tower response to harmonic wave excitation at $\omega = \Omega_n$ (harmonic solution) with and without damping. If the system was linear, such loading would have caused resonance instability. But since the system is nonlinear, an amplitude change (beating) can be seen Fig. 7 (a), indicating that 'jumps' occur from one amplitude to the other (Wilson [17] pp. 147). It can also be seen that although the excitation frequency is constant, the frequency response is not Fig. 7 (b). Again the reason is the nonlinear system characteristics. From the response with friction (figures (c, d)) we see that the response is not smaller since it is unstable, but the ratio between the large and small amplitude of the beating gets smaller.

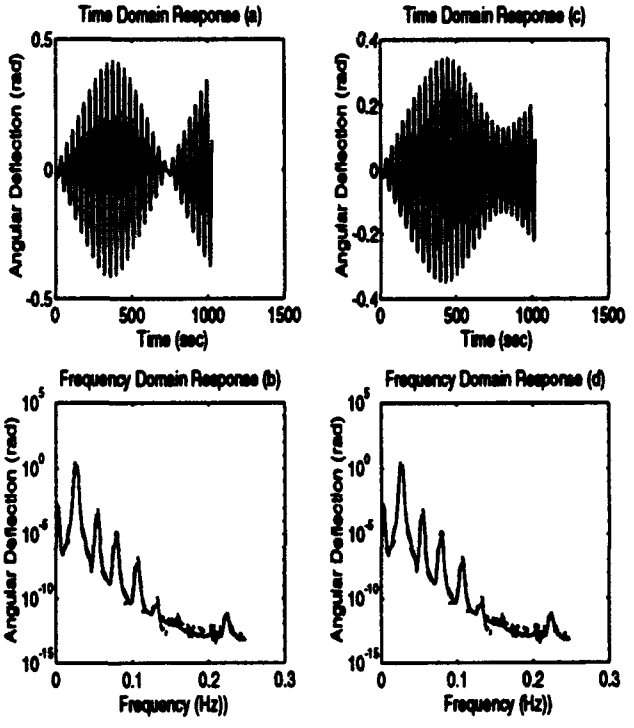

Figure 7: Tower response to harmonic wave excitation at the 'Natural Frequency' - Beating Phenomenon

Fig. 8 shows the response due to harmonic wave excitation at twice the system 'natural frequency' (sub-harmonic solution), with (c, d) and without friction (a, b). We can see the beating phenomenon, and from the frequency domain we see that the response consists of the 'natural frequency'and it multipliers. This is due to the nonlinear nature of the system.

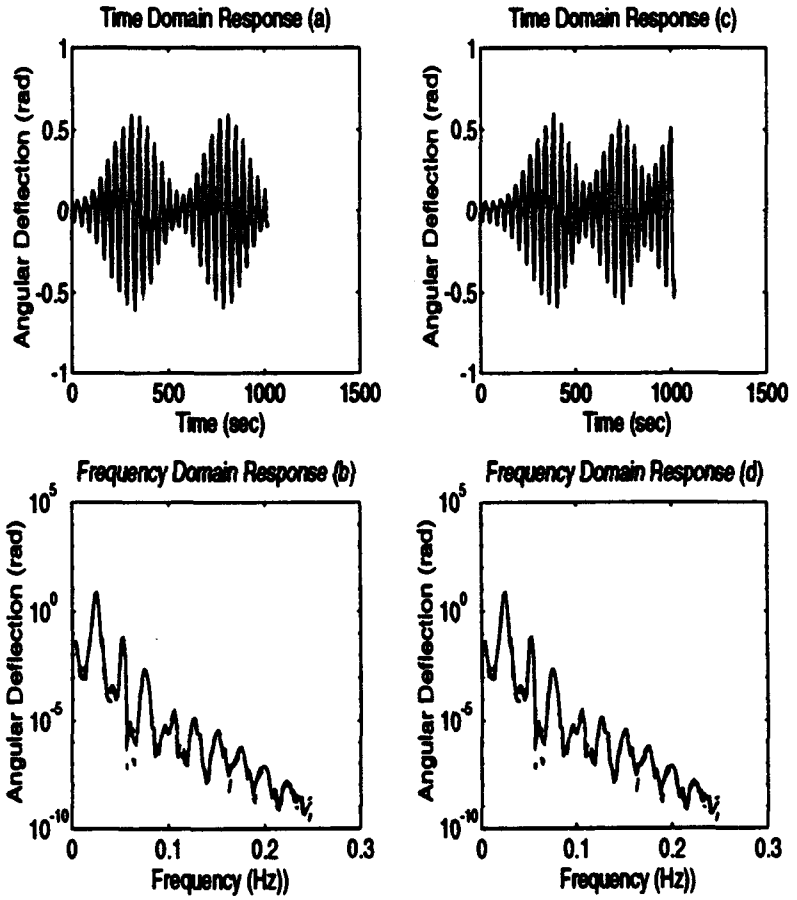

Figure 8: Tower response to sub-harmonic wave excitation at twice 'Natural Frequency'

The direction of the drag force is opposite to the direction of the relative velocity between the tower and the wave. If the direction of the relative velocity is the same as the tower velocity, the drag will always stabilize the system. The reason is that the drag moment will always be opposite to the direction of the deflection angle θ. But if the relative velocity direction is opposite to tower velocity, the drag moment can cause instability. For zero wave velocity the drag force always stabilizes the system, as can be seen from Fig. 5. Fig. 9 describes the horizontal and vertical components of the relative velocity and tower velocity.

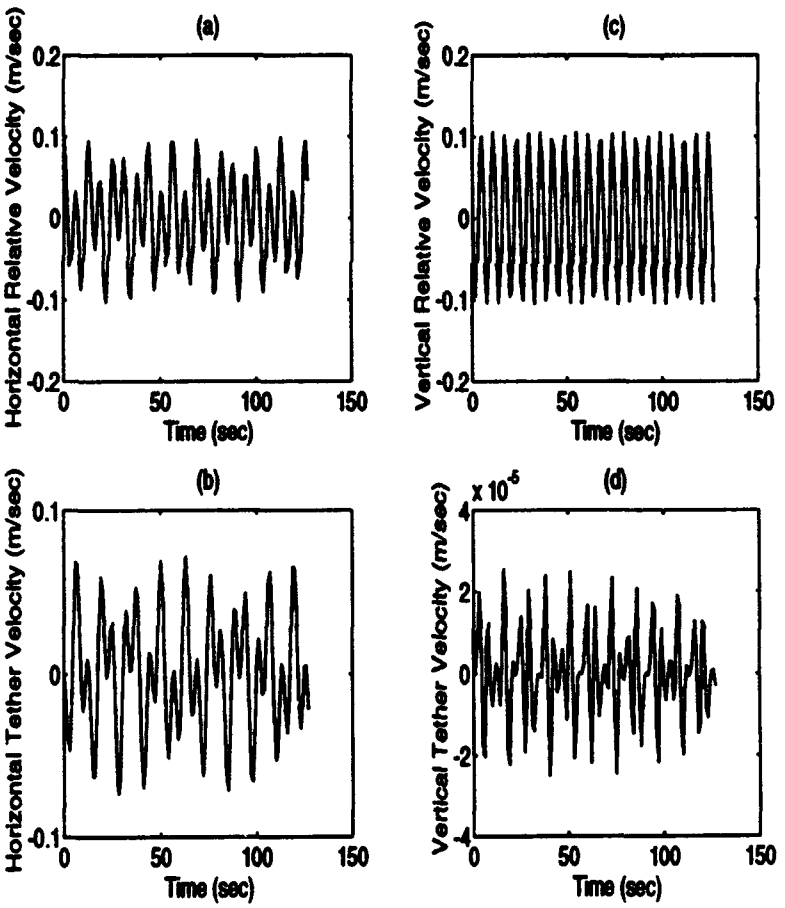

Figure 9: Relative and Tower Velocities - (a, c) Horizontal and (b, d) Vertical

4.1.1 Chaotic Response

Because of the nonlinear characteristics of the system, the governing differential equation of motion, chaotic motion can occure under certain conditions. Fig. 10 shows the response of the tower to a harmonic wave excitation at a frequency $\omega = 0.95\Omega_n$. We see that the response 'jumps' between two stable equilibrium states. This phenomenon can imply a chaotic system.

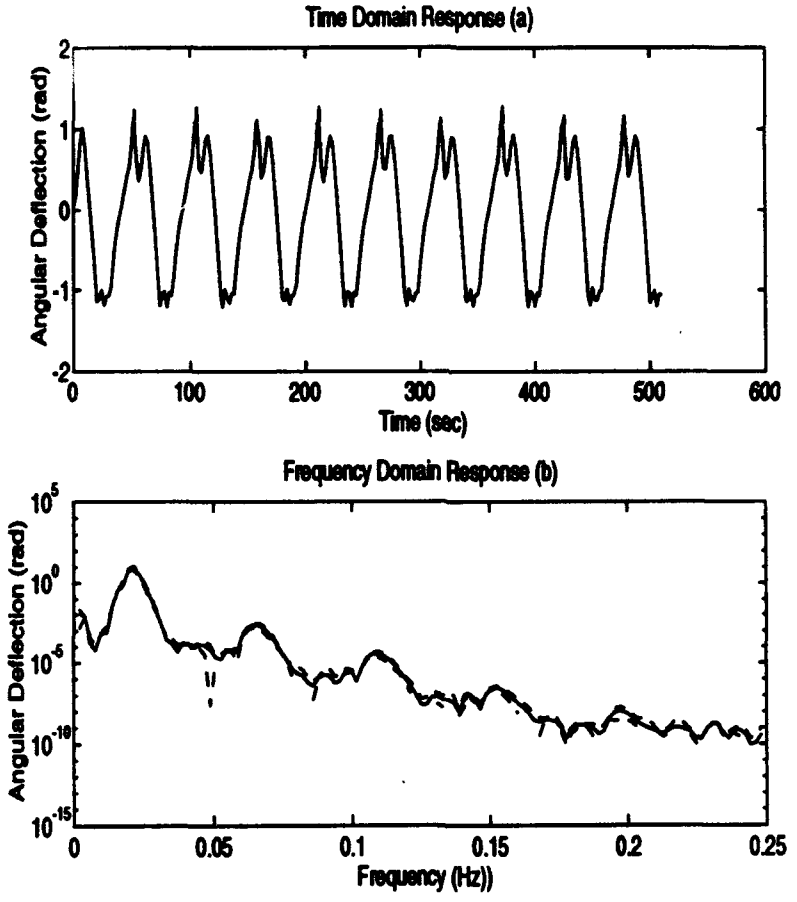

Figure 10: Tower response to harmonic wave excitation at the 'Natural Frequency', $C_D = 0.6$

Moon [11] provides several ways to identify chaotic vibrations. We next use three ways to prove that the system under consideration is chaotic. Fig. 11 describes the response of the tower to a harmonic wave excitation having a frequency of $\omega = 0.09\ (Hz)$. Fig 11 (a, b) shows the response in the time and frequency domains and the phase-plane trajectory (c). From the time history it is clearly seen that the system jumps between two stable equilibrium states. The frequency domain shows multiharmonic energy although the system has one degree of freedom; another indicator of chaos. Finally, from the phase-plane trajectory we see that the orbits never close or repeat. Thus, we conclude that this model has the characteristics of a chaotic system. This chaotic phenomenon appeared only when the wave height was larger than 10 (m).

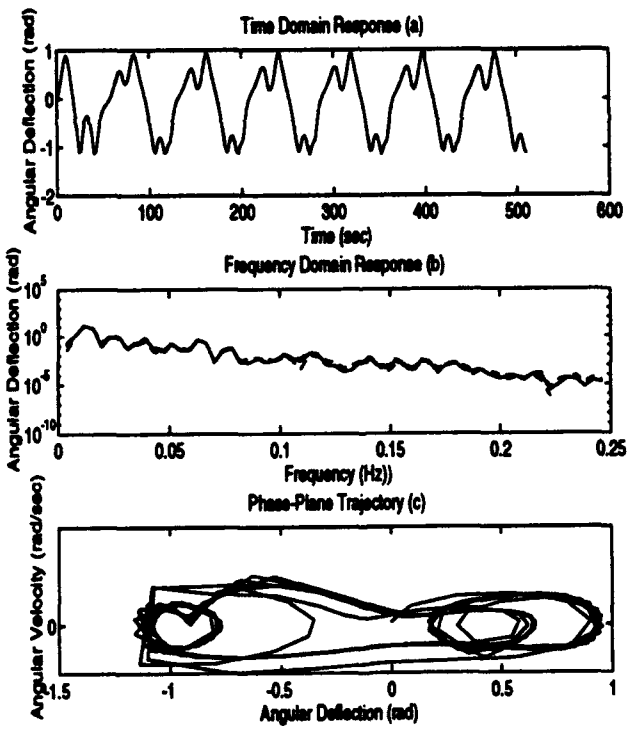

Figure 11: Tower response to a harmonic wave excitation, $\omega = 0.09\ (Hz)$ - Chaos

4.2 Random Wave Height

In this section the tower response to random wave height excitation is investigated. The wave height distribution is generally expressed in the form of a power spectral density. For a simulation of the response in the time domain, the power spectra of the wave height is transformed into a time history. This is accomplished using a method by Borgman [2], described in Wilson's book [17], and presented here.

4.2.1 Synthesis of Time Histories from Power Spectra

The wave elevation $\eta(x,t)$ can be expressed as

$$\eta(x,t) = \int_0^\infty \cos(kx - \omega t + \varepsilon)\sqrt{A^2(\omega)d\omega}, \tag{56}$$

where $A^2(\omega)$ is the amplitude spectrum (height) and ε is a random phase angle having a uniform distribution over an interval 0 to 2π. To evaluate the integral, the spectrum is discretized into equal areas (not equal frequencies). This procedure avoids the presence of periodicities in the resulting time history. Consider the following partition ;

$$\omega_0 < \omega_1 < \omega_2 < .... < \omega_N = F, \tag{57}$$

where ω_0 is a small positive value and F is the frequency above which the spectral amplitude is practically zero. Let

$$\Delta\omega_n = \omega_n - \omega_{n-1} \tag{58}$$

$$\bar{\omega}_n = \frac{\omega_n - \omega_{n-1}}{2}; \quad n = 1,2,...N, \tag{59}$$

where N is the number of partitions of the spectra. Now the integral can be approximated as a sum,

$$\bar{\eta}(x,t) = \sum_{n=1}^{N} \cos(\bar{k}_n x - \bar{\omega}_n t + \varepsilon_n)\sqrt{A^2(\bar{\omega}_n)\Delta\omega_n}, \tag{60}$$

where $\bar{\omega}_n^2 = \bar{k}_n g$ and $\bar{()}$ represents the average of each parameter. Let $S(\omega_n)$ represent the cumulative area under the spectral density curve, or

$$S(\omega_n) = \sum_{n=1}^{N} A^2(\omega_n)\Delta\omega_n. \tag{61}$$

Thus,

$$A^2(\bar{\omega}_n)\Delta\omega_n \approx S(\omega_n) - S(\omega_{n-1}) = a^2, \tag{62}$$

where a^2 is a constant to be determined. It follows that

$$Na^2 = S(\omega_N) \approx S(\infty) = \int_0^\infty A^2(\omega)d\omega. \tag{63}$$

The Pierson-Moskowitz spectrum for the wave height is

$$S_\eta(\omega) = A^2(\omega) = \frac{A_0}{\omega^5} e^{-B/\omega^4}, \tag{64}$$

where A_0 and B are constants defined by

$$\begin{aligned} A_0 &= 8.1 \times 10^{-3} g^2 \qquad (65)\\ B &= \frac{3.11}{H_s^2}. \end{aligned}$$

Then, from equations (61) and (64),

$$S(\omega) = \frac{A_0}{4B} e^{-B/\omega^4}, \tag{66}$$

and, therefore,

$$\begin{aligned} S(\infty) &= \frac{A_0}{4B} \qquad (67)\\ a^2 &= \frac{A_0}{4BN}. \qquad (68) \end{aligned}$$

Now the partition frequencies can be determined for $\omega = F$,

$$\frac{A_0}{4B} = e^{B/F^2} S(F). \tag{69}$$

Because the partition is of equal areas

$$S(\omega_n) = \frac{n}{N} S(F) = \frac{A_0}{4B} e^{-B/\omega_n^4} = S(F) e^{B/F^4} e^{-B/\omega_n^4}, \tag{70}$$

it follows that

$$\frac{N}{n} e^{B/F^4} = e^{B/\omega_n^4}. \tag{71}$$

Solving equation (71) for ω_n leads to the partition frequencies

$$\omega_n = \left(\frac{B}{\ln(N/n) + B/F^4} \right)^{0.25}, \qquad n = 1, 2, ...N. \tag{72}$$

Therefore, the wave elevation $\eta(x,t)$ can be approximated by

$$\bar{\eta}(x,t) = a \sum_{n=1}^{N} \cos(k_n x - \omega_n t + \varepsilon_n). \tag{73}$$

The wave loading on the tower is a function of wave velocity and acceleration. Therefore, in our numerical studies, these have to be expressed as functions of the approximate wave elevation. Thus, in the expressions for wave velocity and acceleration, the following substitutions are made

$$\begin{aligned} H &\implies \sqrt{\frac{A_0}{4BN}} \\ \omega &\implies \omega_n \\ k &\implies k_n, \end{aligned} \tag{74}$$

where $n = 1, 2, ...N$. For example, the horizontal velocity and acceleration will become

$$\begin{aligned} u &= \sum_{n=1}^{N} \frac{A_0}{4BN} \omega_n \frac{\cosh k_n x}{\sinh k_n d} \cos(k_n x \tan\theta - \omega_n t) \\ \dot{u} &= \sum_{n=1}^{N} -\frac{A_0}{4BN} \omega_n \left(-\omega_n + \dot{\theta} \frac{k_n x}{\cos^2\theta} \right) \frac{\cosh k_n x}{\sinh k_n d} \sin(k_n x \tan\theta - \omega_n t). \end{aligned} \tag{75}$$

As mentioned earlier, the wave height is assumed to have the Pierson-Moskowitz spectrum

$$S_\eta(\omega) = \frac{0.0081 * g^2}{\omega^5} \exp\left(-\frac{3.11}{H_s^2 \omega^4}\right). \tag{76}$$

The significant wave height, H_s, changes the maximum wave height and the wave frequency distribution as shown in Fig. 12 for $H_s = 15$ and 9 (m).

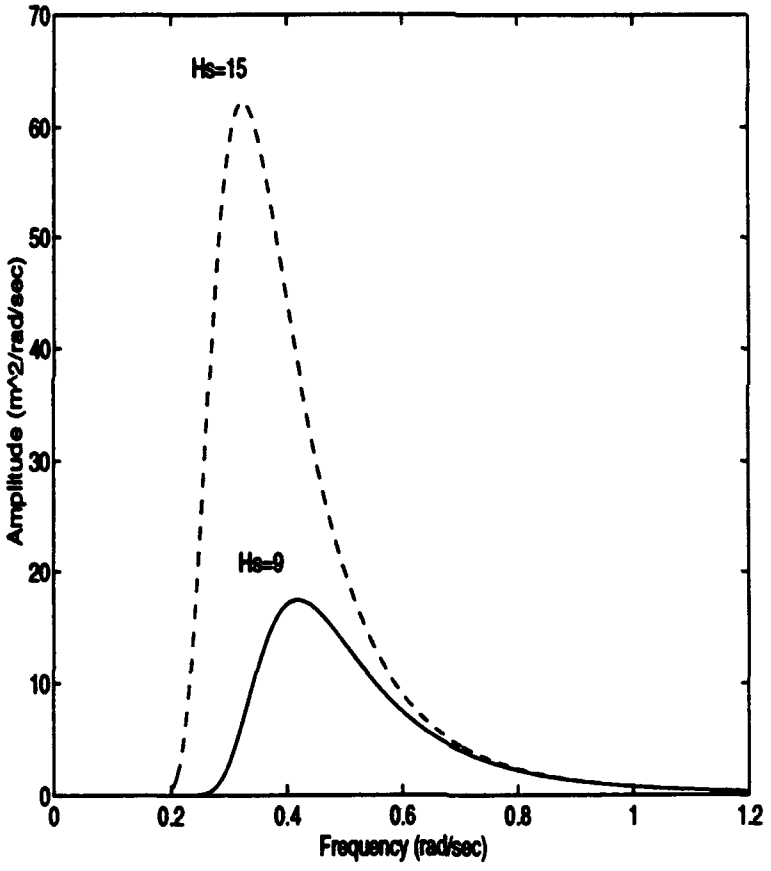

Figure 12: Examples of Two Pierson-Moskowitz Wave Height Spectra

4.2.2 Response for Random Wave Height

In this section, the influance of different significant wave heights, drag coefficient , hinge friction and non-zero intial condition on the response is investigated. Fig. 13 compares the tower response for $H_s = 9$ and 15 (m). Here we enlarged the buoyancy force so that the tower 'natural frequency' is $\Omega_n = 0.07\ (Hz) = 0.44\ (rad/sec)$. It can be seen that the deflection angle for $H_s = 9\ (m)$ is of the same magnitude as for for $H_s = 15\ (m)$, although the later maximum wave height is four times larger then the former (as can be seen from Fig. 12). The reason is that the natural frequency of the tower coinsides with where most of the spectral energy for $H_s = 9\ (m)$ is located, as shown in Fig. 12. Since the lowest wave freqency is about $\omega = 0.2\ (rad/sec)$ articulated tower are designed to have a 'natural frequency' lower than that.

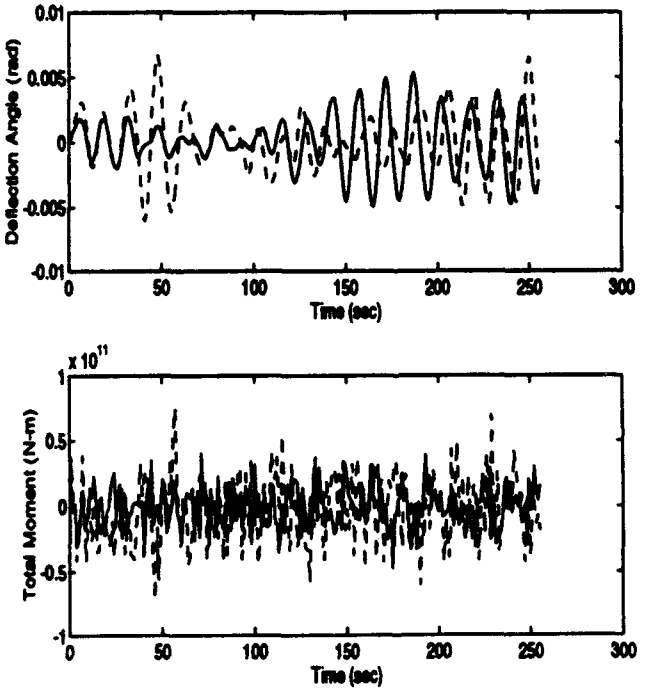

Figure 13: Tower Response - Deflection angle and Total Moment for $H_s = 15$ (dashed line) and 9 (solid line) (m)

A comparison of the tower response for different values of the drag coefficient are plotted in Fig. 14. This figure shows the deflection angle and the total drag moment, $M_d = M_{Dh} - M_{Dv}$, for $C_D = 0.6$ and 1, and $H_s = 9$ (m). It can be seen from the figure that the deflection angle and the drag moment are larger for $C_D = 1$, since the drag moment in the Morison equation is proportional to the drag coefficient. The results were similar for different significant wave heights.

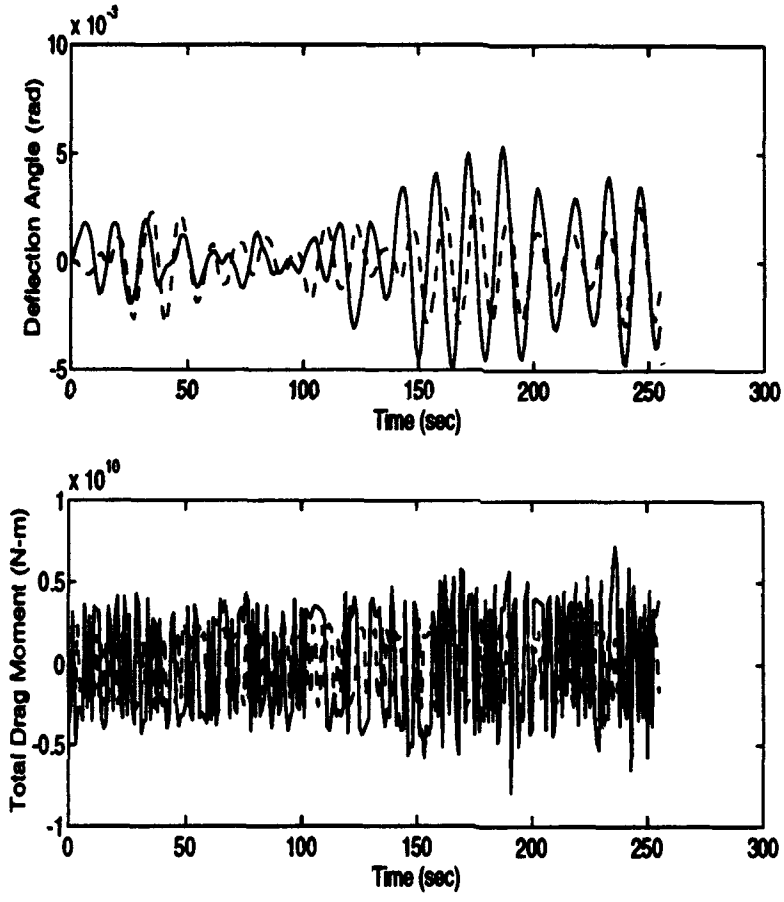

Figure 14: Tower Response - Deflection angle and Total Drag Moment for $H_s = 9$ (m) and $C_D = 0.6$ (dashed line) and 1 (solid line).

The friction effect on the response is shown clearly in Fig. 15. Here the significant wave height is $H_s = 9$ and $C_D = 1$. It is seen that the response is much smaller and smoother due to the additional friction in the system.

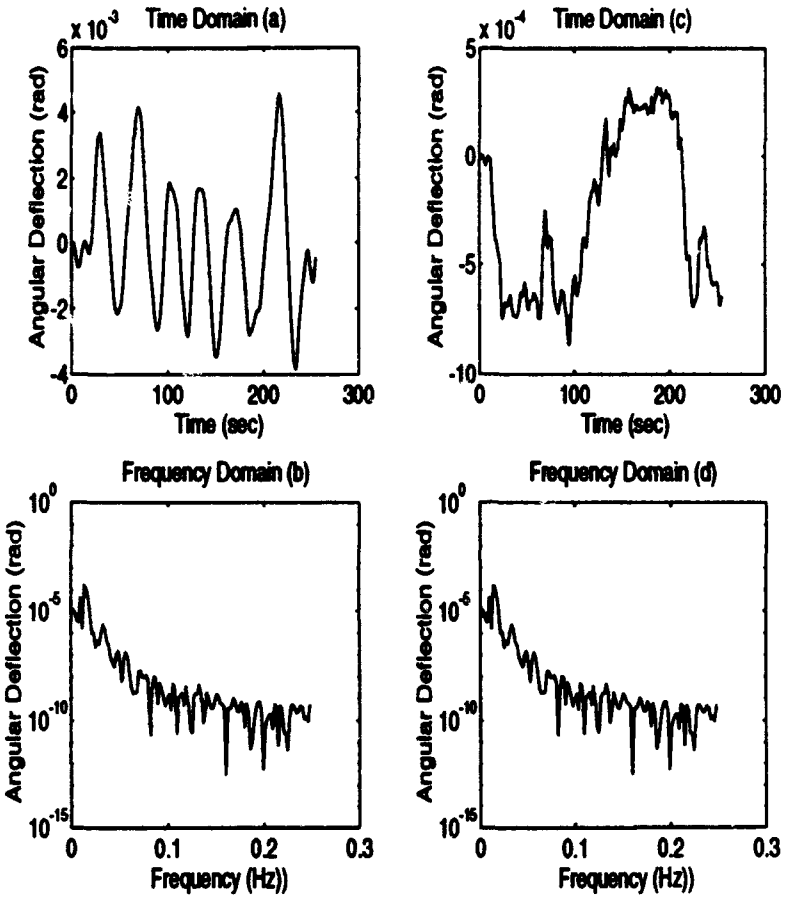

Figure 15: Tower Response - Deflection angle - Time and Frequency Domain for $H_s = 9$ (m) and $C_D = 1$, (a, b) $\mu = 0$ and (c, d) $\mu = 0.4$

The response for nonzero initial conditions is depicted in Fig. 16. The response for $\dot{\theta}(t=0) = 0.01(rad/sec)$ (a, b), and $\theta(t=0) = 0.05(rad)$ (c, d). The drag coefficient is $C_D = 0.6$ and $H_s = 9$ (m).

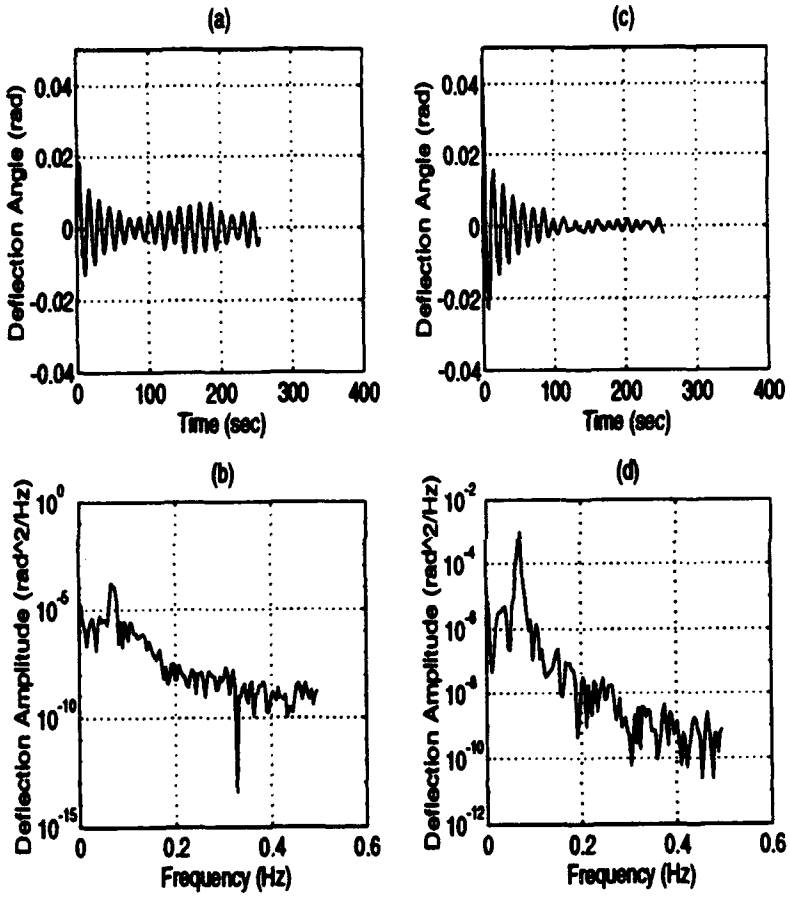

Figure 16: Tower Response - (a, b) Deflection angle $\theta(t=0) = 0.05$ (rad) and (c, d) $\dot{\theta}(t=0) = 0.01$ (rad/sec).

5 Discussion and Summary

The nonlinear differential equation of motion for an articulated tower submerged in the ocean is derived. Geometric as well as force nonlinearities are included in the derivation. The wave velocities and accelerations are determined at the instantaneous position of the tower, a fact that added to the nonlinearities of the equation. The equation is solved numerically using 'ACSL' for deterministic and random wave loading.

The response of the tower to harmonic wave excitation at its 'natural frequency' and at twice its 'natural frequency' demonstrates beating, where the amplitude varies between two extremes. This beating is due to the nonlinear behaviour of the system. Coulomb damping reduces the beating phenomenon and the response amplitude, so it has a stabilizing effect on the system. When the system is excited at an arbitrary frequency, and the wave height is greater than about $10\ (m)$, the response 'jumps' between two stable equilibria, exhibiting chaotic behaviour.

To solve the equation for random wave loading, the Pierson-Moskowitz spectrum that describes the wave height distribution was first transformed into a time history. The equation was solved for two significant wave heights. Again the response was periodic consisting of the fundamental tower frequency and its multipliers. For significant wave height of $9\ (m)$, the response was larger than that for $15\ (m)$, since in the former the tower 'natural frequency' coincides with the frequencies where most of the energy is located. The response with coulomb damping shows that friction stabilizes the system. Notice that in order to reduce stresses in the structure, the friction moment has to be low enough so that the tower can comply with the wave loading.

A more realistic model having two angular degrees of freedom is being analyzed at the present time. The response due to wave, current (colinear and non-colinear) and vortex shedding loading

is investigated loading and results will be published in the near future.

Acknowledgment

This work is supported by the Office of Naval Research grant no. $N00014-93-1-0763$. The authors are grateful for this support and thank ONR and Program Manager Dr. T. Swean for his interest in our work.

References

[1] *ACSL - Advanced Continuous Simulation Language.* Mitchell and Gauthier Associate (MGA), 1993.

[2] E.L. Borgman. Ocean wave simulation for engineering design. *Journal of the waterways and harbors division*, 95:557–583, 1969.

[3] S.K. Chakrabarti and D.C. Cotter. Motion analysis of articulated tower. *Journal of the waterway, port, coastal and ocean division*, 105:281 – 292, 1979.

[4] S.K. Chakrabarti and D.C. Cotter. Transverse motion of articulated tower. *Journal of the waterway, port, coastal and ocean division*, 107:65 – 77, 1980.

[5] H.S. Choi and Lou J.Y.K. Nonlinear behaviour of an articulated offshore loading platform. *Applied Ocean Research*, 12(2):63 – 74, 1991.

[6] T.K. Datta and A.K. Jain. Response of articulated tower platforms to random wind and wave forces. *computer and structures*, 34(1):137 – 144, 1990.

[7] O. Gottlieb, C.S. Yim, and Hudspeth R.T. Analysis of nonlinear response of an articulated tower. *International Journal of Offshore and Polar Engineering*, 2(1):61 - 66, 1992.

[8] A.K. Jain and T.K. Datta. Nonlinear behavior of articulated tower in random sea. *journal of engineering for industry, trans. of ASME*, 113:238 - 240, 1991.

[9] R.K. Jain and C.L Kirk. Dynamic response of a double articulated offshore loading structure to noncollinear waves and current. *Journal of Energy Resources Technology*, 103:41 - 47, 1981.

[10] H.B. Kanegaonkar and A. Haldar. Nonlinear random vibrations of compliant offshore platforms. *Symposium of Nonlinear Stochastic Dynamic Engineering Systems*, pages 351 - 360, 1987.

[11] Francis C. Moon. *Chaotic and Factual Dynamics an introduction for applied scientists and engineers.* John Wiley and Sons, 1992.

[12] A.S. Muhuri, P.K.and Gupta. Stochastic stability of tethered buoyant platforms. *Ocean engineering*, 10(6):471 - 479, 1983.

[13] M.H. Patel. *Dynamics of Offshore Structures.* Butterworths, 1998.

[14] L.L. Seller and Niedzwecki J.M. Response characteristics of multi-articulated offshore towers. *Ocean engineering*, 19(1):1 - 20, 1992.

[15] Hanna S.Y., A. Mangiavacchi, and Suhendra R. Nonlinear dynamics analysis of guyed tower platforms. *Journal of Energy Resources Technology*, 105:205 - 211, 1983.

[16] J.M.T. Thompson, Bokaian A.R., and R. Ghaffai. Stochastic and chaotic motions of compliant offshore structures and articulated mooring towers. *Journal of Energy Resources Technology*, 106:191 - 198, 1984.

[17] J.F. Wilson. *Dynamics of Offshore Structures.* John Wiley and Sons, 1984.

NONLINEAR DYNAMICS OF AN ARTICULATED TOWER IN THE OCEAN

PATRICK BAR-AVI
Department of Mechanical and Aerospace Engineering
Rutgers University
Piscataway, N.J. 08855
HAYM BENAROYA
Department of Mechanical and Aerospace Engineering
Rutgers University
Piscataway, N.J. 08855

ABSTRACT

This paper presents studies on the response of an articulated tower in the ocean subjected to deterministic and random wave loading. The tower is modeled as an upright rigid pendulum with a concentrated mass at the top and having one angular degree of freedom about a hinge with coulomb damping. In the derivation of the differential equation of motion, nonlinear terms due to geometric (large angle) and fluid forces (drag and inertia) are included. The wave loading is derived using Morison's equation in which the velocity and acceleration of the fluid are determined along the instantaneous position of the tower, causing the equation of motion to be highly nonlinear. Furthermore, since the differential equation's coefficients are time-dependent (periodic), parametric instability can occur depending on system parameters such as wave height and frequency, buoyancy, and drag coefficient. The nonlinear differential equation is then solved numerically using 'ACSL' software. The response of the tower to deterministic wave loading is investigated and a stability analysis is performed (resonance and parametric instability). To solve the equation for random loading, the Pierson-Moskowitz power spectrum, describing the wave height, is first transformed into an approximate time history using Borgman's method with slight modification. The equation of motion is then solved, and the influence on the tower response of different parameter values such as buoyancy, initial conditions and wave height and frequency, is investigated.

Key words : Articulated, Dynamics, Random, Stability, Chaos

REVIEW AND PROBLEM DEFINITION

Compliant platforms such as articulated towers are economically attractive for deep water conditions because of their reduced structural weight compared to conventional platforms. The foundation of the tower does not resist lateral forces due to wind, waves and currents; instead, restoring moments are provided by a large buoyancy force, a set of guylines or a combination of both. These structures have a fundamental frequency well below the wave lower frequency. As a result of the relatively large displacements, geometric nonlinearity is an important consideration in the analysis of such a structure. The analysis and investigation of these kind of problems can be divided into two major groups; deterministic and random wave and/or current loading. We briefly review work in this area in the next two subsections.

Deterministic Loading

Chakrabarti and Cotter (1979) [2] analyzed the motion of articulated tower. The tower is articulated by a universal joint having single degree of freedom. They assumed, linear waves, small perturbations about an equilibrium position, linear drag force and that the wind current and wave are colinear. Their resulting equation of motion is,

$$I\ddot{\psi} + B(\dot{\psi}) + D\dot{\psi} + C\psi = M_0 e^{i(\alpha-\beta t)}, \qquad (1)$$

where I is the total moment of inertia including added mass, $B(\dot{\psi})$ is the nonlinear drag term, $D\dot{\psi}$ is the structural damping, $C\psi$ is the restoring moment due to buoyancy and M_0 is the wave moment. An analytical solution is then compared to experimental results to show good agreement as long as the system is inertia predominant, and not drag predominant.

In a later paper, Chakrabarti and Cotter (1980) [3] investigated transverse motion, the motion perpendicular to the horizontal velocity. The tower pivot is assumed to have two angular degrees of freedom and is taken to be frictionless. It is also assumed that the motion is not coupled, so the inline solution is obtained (the same as in the previous paper) from which the relative velocity between the tower and the wave is obtained. The lift force (in the transverse direction) can then be obtained and the linear equation of motion is solved analytically and compared to experimental results. The comparison shows good agreement, especially when the drag terms are small.

Jain and Kirk (1981) [4] investigated the dynamic response of a double articulated offshore structure to waves and current loading. They assumed four degrees of freedom, two angular for each link. The equations of motion were derived using Lagrange equations. In deriving the equations of motion the following assumptions were made: drag and inertia forces tangent to the tower are negligible, and the wave and current velocities are evaluated at the upright position (small angles assumption). The linearized equations were solved to find the natural frequencies of the system and then numerically solved to find the response due to colinear and non-colinear current and wave velocities. They found that when the wave and the current velocities are colinear, the response of the top is sinusoidal, while for noncolinear velocities the response is a complex three dimensional whirling oscillation.

Thompson et al. (1984) [5] investigated the motions of an articulated mooring tower. They modeled the structure as a bilinear oscillator which consists of two linear oscillators having different stiffnesses for each half cycle,

$$m\ddot{x} + c\dot{x} + (k_1, k_2)x = F_0 \sin \omega t, \qquad (2)$$

where k_1, k_2 are the stiffnesses for $x > 0$ and $x < 0$ respectively. The equation is solved numerically for different spring ratios and, as expected, harmonic and subharmonic resonances appeared in the response. A comparison between the response and experimental results of a reduced-scale model showed good agreement in the main phenomenon.

Choi and Lou (1991) [6] have investigated the behaviour of an articulated offshore platform. They modeled it as an upright pendulum having one degree of freedom, with linear springs at the top having different stiffnesses for positive and negative displacements (bilinear oscillator). The equation of motion is simplified by expanding nonlinear terms into a power series and retaining only the first two terms. They assumed that the combined drag and inertia moment is a harmonic function. The discontinuity in the stiffness is assumed to be small, and thus replaced by an equivalent continuous function using a least-squares method to get the following Duffing equation

$$I\ddot{\theta} + c\dot{\theta} + k_1\theta + k_2\theta^2 + k_3\theta^3 = M_0 \cos \omega t, \qquad (3)$$

where k_1, k_2, k_3 are spring constants depending on buoyancy, gravity and the mooring lines. The equation of motion is solved analytically and numerically, and stability analysis is performed. The analytical solution agrees very well with the numerical solution. The main results of their analysis are that as damping decreases, jump phenomena and higher subharmonics occur, and chaotic motion occurs only for large waves and near the first subharmonic (excitation frequency equals twice the fundamental frequency); the system is very sensitive to initial conditions.

Seller and Niedzwecki (1992) [7] investigated the response of a multi-articulated tower in planner motion (upright multi-pendulum) to account for the tower flexibility. The restoring moments (buoyancy and gravity) were taken as linear rotational springs between each link, although the authors say that nonlinear springs are more adequate for this model. Each link is assumed to have a different cross section and density. The equations of motion are derived using Lagrange's equations, in which the generalized coordinates are the angular deflections of each link. The equations in matrix form are

$$[M]\{\ddot{\theta}\} + [K]\{\theta\} = [Q], \qquad (4)$$

where $[M]$ is a mass matrix that includes the actual mass of the link and added mass terms, while the stiffness matrix $[K]$ includes buoyancy and gravity effects. Damping and drag forces are not included in the model. The homogeneous equations for a tri-articulated tower are numerically solved to study the effects of different parameters, such as link length, material density and spring stiffness, on the natural frequency of the system.

Gotlib et al. (1992) [8] analyzed the nonlinear response of a single degree of freedom articulated tower. In the derivation of the equation, the expressions for the buoyancy moment arm, added mass term, and drag and inertia moments are evaluated along the stationary upright tower position and not at the instantaneous position of the tower. The governing equation is of the form

$$\ddot{\theta} + \gamma\dot{\theta} + R(\theta) = M(\dot{\theta}, t), \qquad (5)$$

where $R(\theta) = \alpha \sin\theta$ and α is linear function of buoyancy and gravity, $M(\dot{\theta}, t)$ is the drag moment. Approximated harmonic and subharmonic solutions are derived using a finite Fourier series expansion, and stability

analysis is performed by a Lyapunov function approach. The solution shows a jump phenomenon in primary and the secondary resonances.

Random Loading

Muhuri and Gupta (1983) [9] investigated the stochastic stability of a buoyant platform. They used a linear single degree of freedom model as follows

$$\ddot{x} + 2c\dot{x} + (1 + G(t))x = 0, \qquad (6)$$

where x is the displacement, c is the damping coefficient and $G(t)$ is a stochastic time-dependent function due to buoyancy. It is assumed that $G(t)$ is a narrow-band random process with zero-mean. A criterion for the mean square stability is obtained from which the following results are found: for $c > 1$ the system is always stable, and for $0 < c < 1$ there are regions of stability and instability.

Datta and Jain (1990) [10] investigated the response of an articulated tower to random wave and wind forces. In the derivation of the single degree of freedom equation of motion the tower is discretized into n elements having appropriate masses, volumes and areas lumped at the nodes, and there is viscous damping. The equation of motion is,

$$I(1 + \beta(t))\ddot{\theta} + c\dot{\theta} + R(1 + \nu(t))\theta = F(t), \qquad (7)$$

where $I\beta(t)$ is the time varying added mass term, $R\nu(t)$ is time varying buoyancy moment and $F(t)$ is the random force due to wave and wind. The Pierson-Moskowitz spectrum is assumed for the wave height and Davenport's spectrum assumed for the wind velocity. The equation is solved in the frequency domain using an iterative method, which requires that the deflection angle $\theta(t)$ and the forcing function $F(t)$ be decomposed into Fourier series: The coefficient of the *sin* and *cos* are then found iteratively. From their parametric study, they concluded the following:

1. Nonlinearities such as large displacements and drag force do not influence the response when only wind force is considered.
2. The random wind forces result in higher responses than do wave forces.
3. The r.m.s. response due only to wind forces varies in a linear fashion with the mean wind velocity.

In a later paper, Jain and Datta (1991) [11] used the same equation and the same method of solution to investigate the response due to random wave and current loading. The wave loadings (drag, inertia and buoyancy) are evaluated via numerical integration. The following results were obtained from the parametric study,

1. The dynamic response is very small since its fundamental frequency is well below the wave's fundamental frequency.
2. Nonlinear effects (drag force, variable buoyancy) have considerable influence on the response.
3. Current velocity has a large influence on the response.

Hanna et al. (1983) [12] analyzed the nonlinear dynamics of a guyed tower platform. The tower is represented by a lumped parameter model consisting of discrete masses. Each mass has three degrees of freedom, two translations and one rotation about the vertical axis. The external forces on the structure are approximated by concentrated forces and torques at the nodal points. The equation of motion is

$$[M]\{\ddot{u}\} + [C]\{\dot{u}\} + [K(u)]\{u\} = \{P(t, u, \dot{u})\}, \qquad (8)$$

where $[M]$ is the total mass matrix including added mass terms, $[C]$ is the structural damping matrix assumed to be proportional to the mass matrix and $[K(u)]$ is the total nonlinear stiffness matrix that includes mooring lines effects, soil stiffness and geometric stiffness. $\{P(t, u, \dot{u})\}$ is the nonlinear dynamic load vector due to wave, current and wind. The equation is then solved using normal mode superposition and the response is calculated at each time step. This method is good only if the nonlinearities are not large. Deterministic and random loading are considered. The solution shows insignificant flexure modes while the torsional one has a noticeable effect on the deck rotational response.

Kanegaonkar and Haldar (1988) [13] investigated the nonlinear random vibration of a guyed tower. They included nonlinearities due to guylines stiffnesses, geometry, load and material. The simplified planner equation of motion is

$$I\ddot{\theta} + c\dot{\theta} + K\theta + k_1\theta^3 = M(t), \qquad (9)$$

where K is a spring constant depending on buoyancy, gravity and guyline horizontal stiffness, and k_1 is a constant depending on the guyline vertical stiffness. $M(t)$ is the random wave loading. The equation is then solved numerically where the wave height is defined by the Pierson-Moskowitz spectrum. It was seen that the response is non-Gaussian for significant wave heights greater than 5 m.

Gerber and Engelbrecht (1993) investigated the response of an articulated mooring tower to irregular seas. It is an extension of earlier work done by Thompson et al. (1984) [5]. The tower is modeled as a bilinear oscillator, that is, a linear oscillator with different stiffnesses for positive and negative deflections,

$$m\ddot{x} + c\dot{x} + (k_1, k_2)x = F(t). \qquad (10)$$

The random forcing function $F(t)$ is assumed to be the sum of a large number of harmonic components, each in different frequency, a procedure similar to that proposed by Borgman (1969) [14]. The equation is then solved analytically since it is linear for each half cycle. The solution is obtained for different cases; linear oscillator (both stiffnesses are the same), bilinear oscillator, and for the case of impact oscillator (a rigid cable) in which oscillation can occur only in one half of the cycle. For future study they suggest to include nonlinear stiffness and/or using a different spectrum to describe the wave height.

Problem Definition

In this paper, the response of an articulated tower submerged in the ocean is investigated. The nonlinear differential equation of motion is derived, including nonlinearities due to geometry, coulomb damping, drag force, added mass buoyancy. All forces/moments are evaluated analytically and explicitly at the instantaneous position of the tower and, therefore, they are time-dependent and highly nonlinear. The equation is then numerically solved using 'ACSL' - Advanced Continuous Simulation Language [15], a powerful software language for deterministic and random wave loading using the Pierson-Moskowitz wave height spectrum. A harmonic and subharmonic solutions for deterministic wave heights are obtained. The response to random wave heights for different significant wave heights is investigated, the influence of coulomb damping on the response is analyzed, and chaotic regimes of behavior are identified.

The distinctions between this study and the literature with which we are aware are that,

1. A sound and exact derivation of the nonlinear equation of motion is provided.
2. All terms in the equation of motion are analytically derived.
3. Coulomb friction in the tower hinge is added.
4. Usage of 'ACSL' for the numerical solution provides an easy way to modify parameters and perform a sensitivity study.

PROBLEM DESCRIPTION

A schematic of the structure is shown in Fig. 1. It consists of a tower submerged in a fluid having a concentrated mass at the top and one degree of freedom θ about the z axis. The tower is subjected to wave loading. Two coordinate systems are used; one fixed (x,y,z) and the second attached to the tower (x',y',z'). All forces/moment are derived in the fixed coordinate system, which means that the tower rectilinear velocity is resolved into x, y coordinates. The motion of the tower is assumed to be only in plane.

This problem has similarities to that of an inverted pendulum, but due to the presence of gravity waves, additional considerations are made :

1. Forces due to buoyancy and vertical wave velocity are summed and denoted as T_0.
2. Drag forces proportional to the square of the relative velocity between the fluid and the tower need to be considered.
3. Fluid inertia forces due to fluid acceleration are part of the loading environment.
4. Fluid added mass is directly included in the inertia forces.

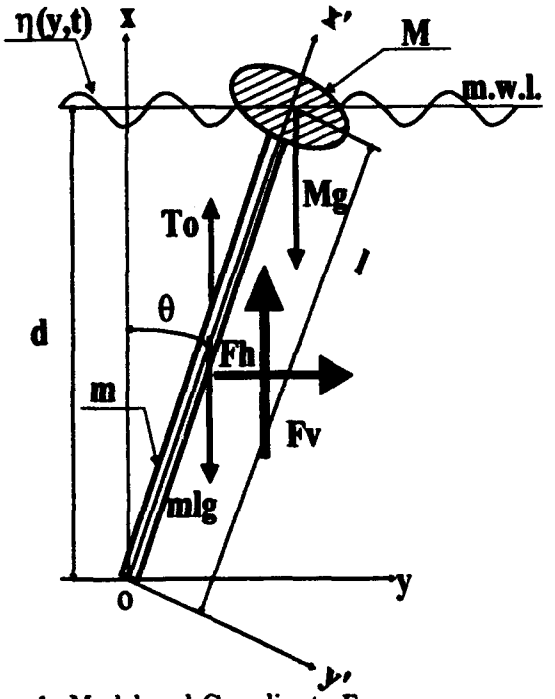

Figure 1: Model and Coordinate Frames

EQUATION OF MOTION

The equation of motion is derived using Newton's second law, setting all moments (external and inertial) acting on the tower about hinge to zero. We will find the equation of motion to be of the form,

$$J(g(\theta))\ddot{\theta} = \sum M\left(t, \omega, f(\theta), \dot{\theta}, sign(\dot{\theta})\right), \qquad (11)$$

where, $J(g(\theta))$ is the effective position dependent moment of inertia, $g(\theta)$, $f(\theta)$ are nonlinear functions of θ (trigonometric functions), ω is the wave frequency and M is the sum of all external moments that act on the tower. Certain assumptions have been made in deriving the nonlinear equation of motion. These are listed below.

Assumptions

1. The tower stiffness is infinite: $EI = \infty$.
2. The hinge has coulomb damping.
3. The tower has a uniform mass per unit length, m and is of length l and diameter D.
4. The tower is a smooth slender structure with uniform cross section.
5. The end mass M is considered to be concentrated at the end of the tower. (It has no volume.)
6. The tower length is greater than the fluid depth, but the dynamics is not limited to the case of M always being above the mean water level.
7. The structure is statically stable due to the buoyancy force.
8. The waves are linear having random height.
9. Morison's fluid force coefficients C_D and C_M are constant.
10. The center of mass (c.g.) of the tower is at its geometric center.
11. Currents, wind and wave slamming forces are not included.

Forces/Moments Acting on the Tower

Fig. 1 describes the external forces acting on the tower. These are :

1. T_0 is a vertical buoyancy force.
2. F_v, F_h are the vertical and horizontal fluid forces due to fluid drag and inertia.
3. Mg, mlg are the forces due gravity.

We next describe these forces and moments.

Inertia Moment

The inertia moment equals the total moment of inertia of the tower plus the fluid added mass term, multiplied by the angular acceleration of the tower,

$$M_I = (J_0 + Ml^2)\ddot{\theta} + M_{fl}, \qquad (12)$$

where J_0 is the moments of inertia of the tower about point 'o' and M_{fl} is the fluid added mass moment. Assuming that the fluid added mass due to the end mass is negligible, the total inertia moment is

$$M_I = J_{eff}\ddot{\theta}, \qquad (13)$$

where J_{eff}, the total moment of inertia, is

$$J_{fl} = \frac{1}{3}(ml + M)l^2 + \frac{1}{3}C_A\rho\pi\frac{D^2}{4}L^3(1 + tan^2\theta). \qquad (14)$$

where L is the projection, in the x direction, of the submerged part of the tower and is quantified later. C_A is the added mass coefficient which equals $C_A = C_M - 1$, where C_M is the inertia coefficient.

Moments due to Gravity, Buoyancy

The following moment is due to terms that do not depend on the fluid velocity, such as gravity and buoyancy forces,

$$M_g = T_0 l_b - (M + m\frac{l}{2})gl\sin\theta, \qquad (15)$$

where g is the gravitational constant, T_0 is the buoyancy force which is time dependent and l_b is its moment arm;

$$T_0 = \rho g\pi\frac{D^2}{4}L_s, \qquad (16)$$

where L_s, which is the length of the submerged paer of the tower, is

$$\mathrm{L}_s = \frac{d + \eta(y,t)}{\cos\theta} \qquad (17)$$

where d is the mean water level, ρ is the fluid density $\eta(y,t)$ is the wave height elevation evaluated at the mean water level,

$$\eta(\theta,t) = \frac{1}{2}H\cos(kd\tan\theta - \omega t + \varepsilon), \qquad (18)$$

H is the wave height, ω is the wave frequency, k is the wave number. The buoyant force acts at the center of mass of the submerged part of the tower l_b,

$$l_b = \frac{D^2}{16L_s}\tan^2\theta\cos\theta + \frac{1}{2}L_s + \frac{D^2}{32L_s}\tan^2\theta\sin\theta \quad (19)$$

Morison's Equation for Wave Force

In general, the fluid forces acting on a slender tower are of two types: drag and inertia. The drag force is proportional to the square of the relative velocity between the fluid and the tower, and the inertia force is proportional to the fluid acceleration. The drag and inertia forces per unit length are given by Morison's equation,

$$\mathbf{F}_{fl} = C_{dd} \mid \mathbf{U} - \mathbf{V} \mid (\mathbf{U} - \mathbf{V}) + C_{mm}\dot{\mathbf{U}}, \quad (20)$$

where,

$$\begin{aligned} C_{dd} &= C_D\rho\frac{D}{2} \\ C_{mm} &= C_M\rho\pi\frac{D^2}{4}, \end{aligned} \quad (21)$$

$\mathbf{F}_{fl}$ is the fluid force per unit length, $\mathbf{V}$ is the tower absolute velocity and $\mathbf{U}$ is the fluid absolute velocity evaluated at the instantanuouse position of the tower. The moments due to the fluid velocity and acceleration are as follows. The inertia moments are

$$\begin{aligned} M_{Ih} &= C_{mm}\int_0^L \dot{u}x dx \\ M_{Iv} &= C_{mm}\int_0^L \dot{w}x\tan\theta dx, \end{aligned} \quad (22)$$

and the drag moments,

$$\begin{aligned} M_{Dh} &= C_{dd}\int_0^L \mid u - v_y \mid (u - v_y)x dx \quad (23) \\ M_{Dv} &= C_{dd}\int_0^L \mid w - v_x \mid (w - v_x)x\tan\theta dx. \end{aligned}$$

where M_{Ih}, M_{Iv} are the inertia moments due to horizontal and vertical accelerations, respectively and M_{Dh}, M_{Dv} are the drag moments due to horizontal and vertical relative velocities, respectively. L, which is the upper limit of the integral, depends on the angle θ as follows :

$$L = \begin{cases} l\cos\theta & \text{if } d > l\cos\theta \\ d & \text{if } d < l\cos\theta. \end{cases} \quad (24)$$

This means that the moments are calculated only for the submerged part of the tower. The integrals in equations (22) and (23) are evaluated analytically using the symbolic software 'MAPLE'.

When solving the equation of motion numerically, the sign of the relative velocities and of $(d - l\cos\theta)$ are checked in each time interval. This is done to set the correct direction of the drag moments and the limits of integration, respectively.

Damping Moment

The tower hinge is assumed to dissipate energy via coulumb friction. In this section the damping moment is evaluated. The general form of the friction force is

$$F_{fr} = N\mu[sgn(\dot{\theta})], \quad (25)$$

where, μ is the friction coefficient, and N, the normal force, is

$$N = \sum F_x\cos\theta + \sum F_y\sin\theta, \quad (26)$$

where $\sum F_x$, $\sum F_y$ are the total forces in the x, y directions, respectively. These forces are due to gravity, buoyancy and fluid drag and inertia. If we assume a hinge radius R_h, then the damping moment is

$$\begin{aligned} M_{fr} &= \left(\sum F_x\cos\theta + \sum F_y\sin\theta\right) \cdot \\ &\quad R_h\mu[sgn(\dot{\theta})] \end{aligned} \quad (27)$$

Finally, adding all the external moments, equations (15), (22), (23), (27), and setting them equal to the total inertia moment, equation (13), yields the governing nonlinear differential equation of motion,

$$J_{eff}\ddot{\theta} = -M_{fr} - M_g + M_{Ih} - M_{Iv} + M_{Dh} - M_{Dv}. \quad (28)$$

Both sides of this equation are a nonlinear functions of θ, $\dot{\theta}$, t and ω.

NUMERICAL SOLUTION

The numerical solution for the nonlinear differential equation (28) was performed using 'ACSL' and the analyses of the results was performed using 'MATLAB'. The 'ACSL' code written for this application is available upon request. In order to build confidence in the solution, some test cases have been solved using the following physical parameters :

Tower properties

1. l - Length of the tower = 400 (m)
2. D - Tower diameter = 15 (m)
3. M - End mass = $2.5 * 10^5$ (Kg)
4. m - Tower mass per unit length = $2 * 10^3$ ($\frac{Kg}{m}$)

5. μ - Friction coefficient = 0.1-0.4

6. R_h - Hinge radius = 1.5 (m)

Fluid properties

1. d - Mean water level = 350 (m)

2. C_D - Drag coefficient =0.6 - 1.0

3. C_M - Inertia Coefficient =1.5

4. ρ - Water density = 1025 $(\frac{Kg}{m^3})$

5. ω - Wave frequency = 0.2 - 1.0 $(\frac{rad}{sec})$

Response for Deterministic Wave Heights

In this section the response of the tower to deterministic wave heights is established. Free vibration and stability analyses are performed.

First, the natural frequency of the tower is found as if it was an upright pendulum subjected to a constant tension force T_0 and gravitational force M_g. Fig. 2 shows the tower response to an impulse for $C_D = 0$ and $H = 0$ in the time and frequency domain. The response is harmonic in the tower natural frequency $\Omega_n = 0.026$ (Hz), and it agrees with the calculation for the natural frequency of a pendulum :

$$\Omega_n = \frac{1}{2\pi}\sqrt{\frac{T_0 l_b - (0.5ml + M)gl}{J_{eff}}}. \qquad (29)$$

Fig 3 (a,b) shows the same but for $\mu = 0$ and $C_D = 1$, the decay here is not linear since the drag force is propotional to the velocity squared. Fig 3 (c,d) shows the free vibration with frictional damping, $\mu = 0.1$, in the time and frequency domain. Here the amplitude decays linearly with time as expected when coulomb damping is present. From the figure we can evaluate the equivalent damping ratio for $C_D = 0$ to be $\xi = 0.02$. Since the damping is nonlinear, the 'natural frequency' and its multipliers are seen in the figure.

Fig. 4 shows the response in the time domain and frequency domain for $H = 1$ (m) and wave loading frequency $\omega = 0.064$ (Hz). Figures (a, b) are with $\mu = 0$ and (c, d) are with $\mu = 0.4$. In the frequency domain, the tower 'natural frequency' and the wave natural frequency are clearly seen. It can be seen that the friction has a damping and stabilizing effect on the system.

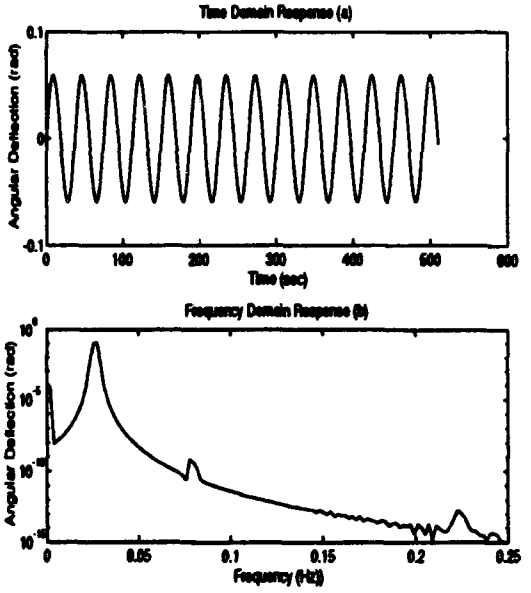

Figure 2: Tower Natural Frequency, $C_D = 0$

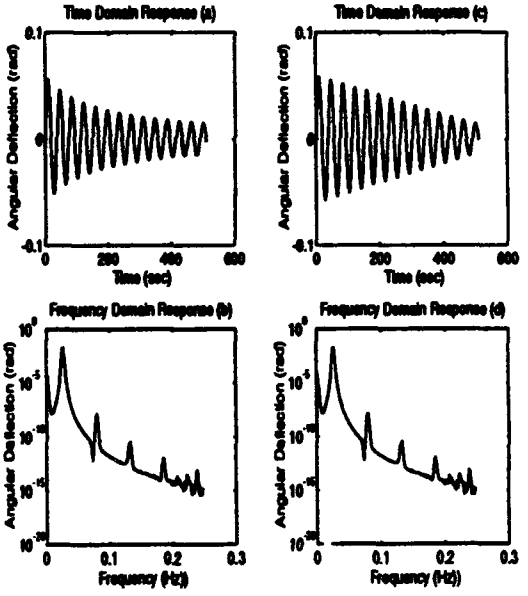

Figure 3: Tower Free Vibration with Damping, (a, b) $\mu = 0.1$, (c, d) $C_D = 1$

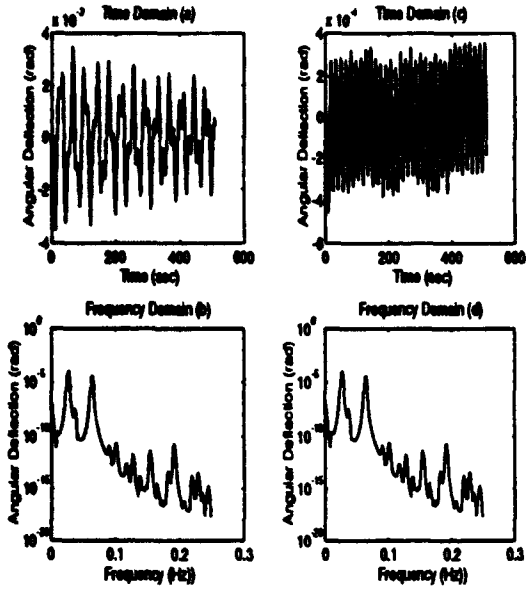

Figure 4: Tower response to wave excitation, Time and Frequency Domain, $H = 1\ (m)$

Since this is a nonlinear system, its response to harmonic excitation at the system's 'natural frequency' or its multipliers can be multivalued, indicating the occurrence of a 'jump'. Fig. 5 shows the tower response to harmonic wave excitation at $\omega = \Omega_n$ (harmonic solution) with and without damping. If the system was linear, such loading would have caused resonance instability. But since the system is nonlinear, an amplitude change (beating) can be seen Fig. 5 (a), indicating that 'jumps' occur from one amplitude to the other (Wilson [16] pp. 147). It can also be seen that although the excitation frequency is constant, the frequency response is not Fig. 5 (b). Again the reason is the nonlinear system characteristics. From the response with friction (figures (c, d)) we see that the response is not smaller since it is unstable, but the ratio between the large and small amplitude of the beating gets smaller.

Fig. 6 shows the response due to harmonic wave excitation at twice the system 'natural frequency' (subharmonic solution), with (c, d) and without friction (a, b). We can see the beating phenomenon, and from the frequency domain we see that the response consists of the 'natural frequency'and it multipliers. This is due to the nonlinear nature of the system.

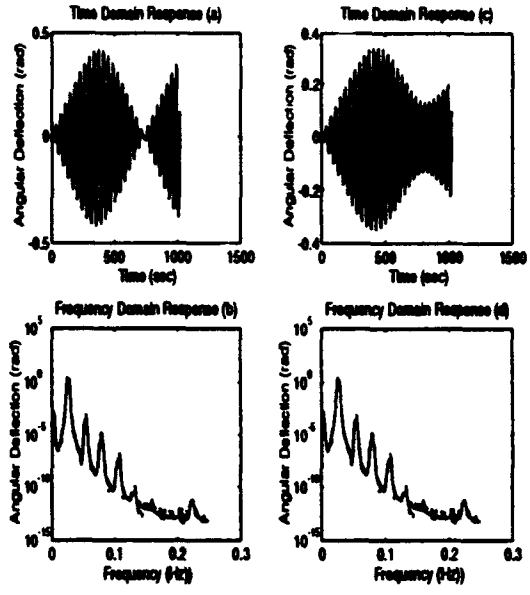

Figure 5: Tower response to harmonic wave excitation at the 'Natural Frequency' - Beating Phenomenon

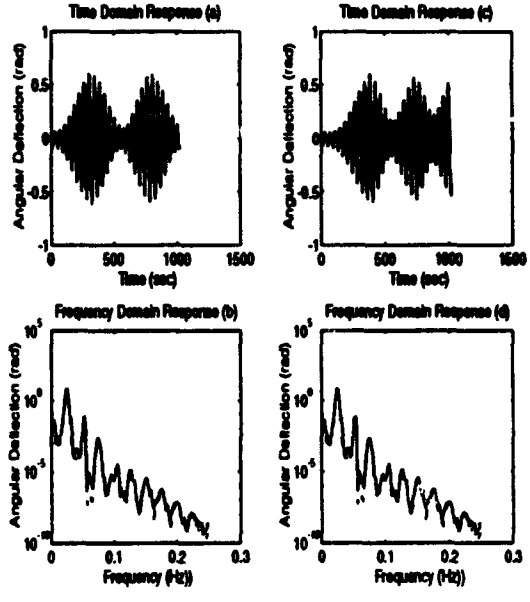

Figure 6: Tower response to sub-harmonic wave excitation at twice 'Natural Frequency'

The direction of the drag force is opposite to the direction of the relative velocity between the tower and the wave. If the direction of the relative velocity is the same as the tower velocity, the drag will always stabilize the system. The reason is that the drag moment will always be opposite to the direction of the deflection angle θ. But if the relative velocity direction is opposite to tower velocity, the drag moment can cause instability. For zero wave velocity the drag force always stabilizes the system, as can be seen from Fig. 3. Fig. 7 describes the horizontal and vertical components of the relative velocity and tower velocity.

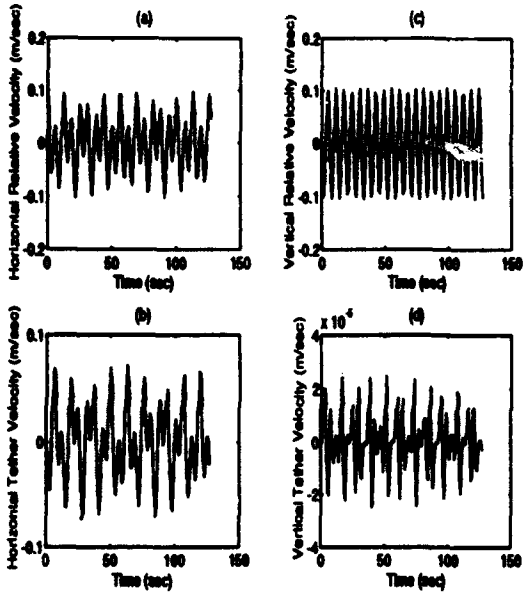

Figure 7: Relative and Tower Velocities - (a, c) Horizontal and (b, d) Vertical

Chaotic Response

Because of the nonlinear characteristics of the system, the governing differential equation of motion, chaotic motion can occure under certain conditions. Fig. 8 shows the response of the tower to a harmonic wave excitation at a frequency $\omega = 0.95\Omega_n$. We see that the response 'jumps' between two stable equilibrium states. This phenomenon can imply a chaotic system.

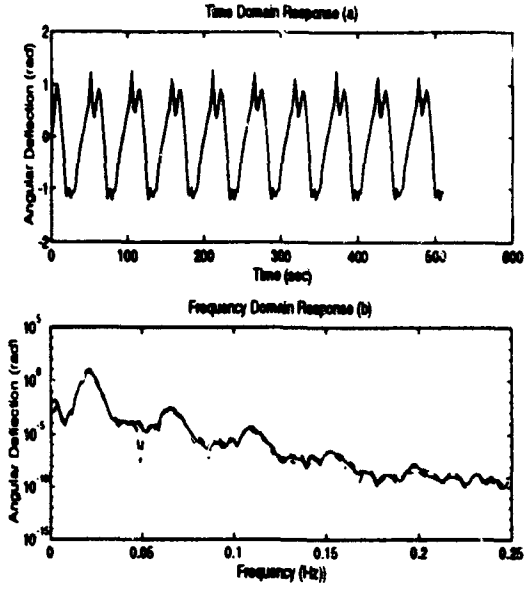

Figure 8: Tower response to harmonic wave excitation at the 'Natural Frequency', $C_D = 0.6$

Moon [17] provides several ways to identify chaotic vibrations. We next use three ways to prove that the system under consideration is chaotic. Fig. 9 describes the response of the tower to a harmonic wave excitation having a frequency of $\omega = 0.09\ (Hz)$. Fig 9 (a, b) shows the response in the time and frequency domains and the phase-plane trajectory (c). From the time history it is clearly seen that the system jumps between two stable equilibrium states. The frequency domain shows multiharmonic energy although the system has one degree of freedom; another indicator of chaos. Finally, from the phase-plane trajectory we see that the orbits never close or repeat. Thus, we conclude that this model has the characteristics of a chaotic system. This chaotic phenomenon appeared only when the wave height was larger than 10 (m).

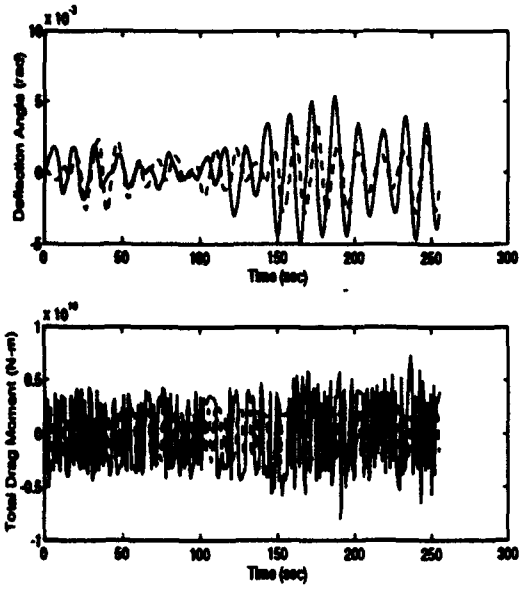

Figure 11: Tower Response - Deflection angle and Total Drag Moment for $H_s = 9$ (m) and $C_D = 0.6$ (dashed line) and 1 (solid line).

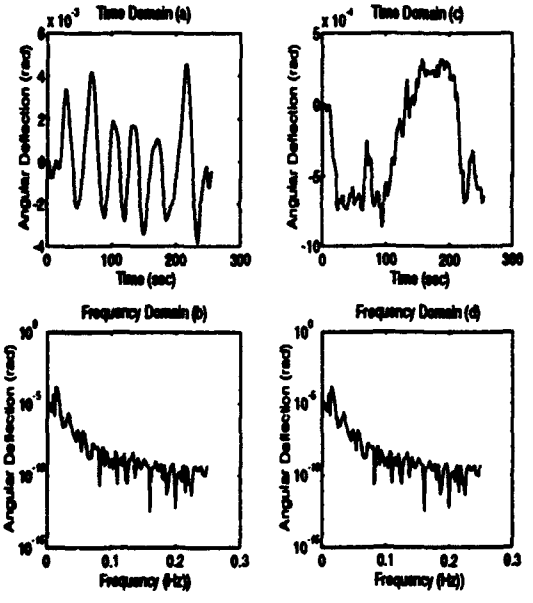

Figure 12: Tower Response - Deflection angle - Time and Frequency Domain for $H_s = 9$ (m) and $C_D = 1$, (a, b) $\mu = 0$ and (c, d) $\mu = 0.4$

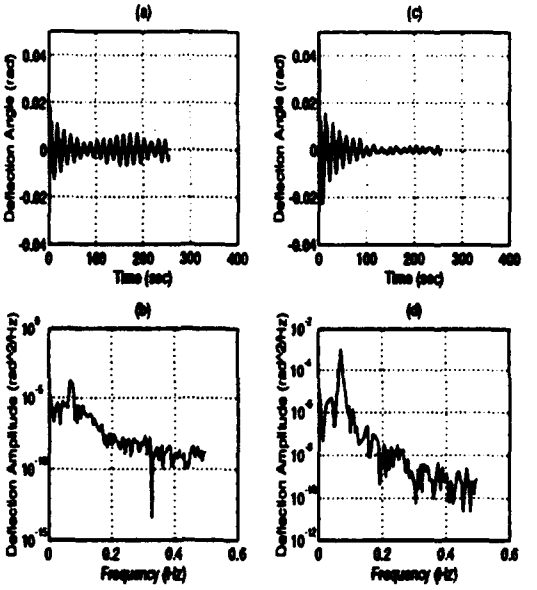

Figure 13: Tower Response - (a, b) Deflection angle $\theta(t = 0) = 0.05$ (rad) and (c, d) $\dot{\theta}(t = 0) = 0.01$ (rad/sec).

DISCUSSION AND SUMMARY

The nonlinear differential equation of motion for an articulated tower submerged in the ocean is derived. Geometric as well as force nonlinearities are included in the derivation. The wave velocities and accelerations are determined at the instantaneous position of the tower, a fact that added to the nonlinearities of the equation. The equation is solved numerically using 'ACSL' for deterministic and random wave loading.

The response of the tower to harmonic wave excitation at its 'natural frequency' and at twice its 'natural frequency' demonstrates beating, where the amplitude varies between two extremes. This beating is due to the nonlinear behaviour of the system. Coulomb damping reduces the beating phenomenon and the response amplitude, so it has a stabilizing effect on the system. When the system is excited at an arbitrary frequency, and the wave height is greater than about 10 (m), the response 'jumps' between two stable equilibria, exhibiting chaotic behaviour.

To solve the equation for random wave loading, the Pierson-Moskowitz spectrum that describes the wave height distribution was first transformed into a time history. The equation was solved for two significant wave heights. Again the response was periodic consisting of the fundamental tower frequency and its multipli-

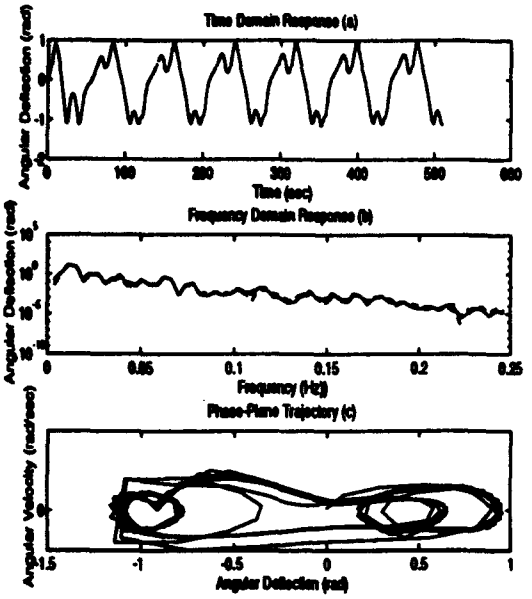

Figure 9: Tower response to a harmonic wave excitation, $\omega = 0.09\ (Hz)$ - Chaos

Random Wave Height

In this section the tower response to random wave height excitation is investigated. The wave height distribution is generally expressed in the form of a power spectral density. For a simulation of the response in the time domain, the Pierson-Moskowitz spectrum, which is assumed to describe the spectrum of the wave height, is transformed into a an infinite series of time-dependent harmonic functions. This is accomplished using a method by Borgman [14], described also in Wilson's book [16].

Response for Random Wave Height

In this section, the influance of different significant wave heights, drag coefficient , hinge friction and non-zero intial condition on the response is investigated.

Fig. 10 compares the tower response for $H_s = 9$ and 15 (m). Here we enlarged the buoyancy force so that the tower 'natural frequency' is $\Omega_n = 0.07\ (Hz)$ $= 0.44\ (rad/sec)$. It can be seen that the deflection angle for $H_s = 9\ (m)$ is of the same magnitude as for for $H_s = 15\ (m)$, although the later maximum wave height is four times larger then the former. The reason is that the natural frequency of the tower coinsides with where most of the spectral energy for $H_s = 9\ (m)$ is located. Since the lowest wave freqency is about $\omega =$ $0.2\ (rad/sec)$ articulated tower are designed to have a 'natural frequency' lower than that.

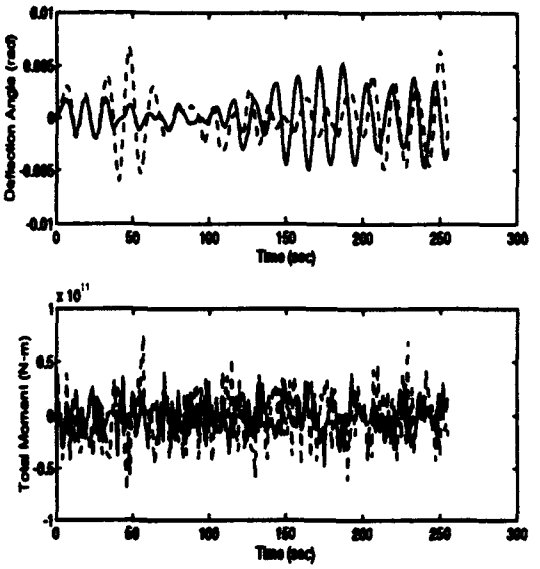

Figure 10: Tower Response - Deflection angle and Total Moment for $H_s = 15$ (dashed line) and 9 (solid line) (m)

A comparison of the tower response for different values of the drag coefficient are plotted in Fig. 11. This figure shows the deflection angle and the total drag moment, $M_d = M_{Dh} - M_{Dv}$, for $C_D = 0.6$ and 1, and $H_s = 9\ (m)$. It can be seen from the figure that the deflection angle and the drag moment are larger for $C_D = 1$, since the drag moment in the Morison equation is proportional to the drag coefficient. The results were similar for different significant wave heights.

The friction effect on the response is shown clearly in Fig. 12. Here the significant wave height is $H_s = 9$ and $C_D = 1$. It is seen that the response is much smaller and smoother due to the additional friction in the system.

The response for nonzero initial conditions is depicted in Fig. 13. The response for $\dot{\theta}(t = 0) = 0.01(rad/sec)$ (a, b), and $\theta(t = 0) = 0.05(rad)$ (c, d). The drag coefficient is $C_D = 0.6$ and $H_s = 9\ (m)$.

ers. For significant wave height of 9 (m), the response was larger than that for 15 (m), since in the former the tower 'natural frequency' coincides with the frequencies where most of the energy is located. The response with coulomb damping shows that friction stabilizes the system. Notice that in order to reduce stresses in the structure, the friction moment has to be low enough so that the tower can comply with the wave loading.

A more realistic model having two angular degrees of freedom is being analyzed at the present time. The response due to wave, current (colinear and non-colinear) and vortex shedding loading is investigated loading and results will be published in the near future.

Acknowledgment

This work is supported by the Office of Naval Research grant no. $N00014-93-1-0763$. The authors are grateful for this support and thank ONR and Program Manager Dr. T. Swean for his interest in our work.

References

[1] M.H. Patel. *Dynamics of Offshore Structures*. Butterworths, 1998.

[2] S.K. Chakrabarti and D.C. Cotter. Motion analysis of articulated tower. *Journal of the waterway, port, coastal and ocean division*, 105:281 – 292, 1979.

[3] S.K. Chakrabarti and D.C. Cotter. Transverse motion of articulated tower. *Journal of the waterway, port, coastal and ocean division*, 107:65 – 77, 1980.

[4] R.K. Jain and C.L Kirk. Dynamic response of a double articulated offshore loading structure to noncollinear waves and current. *Journal of Energy Resources Technology*, 103:41 – 47, 1981.

[5] J.M.T. Thompson, Bokaian A.R., and R. Ghaffai. Stochastic and chaotic motions of compliant offshore structures and articulated mooring towers. *Journal of Energy Resources Technology*, 106:191 – 198, 1984.

[6] H.S. Choi and Lou J.Y.K. Nonlinear behaviour of an articulated offshore loading platform. *Applied Ocean Research*, 12(2):63 – 74, 1991.

[7] L.L. Seller and Niedzwecki J.M. Response characteristics of multi-articulated offshore towers. *Ocean engineering*, 19(1):1 – 20, 1992.

[8] O. Gottlieb, C.S. Yim, and Hudspeth R.T. Analysis of nonlinear response of an articulated tower. *International Journal of Offshore and Polar Engineering*, 2(1):61 – 66, 1992.

[9] A.S. Muhuri, P.K.and Gupta. Stochastic stability of tethered buoyant platforms. *Ocean engineering*, 10(6):471 – 479, 1983.

[10] T.K. Datta and A.K. Jain. Response of articulated tower platforms to random wind and wave forces. *computer and structures*, 34(1):137 – 144, 1990.

[11] A.K. Jain and T.K. Datta. Nonlinear behavior of articulated tower in random sea. *journal of engineering for industry, trans. of ASME*, 113:238 – 240, 1991.

[12] Hanna S.Y., A. Mangiavacchi, and Suhendra R. Nonlinear dynamics analysis of guyed tower platforms. *Journal of Energy Resources Technology*, 105:205 – 211, 1983.

[13] H.B. Kanegaonkar and A. Haldar. Nonlinear random vibrations of compliant offshore platforms. *Symposium of Nonlinear Stochastic Dynamic Engineering Systems*, pages 351 – 360, 1987.

[14] E.L. Borgman. Ocean wave simulation for engineering design. *Journal of the waterways and harbors division*, 95:557–583, 1969.

[15] *ACSL - Advanced Continuous Simulation Language*. Mitchell and Gauthier Associate (MGA), 1993.

[16] J.F. Wilson. *Dynamics of Offshore Structures*. John Wiley and Sons, 1984.

[17] Francis C. Moon. *Chaotic and Factual Dynamics an introduction for applied scientists and engineers*. John Wiley and Sons, 1992.

The van Kampen expansion for the Fokker-Planck equation of a Duffing oscillator

E. Weinstein*and H. Benaroya†

January 23, 1994

*Senior Research Engineer, Galaxy Scientific Corporation, Pleasantville, N.J.
†Associate Professor, Rutgers University, New Brunswick, NJ

Abstract

In Rodríguez and Van Kampen's 1976 paper [1], a method of extracting information from the Fokker-Planck equation without having to solve the equation is outlined. The Fokker-Planck equation for a Duffing oscillator excited by white noise is expanded about the intensity of the forcing function, α. This expansion is carried to order $\mathcal{O}(\alpha^{\frac{1}{2}})$. However no studies are made of the effects of the order of the expansion, variation of the parameters, nor are comparisons made to experimental results. In this paper, the expansion is carried to a higher order, $\mathcal{O}(\alpha^{\frac{3}{2}})$, results are presented and compared to Monte-Carlo experiments using both white and colored noise, and parametric studies are performed on the intensity of the forcing function and the damping coefficient. It is found that the expansion method works well for the case of white noise and for colored noise where the correlation time is less than 0.1 seconds, but fails to give certain details. It is also found that the system behaves as expected when the parameters are varied.

List of Figures

1 Introduction

The Fokker-Planck equation has proven to be a useful tool in the analysis of simple nonlinear oscillators excited by stochastic processes. As a partial differential equation for the probability density function of the response, its solution completely defines the solution of the problem. It can be used to analyze both a single oscillator of the form

$$m\ddot{x} + \gamma(\dot{x}, x)\dot{x} + k(\dot{x}, x)x = \mathcal{F}(t), \tag{1}$$

or a system of multiple, linked, oscillators of the form

$$\mathbf{M}\underline{\ddot{x}} + \mathbf{\Gamma}(\dot{x}, x)\underline{\dot{x}} + \mathbf{K}(\dot{x}, x)\underline{x} = \underline{\mathcal{F}}(t). \tag{2}$$

In many cases, a physical system can be approximated by such a system of nonlinear oscillators. The systems so modeled can range from a Brownian particle to structures excited by von Karman vortex shedding. Such modeling can be useful for gaining insight into a problem and the way in which the system will behave as certain parameters are varied.

Once one has decided on the system of oscillators to be used to represent the physical system, the derivation of the Fokker-Planck equation is relatively straightforward, although tedious. The problem remains of how to solve it for the probability distribution of the response. In a very few cases, the Fokker-Planck equation can be solved analytically, but in most cases no analytical solution exists and one usually must resort to a numerical solution. However this can be computationally intensive and gives little insight into the larger problem.

In their 1976 paper, Rodríguez and van Kampen outline a method of dealing with the case of an oscillator excited by weak Gaussian white noise. The Fokker-Planck equation of the system is expanded about the intensity, α, of the driving function. This expansion is carried to the order $\mathcal{O}(\alpha^{\frac{1}{2}})$. In this way the statistics of the fluctuations can be obtained directly. This method shows promise as a way to use the Fokker-Planck equation to gain useful information about a wider variety of systems than was possible before.

This is the first of a planned series of papers exploring the usefullness of this method. As in the original paper, the method is applied to the problem of a Duffing oscillator excited by Gaussian white noise. The inherent assumptions of the method are explained here in detail. The expansion is carried both to the same order as in the original paper, and to order $\mathcal{O}(\alpha^{\frac{3}{2}})$. Results are presented and compared to a Monte Carlo experiment. Parametric studies were done on the parameter of expansion as well as on the other important variable in the expansion: the coefficient of damping.

2 Expansion of the Fokker Planck Equation for a Duffing Oscillator

As in the Rodríguez and van Kampen paper, heretofore called the "Original paper," the system under consideration is a Duffing oscillator in a heat bath. The equation of motion can be written simply as

$$\ddot{x} + \gamma\dot{x} + x + x^3 = F(t). \tag{3}$$

$F(t)$ is a Langevin force [2] and is assumed to be Gaussian white noise with the following properties:

$$\begin{aligned} < F(t) > &= 0 \\ < F(t)F(t') > &= 2\alpha\delta(t - t'). \end{aligned} \tag{4}$$

It is assumed that the immersion of the oscillator takes place at time $t = 0$ and that the system is not necessarily at rest.

$f(x, v; t)$ is defined as the joint probability density function of x and $v = \dot{x}$ at time t. This leads to the following Fokker-Planck equation (see Ochi [3] for a complete derivation):

$$\frac{\partial f}{\partial t} + v\frac{\partial f}{\partial x} - (x + x^3)\frac{\partial f}{\partial v} = \gamma\frac{\partial}{\partial v}(vf) + \alpha\frac{\partial^2 f}{\partial v^2}. \tag{5}$$

As $f(x, v; t)$ is a complete description of the system response, solution of the above differential equation for f constitutes a solution of the problem.

The same assumptions on the sizes of the variables in Eq. 5 are made as in the original paper: namely that γ, x and v will all be assumed to be of the same order of magnitude, and much larger than α.

In the original paper, it is assumed that the system response due to the forcing function will be small as compared to the deterministic response due to the initial conditions. Therefore, the total response can be viewed as random fluctuations, Δ_x and Δ_v, superimposed onto the deterministic response to the initial conditions. Furthermore, the random fluctuations will be of order $\alpha^{\frac{1}{2}}$. Because the only source of energy is $F(t)$, the power input to the system is proportional to α. But if the system is to remain stable, then the viscous power dissipation of the fluctuations caused by the influence of $F(t)$ must be of equal average magnitude as the power input. Therefore $\mathcal{O}(\gamma\ \eta^2) = \mathcal{O}(\alpha)$ or $\mathcal{O}(\eta) = \mathcal{O}(\alpha^{\frac{1}{2}})$. But the kinetic energy of the fluctuations must be of the same order as the potential energy. So $\mathcal{O}(\zeta^2) = \mathcal{O}(\eta^2)$ which implies that $\mathcal{O}(\zeta) = \mathcal{O}(\alpha^{\frac{1}{2}})$. Therefore, $\Delta_x = \alpha^{\frac{1}{2}}\zeta$ and $\Delta_v = \alpha^{\frac{1}{2}}\eta$ where ζ and η are of order unity. Therefore the following substitutions are made:

$$x = \phi(t) + \alpha^{\frac{1}{2}}\zeta, \tag{6}$$

$$v = \psi(t) + \alpha^{\frac{1}{2}}\eta. \tag{7}$$

In the original paper, the initial conditions, $\phi(0)$, and $\psi(0)$, are assumed to be zero and the expansion carried through to give the time derivatives of the second order moments. In Weinstein and Benaroya, [4], the expansion is explained in somewhat greater detail and the fourth order moments are also derived. In total the following eight equations are derived:

$$\frac{d}{dt} < \zeta^2 >= 2 < \zeta\eta > \tag{8}$$

$$\frac{d}{dt} < \zeta\eta >=< \eta^2 > - < \zeta^2 > -\gamma < \zeta\eta > -\alpha < \zeta^4 > + \mathcal{O}(\alpha^{\frac{3}{2}}) \tag{9}$$

$$\frac{d}{dt} < \eta^2 >= -2 < \zeta\eta > -2\gamma < \eta^2 > -2\alpha < \zeta^3\eta > +2 + \mathcal{O}(\alpha^{\frac{3}{2}}) \tag{10}$$

$$\frac{d}{dt} < \zeta^4 >= 4 < \zeta^3\eta > \tag{11}$$

$$\frac{d}{dt} < \zeta^3\eta >= 3 < \zeta^2\eta^2 > - < \zeta^3\eta > - < \zeta^4 > + \mathcal{O}(\alpha^{\frac{3}{2}}) \tag{12}$$

$$\frac{d}{dt} < \zeta^2\eta^2 >= 2 < \zeta\eta^3 > -2\gamma < \zeta^2\eta^2 > -2 < \zeta^3\eta > +2 < \zeta^2 > + \mathcal{O}(\alpha^{\frac{3}{2}}) \tag{13}$$

$$\frac{d}{dt} < \zeta\eta^3 >=< \eta^4 > -3\gamma < \zeta\eta^3 > -3 < \zeta^2\eta^2 > +6 < \zeta\eta > + \mathcal{O}(\alpha^{\frac{3}{2}}) \tag{14}$$

$$\frac{d}{dt} < \eta^4 >= -4\gamma < \eta^4 > -4 < \zeta\eta^3 > +12 < \eta^2 > + \mathcal{O}(\alpha^{\frac{3}{2}}). \tag{15}$$

If it is the stationary behavior that is of interest, then one can obtain the equilibrium values of these quantities by setting each time derivative equal to zero. Then the equilibrium, or stationary, states of each expectation can be found by simple linear algebra:

$$\begin{aligned} <\zeta^2>_{eq} &= \frac{1}{\gamma} - \alpha\frac{3}{\gamma^2} & <\zeta^3\eta>_{eq} &= 0 + \mathcal{O}(\alpha^{\frac{3}{2}}) \\ <\zeta\eta>_{eq} &= 0 & <\zeta^2\eta^2>_{eq} &= \frac{1}{\gamma^2} + \mathcal{O}(\alpha^{\frac{3}{2}}) \\ <\eta^2>_{eq} &= \frac{1}{\gamma} + \mathcal{O}(\alpha^{\frac{1}{2}}) & <\zeta\eta^3>_{eq} &= 0 + \mathcal{O}(\alpha^{\frac{3}{2}}) \\ <\zeta^4>_{eq} &= \frac{3}{\gamma^2} + \mathcal{O}(\alpha^{\frac{3}{2}}) & <\eta^4>_{eq} &= \frac{3}{\gamma^2} + \mathcal{O}(\alpha^{\frac{3}{2}}). \end{aligned}$$

If one is interested in the transient response of the system, and if one can accept a solution of order $\mathcal{O}(\alpha^{\frac{1}{2}})$, then one can obtain it analytically. Equations 8 to 10 can be written in matrix form as follows:

$$\frac{d}{dt}\begin{pmatrix} <<\zeta^2>> \\ <<\zeta\eta>> \\ <<\eta^2>> \end{pmatrix} = \mathcal{M}_3 \begin{pmatrix} <<\zeta^2>> \\ <<\zeta\eta>> \\ <<\eta^2>> \end{pmatrix} + \begin{pmatrix} 0 \\ 0 \\ 2 \end{pmatrix} + \mathcal{O}(\alpha^{\frac{3}{2}})$$

$$\text{where} \quad \mathcal{M}_3 = \begin{Bmatrix} 0 & 2 & 0 \\ -1 & -\gamma & 1 \\ 0 & -2 & -2\gamma \end{Bmatrix}. \tag{16}$$

This can be solved through standard techniques to yield the time evolving variances. It must be noted that by solving only these three equations, the order of the solution has been reduced to $\mathcal{O}(\alpha^{\frac{1}{2}})$:

$$\begin{pmatrix} <<\zeta^2>> \\ <<\zeta\eta>> \\ <<\eta^2>> \end{pmatrix} = \begin{Bmatrix} 1/\lambda_1 & -1/2\lambda_2 & -1/\lambda_3 \\ 1/2 & -1/4 & -1/4 \\ 1/\lambda_1 & -1/\lambda_2 & -1/2\lambda_3 \end{Bmatrix} \begin{pmatrix} e^{\lambda_1 t} \\ e^{\lambda_2 t} \\ e^{\lambda_3 t} \end{pmatrix} + \begin{pmatrix} 1/\gamma \\ 0 \\ 1/\gamma \end{pmatrix} \tag{17}$$

where

$$\begin{aligned} \lambda_1 &= -\gamma \\ \lambda_2 &= -\gamma + 2iw \\ \lambda_2 &= -\gamma - 2iw \\ \text{and} \quad w &= \sqrt{1 - \frac{1}{4}\gamma^2}. \end{aligned}$$

If one is interested in the transient response and desires a solution of order $\mathcal{O}(\alpha^{\frac{3}{2}})$, one could cast all of Equations 8 to 15 into a matrix equation of the form of Equation 16. This would yield a matrix of rank 8. To solve this analytically would require the analytical eigensolution of this rank 8 matrix. This is a difficult proposition at best with unclear practical need. Instead, for each particular set of parameters, γ and μ, a numerical matrix is obtained. The eigensolution is then obtained numerically and the results calculated. It should be noted that there is no theoretical loss of accuracy in solving the system of equations this way; only roundoff error degrades the accuracy of the solution.

Thus we have a method for obtaining in closed form the time evolving moments of the Duffing oscillator subjected to a white noise forcing function.

3 Results

The response of a Duffing oscillator with damping coefficient $\gamma = 1.0$ excited by white noise of intensity $\alpha = 0.1$, was calculated using Equation 17 and by solution of all of Equations 8 to 15. As a point of comparison, a Monte Carlo experiment simulating a Duffing oscillator with the same parameters was performed. This Monte Carlo experiment consisted of one thousand iterations of a fourth order Runge-Kutta integration of the following restatement of Equations 3:

$$\frac{d}{dt}x = v, \qquad \frac{d}{dt}v = \mathcal{F}(t) - v - x - x^3. \tag{18}$$

The results of the order $\mathcal{O}(\alpha^{\frac{1}{2}})$ analysis, the order $\mathcal{O}(\alpha^{\frac{3}{2}})$ analysis, and the Monte Carlo experiment are plotted in Figures 1 to 3.

Figure 1 shows the time evolution of $< \zeta^2 >$ as calculated by all three methods. The order $\mathcal{O}(\alpha^{\frac{1}{2}})$ analysis shows $< \zeta^2 >$ increasing monotonically to its steady state value of approximately one. The higher order analysis shows $< \zeta^2 >$ increasing in nearly monotonic fashion to its steady state value of about 0.75. However this curve does exhibit some overshoot at about 2.5 seconds. The results of the Monte Carlo analysis are quite close to those of the higher order analysis, reaching the same steady state value. The main difference between the two curves is the slightly greater rise time of the Monte Carlo results. The higher limit of the order $\mathcal{O}(\alpha^{\frac{1}{2}})$ analysis and the overshoot of the order $\mathcal{O}(\alpha^{\frac{3}{2}})$ analysis are artifacts of the expansion process. The higher order, $\mathcal{O}(\alpha^{\frac{3}{2}})$, time derivatives differ from the lower order, $\mathcal{O}(\alpha^{\frac{1}{2}})$, ones by the subtraction of $\alpha < \zeta^4 >$ in the case of $\frac{d}{dt} < \zeta\eta >$ and $2\alpha < \zeta^3\eta >$ in the case of $\frac{d}{dt} < \zeta^2 >$. However it can be seen from Figure 4 that $< \zeta^4 > \geq 0$ during the entire time span of interest and rises in magnitude quickly, and $< \zeta^3\eta >$ is greater than zero during the first half of the time span of interest where the second order moments are changing most rapidly. This would explain the slower rise in the magnitude of the order $\mathcal{O}(\alpha^{\frac{3}{2}})$ solutions than the order $\mathcal{O}(\alpha^{\frac{1}{2}})$ solutions. It also indicates that inclusion of the higher order terms serve to lower the overall value of the analytical results and that the omission thereof causes the higher overall values of the analytical methods than those of the Monte-Carlo methods. As one would expect, the higher order analyses consistently show more points of inflection than do the lower order analyses.

Figure 2 shows nearly identical curves for all methods. As in Figure 1, the order $\mathcal{O}(\alpha^{\frac{3}{2}})$ analysis shows more overshoot in one place than does the lower order analysis. Here this overshoot occurs at about four seconds, at the second local extreme. It is also noted that, only the order $\mathcal{O}(\alpha^{\frac{3}{2}})$ method accurately reflects the region where the Monte-Carlo curve is negative. The initial excursion of the Monte Carlo curve is not as great as that of the other two curves, although all three approach the x-axis as time increases.

Figure 3 Provides a qualitatively similar comparison of results with both analyses almost coincidental and again slightly greater in the transient region than the Monte Carlo experiment. All three curves approach a steady state value of approximately 1.

Figure 5 shows how the time evolution of $< \zeta^2 >$, as calculated by the order $\mathcal{O}(\alpha^{\frac{3}{2}})$ analysis, is affected by increasing γ. Figure 6 shows the same study for the Monte Carlo experiment. Figure 5 shows not only a decrease in the steady state values of $< \zeta^2 >$ with increasing values of γ, but also a smoothing of the curves. The decrease in the steady state values is also seen in the Monte Carlo curves. The cause of the decrease is a physical one: increased damping implies increased viscous energy dissipation which leads to smaller excursions of the oscillator. Comparison of Figures 5 and 6 shows that even when γ becomes large enough to violate

the order unity assumption, the analysis still gives reasonable results. In fact the agreement between results becomes better at higher values of γ. It can be seen that, even for $\gamma = 0.6$, the Monte Carlo curves are relatively smooth with the exception of the small scale "wiggles" inherent in Monte-Carlo analysis. This indicates that the multiple local maxima and minima, i.e., at 3, 5, 7, 9 seconds, in the analytical curves at $\gamma = 0.6$ are due to the low order of γ of the analysis. It was assumed at the beginning of the analysis that γ is of order unity. However it can be seen from these curves that the further γ is from this assumption, the worse the results of the analysis.

The behavior of the system as γ becomes small is further investigated in Figures 7 and 8. These curves show how, as γ goes from 0.4 to 0.3 the analysis breaks down completely. It was shown in Figures 5 and 6 that the $\gamma = 0.3$ analysis differed significantly from the Monte Carlo analysis in the transient region of 0 to 5 seconds, although its large time behaviour was accurate. Figures 7 and 8 show that as γ is made smaller, even the large time behaviour becomes unreasonable with $< \zeta^2 >$ becoming negative which is clearly impossible.

Figures 9 and 10 show how the time evolutions of $< \zeta^2 >$ are affected by increasing values of α. It can be seen in Figure 9 what happens as the assumption that α is small as compared to unity is violated. As is shown in Figure 9, the curve for $\alpha = 0.3$ exhibits oscillations that damp out slowly with time. As α becomes even larger, negative values for $< \zeta^2 >$ develop. However, since the average of a squared quantity cannot be negative, these results are spurious. The trend of the steady state value of $< \zeta^2 >$ decreasing with increasing values of α is common to both figures. This does not violate the basic assumption that ζ is of order unity when α is small. ζ does indeed remain of order *unity*; *it was not* assumed that ζ was independent of α. $< \zeta^2 >$ decreases with increasing α due to the nonlinearity of the Duffing oscillator. The energy stored in the nonlinear spring is greater than that stored in the linear spring by $\mathcal{E}_{nonlinear} - \mathcal{E}_{linear} = \frac{1}{4}x^4$. Therefore the effect of the nonlinearity of the Duffing oscillator is to decrease $< \zeta^2 >$, and this effect will increase with increasing $< \zeta^2 >$ and therefore increasing $< \alpha >$

Figures 11 to 13 show the results of Monte-Carlo experiments for the system driven by colored noise. In each curve the time evolving behaviour of the second order moment is depicted for various values of the correlation time, τ_c. All three figures show essentially the same behaviour for the case of $\tau_c = 0.001$ and $\tau_c = 0.01$ as for the white noise case, Figures 1 to 3. For the case of $\tau_c = 0.1$, the of the correlated nature of the noise is noticeable, but perhaps acceptable for some applications. It is clear that when the correlation time becomes greater than 0.1, the results differ significantly from the white noise case. This is as one would expect: at $\tau_c > 0.1$ the correlation time becomes comparable to the natural period of the oscillator, which is about one second. The correlated nature of the noise appears as a effect of time scale τ_c on the time history of the correlated noise. If the time scale of the correlation is much smaller than the natural period of the oscillator, then the oscillator cannot respond to this effect. However as τ_c approaches the natural period of the oscillator, the oscillator can be, and is, affected.

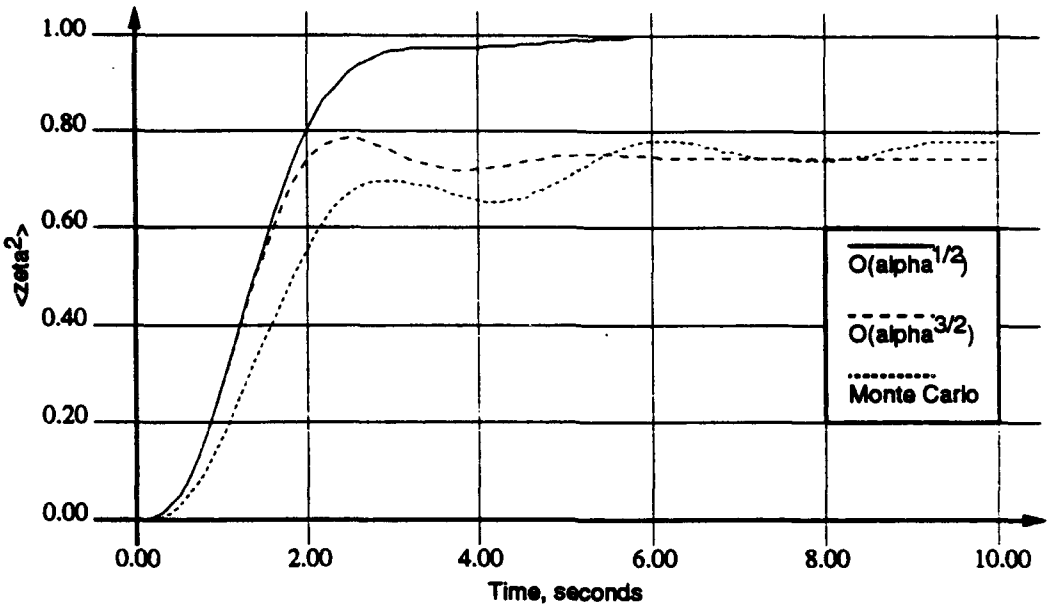

Figure 1: Time evolution of $< \zeta^2 >$

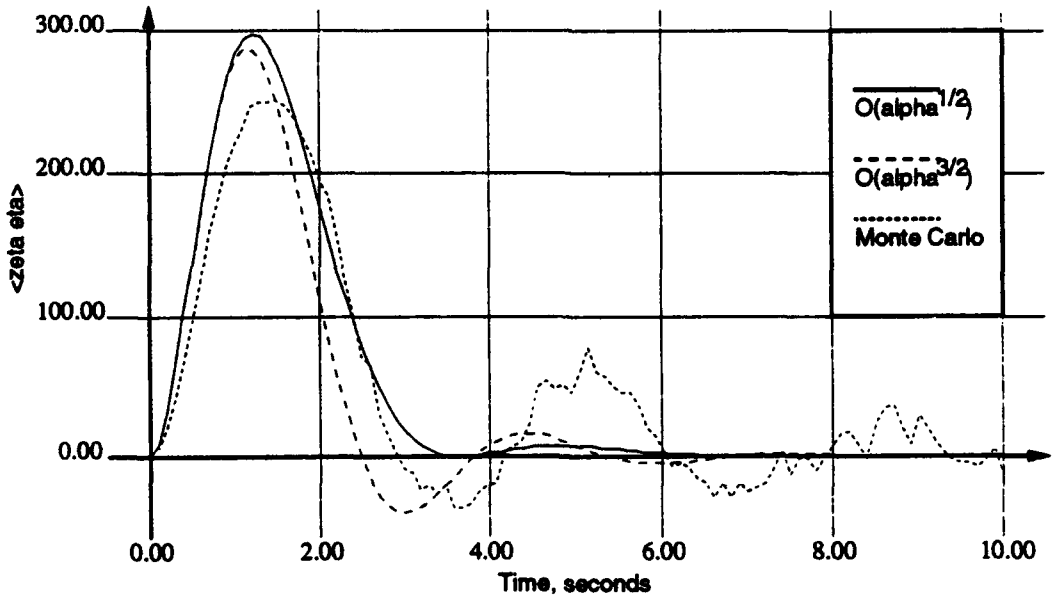

Figure 2: Time evolution of $< \zeta\eta >$

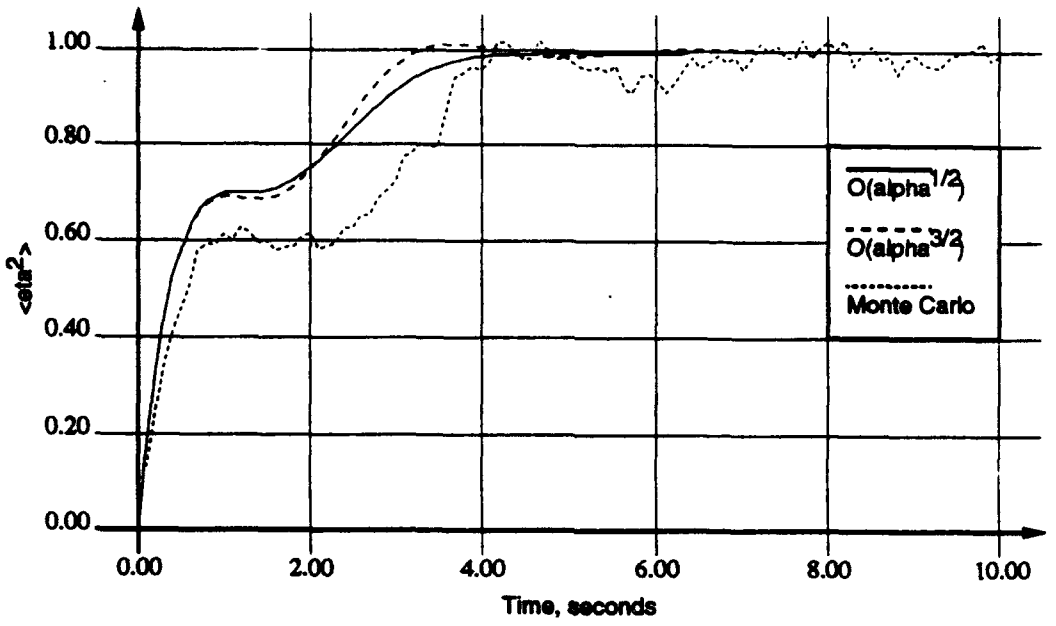

Figure 3: Time evolution of $< \eta^2 >$

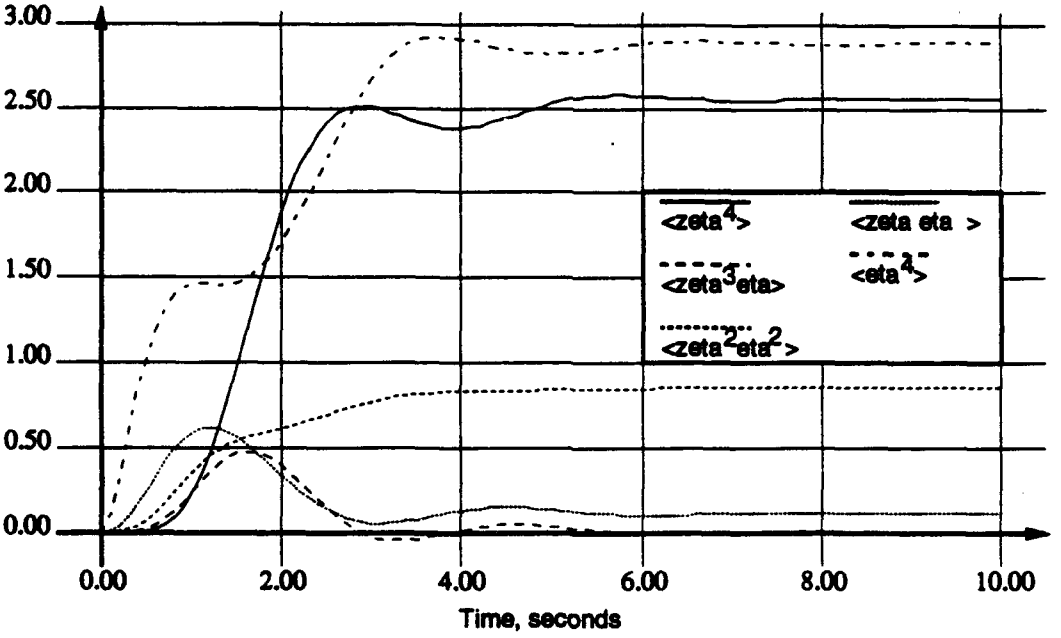

Figure 4: The time evolution of the fourth order moments for $\gamma = 1.0$, $\alpha = 0.1$.

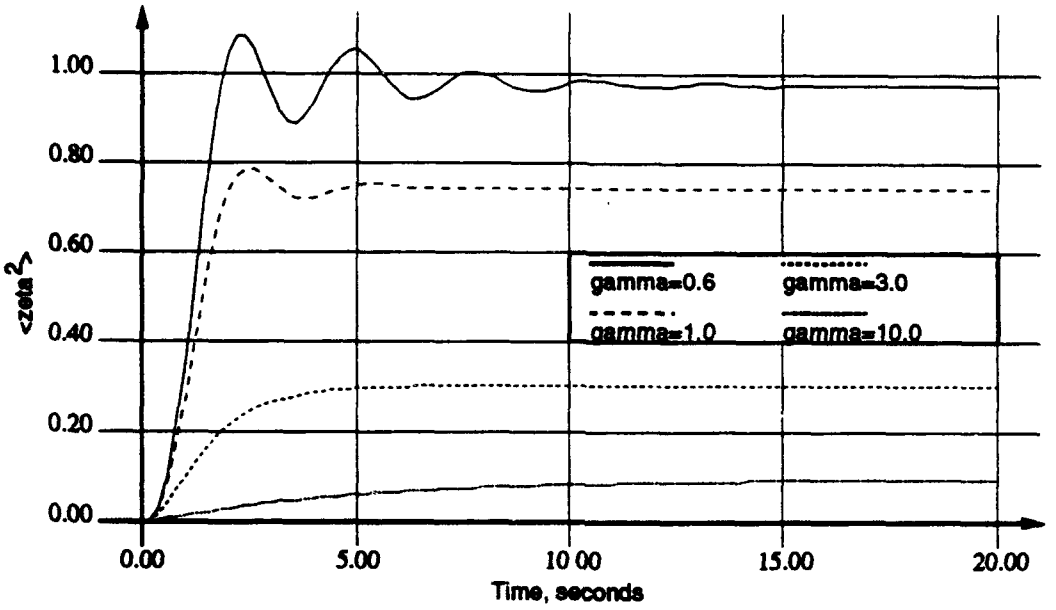

Figure 5: $< \zeta^2 >$ vs Time for increasing values of γ, $\alpha = 0.1$, calculated analytically to order $\mathcal{O}(\alpha^{\frac{2}{2}})$

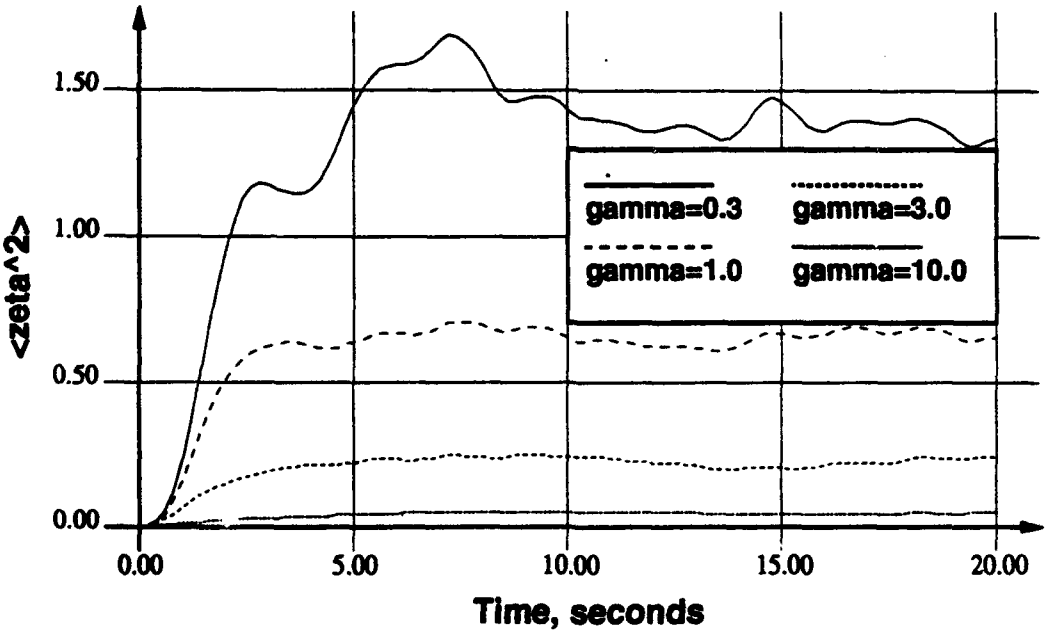

Figure 6: $< \zeta^2 >$ vs Time for increasing values of γ, $\alpha = 0.1$, from Monte Carlo analysis

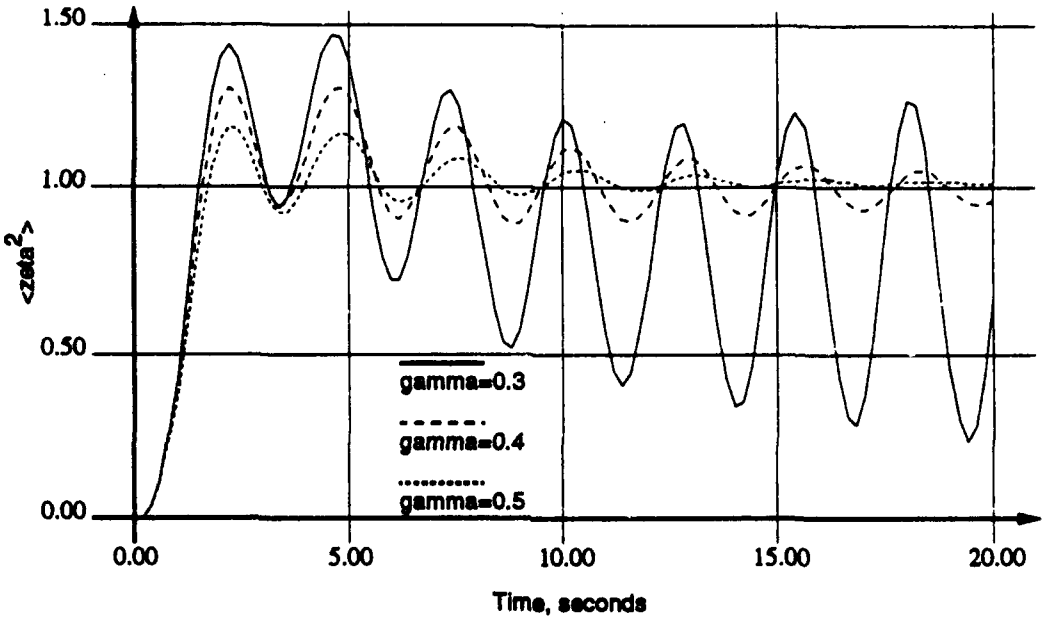

Figure 7: $< \zeta^2 >$ versus T for decreasing values of γ, $\alpha = .1$, calculated analytically to order $\mathcal{O}(\alpha^{\frac{3}{2}})$

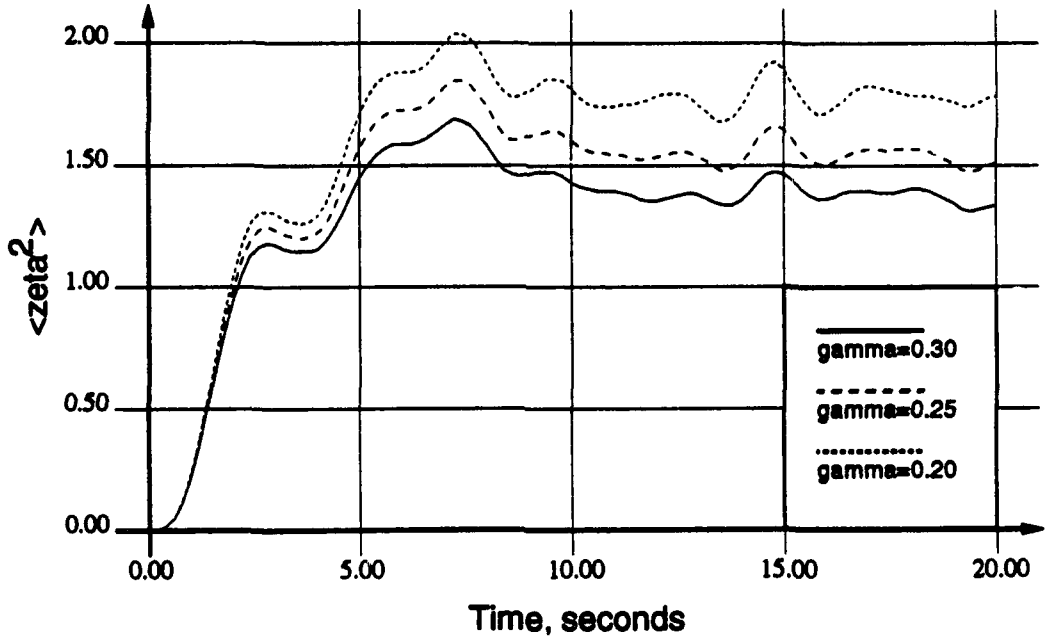

Figure 8: $< \zeta^2 >$ versus T for decreasing values of γ, $\alpha \doteq 0.1$, calculated by Monte-Carlo simulation

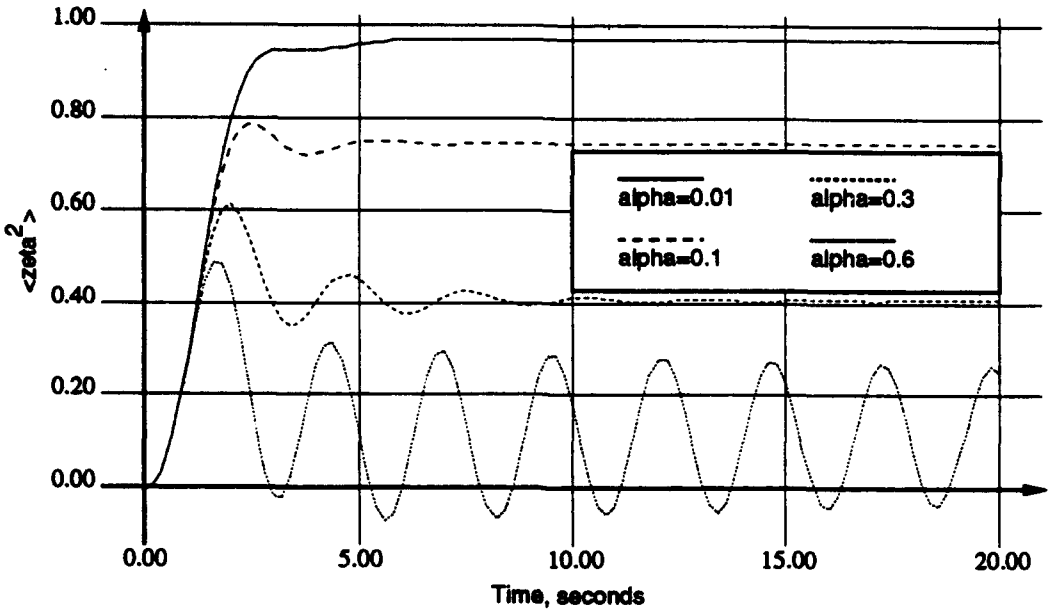

Figure 9: $< \zeta^2 >$ versus T for different values of α, $\gamma = 1.0$, calculated analytically to order $\mathcal{O}(\alpha^{\frac{2}{2}})$

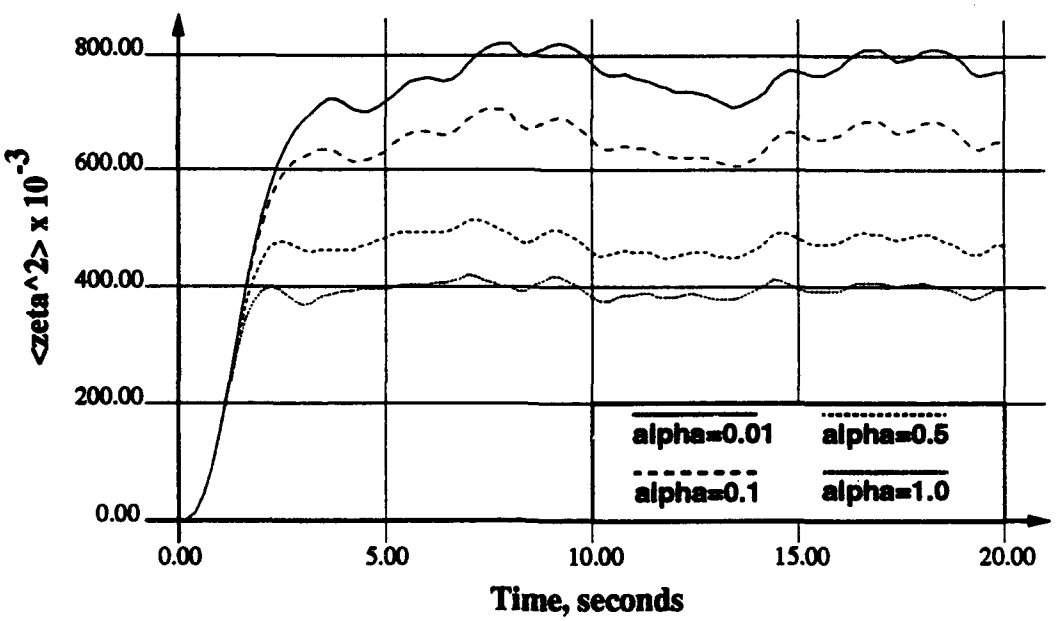

Figure 10: $< \zeta^2 >$ versus T for different values of α, $\gamma = 1.0$, calculated by Monte-Carlo simulation

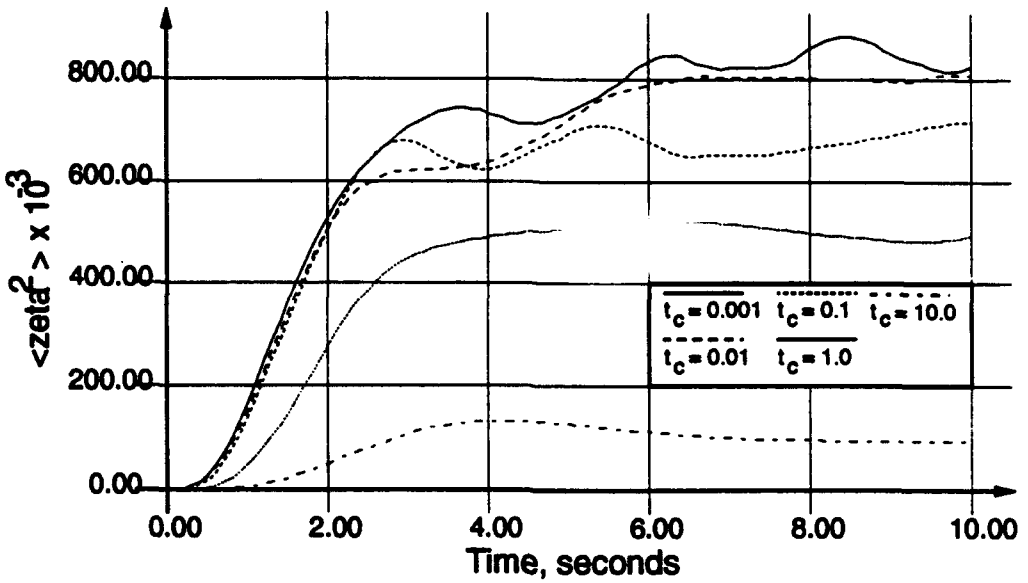

Figure 11: $< \zeta^2 >$ versus T for different values of τ_c, of $\gamma = 1.0$, $\alpha = .1$, Calculated by Monte-Carlo simulation

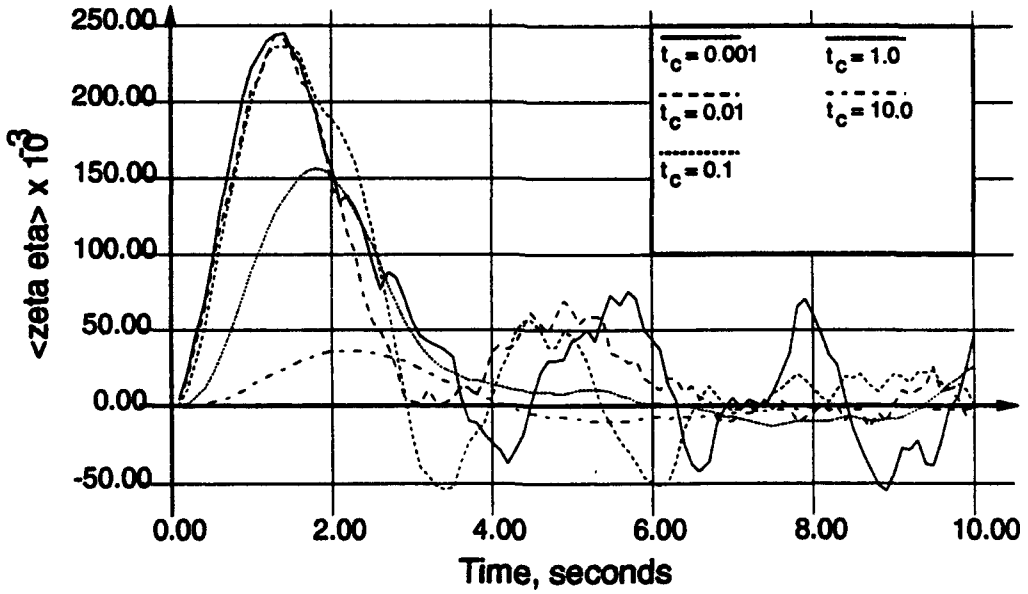

Figure 12: $< \zeta\eta >$ versus T for different values of τ_c, of $\gamma = 1.0$, $\alpha = .1$, Calculated by Monte-Carlo simulation

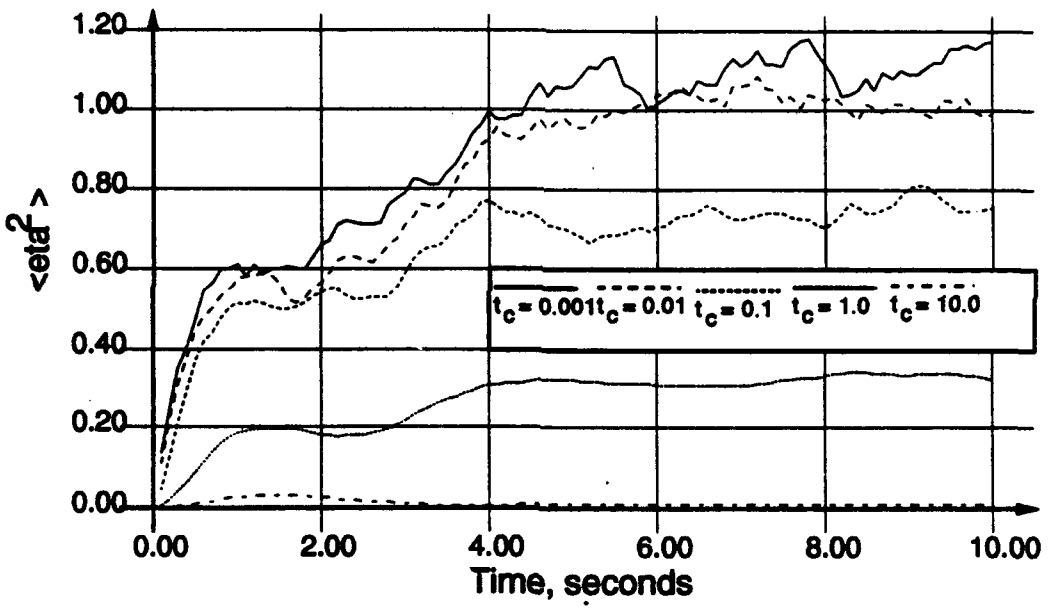

Figure 13: $< \eta^2 >$ versus T for different values of τ_c, $\gamma = 1.0$, $\alpha = .1$, Calculated by Monte-Carlo simulation

4 Conclusions

It can be seen from the figures that the agreement between the results of the various methods of solution is good. The trends observed are not surprising. The further the parameters of the system are from violating the assumptions of the analysis, the better the analytical results agreed with those of the Monte Carlo experiment. It is also seen that by and large, the higher order analysis is more accurate. One interesting point is that the analytical techniques are consistently, albeit slightly, greater than the Monte Carlo experiments. This conservative nature of the analytical method should be noted in applying it.

The method can be applied to systems where the three basic conditions of the expansion are met: that the intensity of the forcing function, α be of order smaller than unity, the damping of the system be of order at least unity, and the forcing function be essentially uncorrelated in time, i.e., correlation time $\tau_c < 0.1$

This technique is a valid analytical tool. It is well suited to studying the behavior of a system under a variety of conditions. The results it gives are accurate and computationally fast enough to embed such a model as an element of a larger model.

5 Acknowledgments

This work is prepared in partial fulfillment of the requirements for the degree of Doctor of Philosophy of the first author. The work was performed under the support of the Federal Aviation Administration Technical Center. The authors would like to thank Lawrence Neri of the Technical Center for his interest and support, Harry Kemp, also of the Technical Center for his support and expertise, and also the Department of Mechanical and Aerospace Engineering at Rutgers, the State University of New Jersey. The second author would also like to thank the Office of Naval Research and scientific officer Thomas F. Swean for support under grant number N00014-93-1-0763.

References

[1] R. Rodríguez and N.G. van Kampen. Systematic treatment of fluctuations in a nonlinear oscillator. *Physica*, 1976.

[2] C. Gardiner. *Handbook of Stochastic Methods.* Springer-Verlag, New York, 2cd edition, 1985.

[3] M. Ochi. *Applied Probability and Stochastic Processes in Engineering and Physical Sciences.* John Wiley and Sons, New York, 1990.

[4] E. Weinstein and H. Benaroya. Solution techniques for the Fokker-Planck equation via the van kampen expansion. In A. Cheng, editor, *Probabilistic Computational Mechnics.* Computational Mechanics Publishers, London, 1993.

The van Kampen expansion for the Fokker-Planck equation of a Duffing oscillator excited by colored noise

E. M. Weinstein*and H. Benaroya†

March 4, 1994

*Senior Research Engineer, Galaxy Scientific Corporation, Pleasantville, N.J.

†Associate Professor, Rutgers University, New Brunswick, NJ

Abstract

In Rodríguez and Van Kampen's 1976 paper [1], a method of extracting information from the Fokker-Planck equation without having to solve the equation is outlined. The Fokker-Planck equation for a Duffing oscillator excited by white noise is expanded about the intensity of the forcing function, α. In Weinstein and Benaroya, the effect of the order of expansion is investigated by carrying the expansion to a higher order. The effects of varying the system parameters is also investigated. All results are verified by comparison to Monte Carlo experiments. In this paper, the van Kampen expansion is modified and applied to the case of a Duffing oscillator excited by colored noise. The effect of the correlation time is investigated. Again the results are compared to those of Monte Carlo experiments. It was found that the expansion compared closely with those of the Monte Carlo experiments as the correlation time, τ_c, was varied from 0.001 to 10 seconds. Examination of the results revealed that the colored noise can be categorized in one of four ways: 1) for $\tau_c < \mathcal{O}(0.01)$sec the noise can be considered as white for all intents and purposes, 2) for $\tau_c = \mathcal{O}(0.1)$ the noise could be considered white for some purposes, 3) for $\tau_c = \mathcal{O}(1.0sec)$ the correlated nature of the noise must be considered in an analysis, and 4) for $\mathcal{O}(1.0) < \tau_c$ the noise can be considered as deterministic.

List of Figures

1 Introduction

The Fokker-Planck equation has proven to be a useful tool in the analysis of simple nonlinear oscillators excited by stochastic processes. As a partial differential equation for the probability density function of the response, its solution completely defines the solution of the problem. It can be used to analyze both a single oscillator of the form

$$m\ddot{x} + \gamma(\dot{x}, x)\dot{x} + k(\dot{x}, x)x = \mathcal{F}(t), \tag{1}$$

or a system of multiple, linked, oscillators of the form

$$\mathbf{M}\underline{\ddot{x}} + \mathbf{\Gamma}(\dot{x}, x)\underline{\dot{x}} + \mathbf{K}(\dot{x}, x)\underline{x} = \underline{\mathcal{F}}(t). \tag{2}$$

In many cases, a physical system can be approximated by such a system of nonlinear oscillators. The systems so modeled can range from a Brownian particle to structures excited by von Karmann vortex shedding. Such modeling can be useful for gaining insight into a problem and the way in which the system will behave as certain parameters are varied.

Once one has decided on the system of oscillators to be used to represent the physical system, the derivation of the Fokker-Planck equation is relatively straightforward, although tedious. The problem remains of how to solve it for the probability distribution of the response. In a very few cases, the Fokker-Planck equation can be solved analytically, but in most cases no analytical solution exists and one usually must resort to a numerical solution. However this can be computationally intensive and gives little insight into the larger problem.

In their 1976 paper, Rodríguez and van Kampen outline a method of dealing with the case of an oscillator excited by weak Gaussian white noise. The Fokker-Planck equation of the system is expanded about the intensity, α, of the driving function. This expansion is carried to the order $\mathcal{O}(\alpha^{\frac{1}{2}})$. In this way the statistics of the fluctuations are obtained directly. This

method shows promise as a way to use the Fokker-Planck equation to gain useful information about a wider variety of systems than was possible before.

This is the second of a planned series of papers exploring the usefulness of this method. In the previous paper [2], the method was applied to the problem of a Duffing oscillator excited by Gaussian white noise. The inherent assumptions of the method were explained there in detail, the expansion was carried both to the same order as in the original paper, and to order $\mathcal{O}(\alpha^{\frac{3}{2}})$, and results were presented and compared to Monte Carlo experiments. Parametric studies were also performed on the parameter of expansion as well as on the other important variable in the expansion: the coefficient of damping.

In this paper, the expansion is applied to the case of a Duffing oscillator excited by exponentially correlated noise. A parametric study is performed on the correlation time, τ_c and the results are compared to those of Monte Carlo experiments. The range of τ_c for which the correlated noise can be treated as white is identified as well as the range of τ_c for which the correlated nature of the noise cannot be ignored.

2 Expansion of the Fokker Planck Equation for a Duffing Oscillator Excited By Correlated Noise

In Gang [3], a method is outlined for deriving the Fokker Planck Equation of a system driven by colored noise. The procedure outlined consists of defining a dummy variable, y, to represent the colored noise process. y is defined as a first order, linear, differential filter of the white noise process:

$$c_1\dot{y}(t) = c_2 y(t) + c_3\mathcal{F}(t), \tag{3}$$

where c_i are constants and $\mathcal{F}(t)$ is the Gaussian white noise process defined by

$$\begin{aligned} < F(t) > &= 0 \\ < F(t)F(t') > &= 2\alpha\delta(t-t'). \end{aligned} \tag{4}$$

The system is now formulated as a system of first order differential equations driven by $y(t)$:

$$\dot{y} = \frac{c_2}{c_1}y + \frac{c_3}{c_1}\mathcal{F} \tag{5}$$

$$\dot{x} = F_x(x, v, y) \tag{6}$$

$$\dot{v} = F_v(x, v, y). \tag{7}$$

Several examples of colored noise filters exist in the literature. Billah and Shinozuka [4] use the following

$$\tau_c\dot{y}(t) = -y(t) + F(t), \tag{8}$$

where τ_c is the correlation time. It can be seen that as $\tau_c \to 0$, $y(t) \to F(t)$. For this derivation, it will be assumed that τ_c is not vanishingly small, so that Equation 8 can be written as:

$$\dot{y}(t) = -\mu y(t) + \mu F(t), \tag{9}$$

where $\mu = \frac{1}{\tau_c}$.

The Duffing oscillator excited by colored noise can now be written as

$$\ddot{x}(t) + \gamma\dot{x}(t) + x(t) + x^3(t) = y(t), \tag{10}$$

where γ is the coefficient of damping.

By defining $v(t) \equiv \dot{x}(t)$, the system can be recast as three linked, ordinary differential equations in time in the form of Equations 5 to 7:

$$\dot{x}(t) = v(t) \tag{11}$$

$$\dot{v}(t) = y(t) - \gamma v(t) - x(t) - x^3(t) \tag{12}$$

$$\dot{y}(t) = -\mu y(t) + \mu F(t). \tag{13}$$

Define $f(x, v, y; t)$ to be the joint probability density function of $x(t)$, $v(t)$, and $y(t)$ at time t. The Fokker-Planck equation for $f(x, v, y; t)$, can now be derived as

$$\frac{\partial f}{\partial t} = -v\frac{\partial}{\partial x}f - \frac{\partial}{\partial v}[(y - \gamma v - x - x^3)f] + \mu\frac{\partial}{\partial y}(yf) + \mu^2\alpha\frac{\partial^2}{\partial y^2}f \tag{14}$$

Equation 14 is the governing equation for the time evolution of the transition probability density function $f(x, v, y; t)$. From this point the derivation of the previous paper [2] will be followed.

As was shown in the previous paper, the response of the oscillator can be separated into a deterministic component due to the initial conditions and a random component of magnitude $\mathcal{O}(\sqrt{\alpha})$. However, by assuming that the oscillator is initially at rest, the deterministic component can be shown to be equal to zero. Therefore the following substitutions are made into Equation 14.

$$x = \sqrt{\alpha}\zeta \tag{15}$$

$$v = \sqrt{\alpha}\eta \tag{16}$$

$$y = \sqrt{\alpha}\rho \tag{17}$$

$$f(\sqrt{\alpha}\zeta, \sqrt{\alpha}\eta, \sqrt{\alpha}\rho; t) = \alpha^{-3/2}\Pi(\zeta, \eta, \rho; t). \tag{18}$$

The factor $\alpha^{-3/2}$ will be omitted from the definition of $\Pi(\zeta, \eta, \rho; t)$. If carried through the derivations, it would be divided out at a later stage of the derivation.

It must be explained why, as is implied in Equation 17, y is of the order of magnitude $\alpha^{\frac{1}{2}}$. This is because the magnitude y is of the same order of magnitude of the white noise forcing function, F. But it can be seen from the definition of F, Eqs 4, that $\alpha = 2\sigma_F^2$. Therefore F, and consequently y, are of $\mathcal{O}(\alpha^{\frac{1}{2}})$.

The relationships between the partial derivatives of f and Π are obtained as:

$$\alpha^{\frac{1}{2}}\frac{\partial f}{\partial x} = \frac{\partial \Pi}{\partial \zeta} \tag{19}$$

$$\alpha^{\frac{1}{2}}\frac{\partial f}{\partial v} = \frac{\partial \Pi}{\partial \eta} \tag{20}$$

$$\alpha^{\frac{1}{2}}\frac{\partial f}{\partial y} = \frac{\partial \Pi}{\partial \rho} \tag{21}$$

$$\frac{\partial f}{\partial t} = \frac{\partial \Pi}{\partial t}. \tag{22}$$

This yields the following transformed FPK:

$$\frac{\partial}{\partial t}\Pi = -\eta\frac{\partial}{\partial \zeta}\Pi - \frac{\partial}{\partial \eta}\left[\left(\rho - \gamma\eta - \zeta - \alpha\zeta^3\right)\Pi\right] + \mu\frac{\partial}{\partial \rho}(\rho\Pi) + \mu^2\frac{\partial^2}{\partial \rho^2}\Pi. \tag{23}$$

By manipulating the left hand side of Equattion 23, the following is obtained:

$$\begin{aligned} -\frac{\partial \Pi}{\partial \zeta}\dot{\zeta} - \frac{\partial \Pi}{\partial \eta}\dot{\eta} - \frac{\partial \Pi}{\partial \rho}\dot{\rho} &= -\eta\frac{\partial}{\partial \zeta}\Pi - \frac{\partial}{\partial \eta}\left[\left(\rho - \gamma\eta - \zeta - \alpha\zeta^3\right)\Pi\right] \\ &\quad + \mu\frac{\partial}{\partial \rho}(\rho\Pi) + \mu^2\frac{\partial^2}{\partial \rho^2}\Pi. \end{aligned} \tag{24}$$

If one substitutes the definitions of ζ, η, and ρ into Eqs 11, 12 and 13, one can use the resultant equations to separate Equation 24 into the following three equations:

$$\dot{\zeta}\Pi = \eta\Pi \tag{25}$$

$$\dot{\eta}\Pi = \left\{2\rho - \gamma\eta - \zeta - \alpha\zeta^3\right\}\Pi. \tag{26}$$

$$\dot{\rho}\Pi = -\mu\rho\Pi - \mu^2\Pi_\rho. \tag{27}$$

Using Eqs 27, 25, and 26, one can find the time derivatives of the higher order moments of ζ, η and ρ. As an example, the time derivative of $< \rho^2 >$ will derived. To derive $\frac{d}{dt} < \rho^2 >$, one multiplies Equation 27 by 2ρ, notes that $2\rho\dot{\rho} = \dot{\rho^2}$, and gets

$$\dot{\rho^2}\Pi = -\mu\rho^2\Pi - \mu^2\rho\Pi_\rho. \tag{28}$$

Integrating this over the range of all three arguments of Π and noting the definition of expectation, it is found:

$$\frac{d}{dt} < \rho^2 >= -2\mu < \rho^2 > -2\mu^2 \int\int\int_{-\infty}^{\infty} \rho\Pi_\rho \, d\rho \, d\zeta \, d\eta. \tag{29}$$

The second term on the right hand side can be expanded as follows:

$$\begin{aligned} \int\int\int_{-\infty}^{\infty} \rho\Pi_\rho \, d\rho \, d\zeta \, d\eta &= \int\int\int_{-\infty}^{\infty} [(\rho\Pi)_\rho - \Pi] \, d\rho \, d\zeta \, d\eta \\ &= -1 + \int\int_{-\infty}^{\infty} [\rho\Pi]_{\rho=-\infty}^{\rho=\infty} = -1. \end{aligned} \tag{30}$$

This last step is possible because the existence of $< \rho >$ guarantees that $\rho\Pi \to 0$ as $\rho \to \pm\infty$. Equation 29 becomes:

$$\frac{d}{dt} < \rho^2 >= -2\mu < \rho^2 > +2\mu^2. \tag{31}$$

The time derivatives of the other second order moments are similarly obtained:

$$\frac{d}{dt} < \zeta^2 > = 2 < \zeta\dot{\zeta} >= -2 < \zeta\eta > \tag{32}$$

$$\begin{aligned} \frac{d}{dt} < \eta^2 > &= 2 < \eta\dot{\eta} >= -2 < \zeta\eta > \\ &\quad -2\gamma < \zeta^2 > +4 < \eta\rho > -2\alpha < \zeta^3\eta > \end{aligned} \tag{33}$$

$$\frac{d}{dt} < \zeta\eta > = < \dot{\zeta}\eta > + < \zeta\dot{\eta} >= - < \zeta^2 > -\gamma < \zeta\eta >$$

$$- < \eta^2 > +2 < \zeta\rho > -\alpha < \zeta^4 > \tag{34}$$

$$\frac{d}{dt} < \rho^2 > \;=\; -2\mu < \rho^2 > -2\mu^2 \tag{35}$$

$$\frac{d}{dt} < \zeta\rho > \;=\; -\mu < \zeta\rho > - < \eta\rho > \tag{36}$$

$$\frac{d}{dt} < \eta\rho > \;=\; - < \zeta\rho > -\gamma < \eta\rho > +2 < \rho^2 > -\alpha < \zeta^3\rho > . \tag{37}$$

3 Results and figures

Figures 1, 3 and 5 show the results of the expansion for $\alpha = 0.1$, $\gamma = 1.0$, and different values of the correlation time, τ_c: $\tau_c = 0.001$, $\tau_c = 0.01$, $\tau_c = 0.1$, $\tau_c = 1.0$, $\tau_c = 10.0$. Figures 2, 4 and 6 show the results of Monte Carlo experiments for similar cases.

As in the previous paper, there is very good agreement between the two methods with similar differences as well. The analytical methods consistently give results slightly greater magnitude than do the Monte Carlo experiments. This phenomenon was seen in the previous paper. The analytical results are also consistently smoother, showing none of the small time scale fluctuations inherent in the Monte Carlo technique.

It can be seen in all the curves that the traces representing $\tau_c = 0.001$ and $\tau_c = 0.01$ are almost identical. In some cases, most notably Figures 1 and 3, the two traces are almost indistinguishable. The difference between the traces representing $\tau_c = 0.001$ and $\tau_c = 0.01$ are slightly more pronounced in the Monte Carlo results. However, the difference between the $\tau_c = 0.001$ and $\tau_c = 0.01$ traces of the Monte Carlo results is only of the order of the small time scale fluctuations inherent in the Monte Carlo technique. These figures indicate that for τ_c of order $\mathcal{O}(0.01)$ or less, the noise can be assumed to be uncorrelated, or white. The traces representing the response for $\tau_c = 0.1$ differ noticeably from those representing the results for $\tau_c < 0.1$. However, even for $\tau_c = 0.1$, the results are still quite close to those for $\tau_c < 0.1$ and the white noise approximation may still be useful for some uses. One would expect the effects of the correlated nature of the noise to become significant at about $\tau_c = 0.1$: at $\tau_c = 0.1$, the correlation time begins to become comparable to the natural period of the oscillator, which is about one second. The correlated nature of the noise appears as an effect of time scale, τ_c on the time history of the correlated noise. If the time scale of the correlation is much

smaller than the natural period of the oscillator, then the oscillator cannot respond to this effect. However, as τ_c approaches the natural period of the oscillator, the oscillator can be, and is, affected.

It can likewise be seen that as the correlation time of the noise becomes much greater than the natural period of the oscillator, the magnitude of the random response approaches zero. This is because when the correlation time is much larger than the natural period of the oscillator, the oscillator responds to the noise as if it were deterministic. Hence the figures show little random response for $\tau_c = 1.0$ seconds and almost none at all for $\tau_c = 10.0$ seconds.

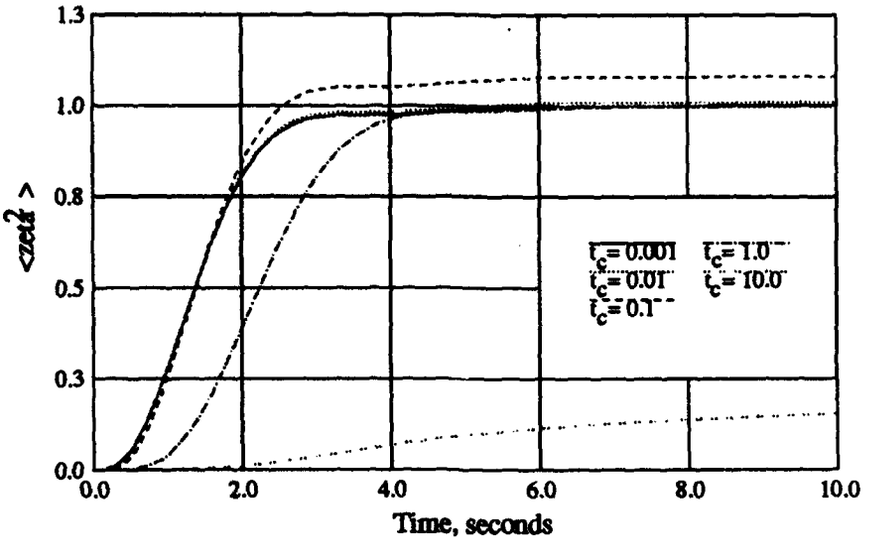

Figure 1: $< \zeta^2 >$ vs Time for different values of τ_c, $\gamma = 1.0$, $\alpha = 0.1$, calculated analytically to order $\mathcal{O}(\alpha^{\frac{3}{2}})$.

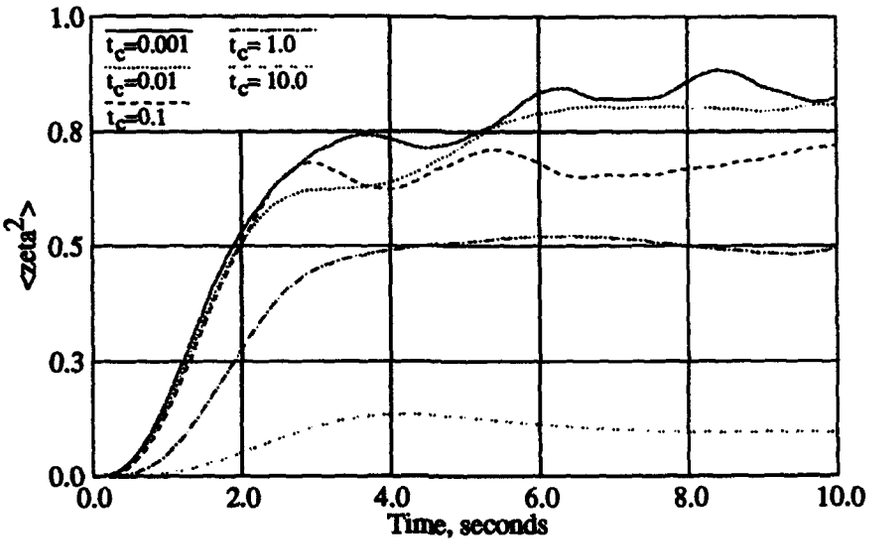

Figure 2: $< \zeta^2 >$ vs Time for different values of τ_c, $\gamma = 1.0$, $\alpha = 0.1$, calculated by Monte-Carlo simulation.

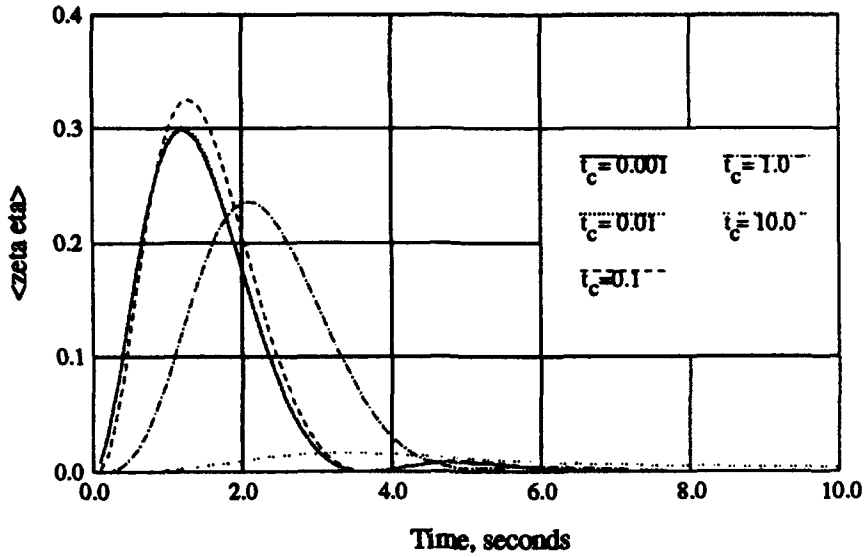

Figure 3: $< \zeta\eta >$ vs Time for different values of τ_c, $\gamma = 1.0$, $\alpha = 0.1$, calculated analytically to order $\mathcal{O}(\alpha^{\frac{3}{2}})$.

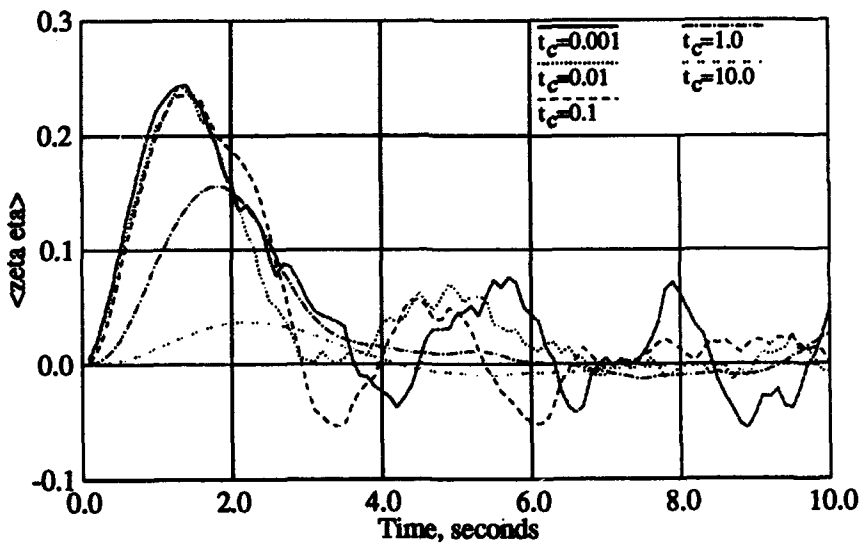

Figure 4: $< \zeta\eta >$ vs Time for different values of τ_c, $\gamma = 1.0$, $\alpha = 0.1$, calculated by Monte-Carlo simulation.

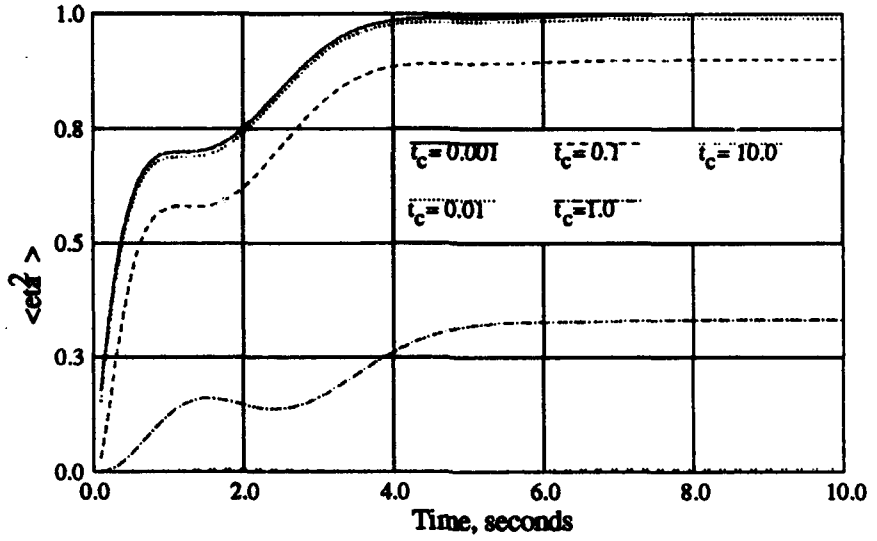

Figure 5: $< \eta^2 >$ vs Time for different values of τ_c, $\gamma = 1.0$, $\alpha = 0.1$, calculated analytically to order $\mathcal{O}(\alpha^{\frac{3}{2}})$.

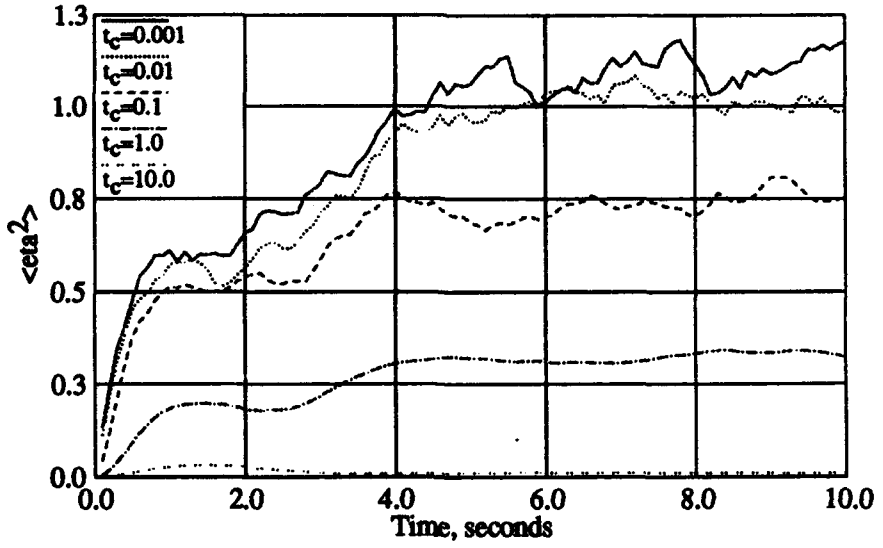

Figure 6: $< \eta^2 >$ vs Time for different values of τ_c, $\gamma = 1.0$, $\alpha = 0.1$, calculated by Monte-Carlo simulation.

4 Conclusions

The overwhelming similarity between the results given by the two methods implies that this adaptation of the van Kampen expansion is an accurate tool for predicting the statistics of the response of an oscillator excited by colored noise. However, it was also seen that, depending on the magnitude of the correlation time, perhaps as compared to the natural period of the oscillator, simplifying assumtions can be made that obviate the need for this adaptation.

5 Acknowledgments

This work is prepared in partial fulfillment of the requirements for the degree of Doctor of Philosophy of the first author. The work was performed under the support of the Federal Aviation Administration Technical Center. The authors would like to thank Lawrence Neri of the Technical Center for his interest and support, Harry Kemp, also of the Technical Center for his support and expertise, and also the Department of Mechanical and Aerospace Engineering at Rutgers, the State University of New Jersey. The second author would also like to thank the Office of Naval Research and scientific officer Thomas F. Swean for support under grant number N00014-93-1-0763.

References

[1] R. Rodríguez and N.G. van Kampen. Systematic treatment of fluctuations in a nonlinear oscillator. *Physica*, 1976.

[2] Edward Weinstein and H. Benaroya. The van Kampen expansion for the Fokker-Planck equation of a Duffing oscillator. *Journal of Statistical Physics. Submitted.*

[3] H. Gang. Two-dimensional probability distribution of systems driven by colored noise. *Physical Review*, 43(2), Jan 1991.

[4] K.Y.R. Billah and M. Shinozuka. Numerical method for colored noise generation and its application to a bistable system. *Physical Review*, 12(42), Dec 1990.

DRAFT

The van Kampen expansion for a linked Duffing-linear oscillator excited by colored noise

E. M. Weinstein*and H. Benaroya†

June 17, 1994

Abstract

In Rodríguez and Van Kampen's 1976 paper [1], a method of extracting information from the Fokker-Planck equation without having to solve the equation is outlined. The Fokker-Planck equation for a Duffing oscillator excited by white noise is expanded about the intensity of the forcing function, α. In Weinstein and Benaroya [2], the effect of the order of expansion is investigated by carrying the expansion to a higher order. The effects of varying the system parameters is also investigated. All results are verified by comparison to Monte Carlo experiments. In Weinstein and Benaroya [3] the van Kampen expansion is modified and applied to the case of a Duffing oscillator excited by colored noise. The effect of the correlation time is investigated. Again the results are compared to those of Monte Carlo experiments. In both cases, the results of the analyses agreed closely with those of the Monte Carlo experiments. In this paper the van Kampen expansion is applied to linked linear-Duffing oscillators. Again, parametric studies are done on the system parameters and the correlation coefficient of the driving force and the results compared to those of Monte Carlo experiments. It was found that the analytical results compared closely with the numerical results as long as the initial assumptions of the expansion are not violated.

1 Introduction

The Fokker-Planck equation has proven to be a useful tool in the analysis of simple nonlinear oscillators excited by stochastic processes. As a partial differential equation for the probability density function of the response, its solution completely defines the solution of the problem. It can be used to analyze both a single oscillator of the form

$$m\ddot{x} + \gamma(\dot{x}, x)\dot{x} + k(\dot{x}, x)x = \mathcal{F}(t), \tag{1}$$

or a system of multiple, linked, oscillators of the form

$$\mathbf{M}\underline{\ddot{x}} + \mathbf{\Gamma}(\dot{x}, x)\underline{\dot{x}} + \mathbf{K}(\dot{x}, x)\underline{x} = \underline{\mathcal{F}}(t). \tag{2}$$

*Senior Research Engineer, Galaxy Scientific Corporation, Pleasantville, N.J.

†Associate Professor, Department of Mechanical and Aerospace Engineering, Rutgers University, New Brunswick, NJ

In many cases, a physical system can be approximated by such a system of nonlinear oscillators. The systems so modeled can range from a Brownian particle to structures excited by von Karmann vortex shedding. Such modeling can be useful for gaining insight into a problem and the way in which the system will behave as certain parameters are varied.

Once one has decided on the system of oscillators to be used to represent the physical system, the derivation of the Fokker-Planck equation is relatively straightforward, although tedious. The problem of how to solve it for the probability distribution of the response remains. In a very few cases, the Fokker-Planck equation can be solved analytically, but in most cases no analytical solution exists and one usually must resort to a numerical solution. However, this can be computationally intensive and gives little insight into the larger problem.

In their 1976 paper, Rodríguez and van Kampen outline a method of dealing with the case of an oscillator excited by weak Gaussian white noise. The Fokker-Planck equation of the system is expanded about the intensity, α, of the driving function. This expansion is carried to the order $\mathcal{O}(\alpha^{\frac{1}{2}})$. In this way the statistics of the fluctuations are obtained directly. This method shows promise as a way to use the Fokker-Planck equation to gain useful information about a wider variety of systems than was possible before.

This is the of a series of papers exploring the usefulness of this method. In this paper, the van Kampen expansion is applied to coupled linear-Duffing oscillators. This is done for two reasons. The first is to demonstrate that the expansion can be applied to a system of coupled oscillators. The second is that some physical systems are well modeled by such coupled oscillators. An example of such a system is an offshore structure under the influence of ocean waves [4, 5]. These waves have a certain periodic nature, but are of random height and intensity. The structure itself can be modelled as a series of oscillators.

There are several ways in which such coupled oscillators can be formulated. The external force can drive either the linear or the Duffing oscillator. Here, it is decided to have the external force drive the linear oscillator. The formulation of the solution would be the same if the situation was reversed. There are also several ways in which the two oscillators can be coupled: through a damping function, through a spring function, or through a combination of the two. In this analysis, the coupling chosen is of the form of a simple linear spring. Here, the system is formulated in such a way that the effect of the Duffing oscillator would not feed back into the linear oscillator. Such a system would more accurately model a system where the driving force is an overwhelming physical phenomenon impervious to the effect of the structure being modeled. However, it appears that all of the above cases can be modeled using the following technique.

2 Derivation and Expansion of the Fokker-Planck equation

The first step in the derivation of the Fokker-Planck equation for any system is the formulation of the governing equations. The governing equations for the system described in the Introduction are:

$$\dot{y}(t) + \frac{1}{\tau_c} y(t) = \frac{1}{\tau_c} F(t) \tag{3}$$

$$\ddot{x}_1(t) + \gamma_1 \dot{x}_1(t) + x_1(t) = y(t) \tag{4}$$

$$\ddot{x}_2(t) + \gamma_2 \dot{x}_2(t) + x_2(t) + \varepsilon x_2^3(t) = k\left[x_1(t) - x_2(t)\right], \tag{5}$$

where $F(t)$ is defined by

$$\begin{aligned} < F(t) > &= 0, \\ < F(t)F(t') > &= 2\alpha\delta(t-t'). \end{aligned} \tag{6}$$

That the solution of Equation 3 is exponentially colored noise is shown in several sources such as Billah and Shinozuka [6].

Because the Fokker-Planck equation requires that the governing equations be cast as a series of first order differential equations, the following new variables are defined:

$$v_1 = \dot{x}_1 \tag{7}$$

$$v_2 = \dot{x}_2. \tag{8}$$

Using these variables the governing equations can be rewritten in the following, equivalent, form:

$$\dot{y}(t) = -\frac{1}{\tau_c}y(t) + \frac{1}{\tau_c}F(t) \tag{9}$$

$$\dot{x}_1(t) = v_1(t) \tag{10}$$

$$\dot{v}_1(t) = y(t) - \gamma_1 v_1(t) - x_1(t) \tag{11}$$

$$\dot{x}_2(t) = v_2(t) \tag{12}$$

$$\dot{v}_2(t) = kx_1(t) - \gamma_2 v_2(t) - (1+k)x_2(t) - \varepsilon x_2^3(t). \tag{13}$$

The Fokker-Planck equation of this system can be derived as:

$$\begin{aligned} \frac{d}{dt}f = {} & \mu\frac{d}{dy}(yf) - v_1\frac{d}{dx_1}f - \frac{d}{dv_1}[(y-\gamma_1 v_1 - x_1)f] - v_2\frac{d}{dx_2}f \\ & -\frac{d}{dv_2}[(kx_1 - \gamma_2 v_2 - (1+k)x_2 - \varepsilon x_2^3)f] + \mu^2\alpha\frac{d^2}{dy^2}f. \end{aligned} \tag{14}$$

As was shown in Weinstein and Benaroya [2], the response of the oscillator can be separated into a deterministic component arising from the initial conditions, and a random component of magnitude $\mathcal{O}(\sqrt{\alpha})$. However, by assuming the oscillator to be initially at rest, the deterministic component can be shown to be equal to zero. Therefore, the following substitutions are made into Equation 14:

$$y = \sqrt{\alpha}\,\rho \tag{15}$$

$$x_1 = \sqrt{\alpha}\,\zeta_1 \tag{16}$$

$$v_1 = \sqrt{\alpha}\,\eta_1 \tag{17}$$

$$x_2 = \sqrt{\alpha}\,\zeta_2 \tag{18}$$

$$v_2 = \sqrt{\alpha}\,\eta_2 \tag{19}$$

$$f(y, x_1, v_1, x_2, v_2; t) = \alpha^{-\frac{5}{2}}\Pi(\rho, \zeta_1, \eta_1, \zeta_2, \eta_2; t). \tag{20}$$

$\Pi(\rho, \zeta_1, \eta_1, \zeta_2, \eta_2; t)$ is the joint probability density of the transformed variables. The factor $\alpha^{-\frac{5}{2}}$ will be omitted from the definition of Π. If carried through the derivations, it would be divided out at a later stage.

The relationships between the partial derivatives of f and Π are easily obtained as:

$$\sqrt{\alpha}\,\frac{\partial f}{\partial y} = \frac{\partial \Pi}{\partial \rho} \tag{21}$$

$$\sqrt{\alpha}\,\frac{\partial f}{\partial x_1} = \frac{\partial \Pi}{\partial \zeta_1} \tag{22}$$

$$\sqrt{\alpha}\,\frac{\partial f}{\partial v_1} = \frac{\partial \Pi}{\partial \eta_1} \tag{23}$$

$$\sqrt{\alpha}\,\frac{\partial f}{\partial x_2} = \frac{\partial \Pi}{\partial \zeta_2} \tag{24}$$

$$\sqrt{\alpha}\,\frac{\partial f}{\partial v_2} = \frac{\partial \Pi}{\partial \eta_2} \tag{25}$$

$$\frac{\partial f}{\partial t} = \frac{\partial \Pi}{\partial t}. \tag{26}$$

Equations 15 to 19, as well as the equations above, Eqs 21 to 26, can be substituted into the Fokker-Planck equation, Equation 14, yielding:

$$\begin{aligned}\Pi_t = {} & \mu(\rho\Pi)_\rho - \eta_1\Pi_{\zeta_1} - [(\rho - \gamma_1\eta_1 - \zeta_1)\Pi]_{\eta_1} - \eta_2\Pi_{\zeta_2} \\ & - \left[(k\zeta_1 - \gamma_2\eta_2 - (1+k)\zeta_2 - \varepsilon\alpha\eta_2^3)\Pi\right]_{\eta_2} + \mu^2\Pi_{\rho,\rho}.\end{aligned} \tag{27}$$

The left hand side of Equation 27 is transformed into partial derivatives of Π in the transformed variables, ρ, ζ_1, η_1, ζ_2, η_2, yielding

$$\begin{aligned}\dot{\rho}\Pi_\rho - \dot{\zeta}_1\Pi_{\zeta_1} - \dot{\eta}_1\Pi_{\eta_1} - \dot{\zeta}_2\Pi_{\zeta_2} - \dot{\eta}_2\Pi_{\eta_2} = {} & \\ \mu(\rho\Pi)_\rho - \eta_1\Pi_{\zeta_1} - [(\rho - \gamma_1\eta_1 - \zeta_1)\Pi]_{\eta_1} - \eta_2\Pi_{\zeta_2} & \\ - \left[(k\zeta_1 - \gamma_2\eta_2 - (1+k)\zeta_2 - \varepsilon\alpha\eta_2^3)\Pi\right]_{\eta_2} + \mu^2\Pi_{\rho,\rho}. &\end{aligned} \tag{28}$$

One can now substitute the definitions of ρ, ζ_1, η_1 ζ_2, and η_2 into Equations 10 to 13 and multiply by $\alpha^{-\frac{1}{2}}$. The resulting four equations are:

$$\dot{\zeta}_1 = \eta_1 \tag{29}$$

$$\dot{\eta}_1 = \rho - \gamma_1\eta_1 - \zeta_1 \tag{30}$$

$$\dot{\zeta}_2 = \eta_2 \tag{31}$$

$$\dot{\eta}_2 = k\zeta_1 - \gamma_2\eta_2 - (1+k)\zeta_2 - \varepsilon\alpha\zeta_2^3. \tag{32}$$

If one multiplies each of the above equations by Π and differentiates Equation 29 with respect to ζ_1, Equation 30 with respect to η_1, Equation 31 with respect to ζ_2, and Equation 32 with respect to η_2, each of the resulting equations can be added to the transformed Fokker-Planck equation, Equation 28. The resultant is the following equation:

$$-\dot{\rho}\frac{\partial \Pi}{\partial \rho} = \mu[\rho\Pi]_\rho + \mu^2\Pi_{\rho,\rho}. \tag{33}$$

This can be integrated with respect to ρ to give

$$-\dot{\rho}\Pi = \mu\rho\Pi + \mu^2\Pi_\rho. \tag{34}$$

Thus, the Fokker-Planck equation of the system of linked oscillators has been transformed to the following five equations:

$$\dot{\rho}\Pi = -\mu\rho\Pi + \mu^2\Pi_\rho \tag{35}$$
$$\dot{\zeta}_1\Pi = \eta_1\Pi \tag{36}$$
$$\dot{\eta}_1\Pi = (\rho - \gamma_1\eta_1 - \zeta_1)\,\Pi \tag{37}$$
$$\dot{\zeta}_2\Pi = \eta_2\Pi \tag{38}$$
$$\dot{\eta}_2\Pi = \left[k\zeta_1 - \gamma_2\eta_2 - (1+k)\zeta_2 - \varepsilon\alpha\zeta_2^3\right]\Pi. \tag{39}$$

As shown in Weinstein and Benaroya [2], the time derivatives of the second order moments can be found as

$$\frac{d}{dt}<\zeta_1^2> = 2<\zeta_1\eta_1> \tag{40}$$
$$\frac{d}{dt}<\eta_1^2> = -2\gamma_1<\eta_1^2> -2<\zeta_1\eta_1> +2<\eta_1\rho> \tag{41}$$
$$\frac{d}{dt}<\zeta_1\eta_1> = -<\zeta_1^2> +<\eta_1^2> -\gamma_1<\zeta_1\eta_1> +<\zeta_1\rho> \tag{42}$$
$$\frac{d}{dt}<\zeta_2^2> = 2<\zeta_2\eta_2> \tag{43}$$
$$\frac{d}{dt}<\zeta_1\zeta_2> = <\eta_1\zeta_2> +<\zeta_1\eta_2> \tag{44}$$
$$\frac{d}{dt}<\eta_1\zeta_2> = -<\zeta_1\zeta_2> -\gamma_1<\eta_1\zeta_2> +<\eta_1\eta_2> +<\zeta_2\rho> \tag{45}$$
$$\frac{d}{dt}<\eta_2^2> = 2k<\zeta_1\eta_2> -2(1+k)<\zeta_2\eta_2> -2\gamma_2<\eta_2^2> \tag{46}$$
$$\frac{d}{dt}<\zeta_1\eta_2> = k<\zeta_1^2> -(1+k)<\zeta_1\zeta_2> -\gamma_2<\zeta_1\eta_2> +<\eta_1\eta_2> \tag{47}$$
$$\frac{d}{dt}<\eta_1\eta_2> = k<\zeta_1\eta_1> -(1+k)<\eta_1\zeta_2> -<\zeta_1\eta_2> -(\gamma_1+\gamma_2)<\eta_1\eta_2> +<\eta_2\rho> \tag{48}$$
$$\frac{d}{dt}<\zeta_2\eta_2> = -(1+k)<\zeta_2^2> +k<\zeta_1\zeta_2> +<\eta_2^2> -\gamma_2<\zeta_2\eta_2> \tag{49}$$
$$\frac{d}{dt}<\rho^2> = -2\mu<\rho^2> -2\mu^2 \tag{50}$$
$$\frac{d}{dt}<\zeta_1\rho> = -\mu<\zeta_1\rho> +<\eta_1\rho> \tag{51}$$
$$\frac{d}{dt}<\eta_1\rho> = <\rho^2> -<\zeta_1\rho> -(\gamma_1+\mu)<\eta_1\rho> \tag{52}$$
$$\frac{d}{dt}<\zeta_2\rho> = -\mu<\zeta_2\rho> +<\eta_2\rho> \tag{53}$$
$$\frac{d}{dt}<\eta_2\rho> = k<\zeta_1\rho> -(1+k)<\zeta_2\rho> -(\gamma_2+\mu)<\eta_2\rho>\,. \tag{54}$$

The previous 15 equations, Equations 40 to 54, can be cast as a single matrix equation,

$$\frac{d}{dt}\vec{x} = A\vec{x} + \vec{b}, \tag{55}$$

where

$$\vec{x} = \begin{Bmatrix} <\zeta_1^2> \\ <\eta_1^2> \\ <\zeta_1\eta_1> \\ <\zeta_2^2> \\ <\zeta_1\zeta_2> \\ <\eta_1\zeta_2> \\ <\eta_2^2> \\ <\zeta_1\eta_2> \\ <\eta_1\eta_2> \\ <\zeta_2\eta_2> \\ <\rho^2> \\ <\zeta_1\rho> \\ <\eta_1\rho> \\ <\zeta_2\rho> \\ <\eta_2\rho> \end{Bmatrix}, \qquad \vec{b} = \begin{Bmatrix} 0 \\ 0 \\ 0 \\ 0 \\ 0 \\ 0 \\ 0 \\ 0 \\ 0 \\ 0 \\ -2\mu^2 \\ 0 \\ 0 \\ 0 \\ 0 \end{Bmatrix}, \tag{56}$$

and

$$\mathcal{A} = \begin{Bmatrix} 0 & 0 & 2 & 0 & 0 & 0 & 0 & 0 \\ 0 & -2\gamma_1 & -2 & 0 & 0 & 0 & 0 & 0 \\ -1 & 1 & -\gamma_1 & 0 & 0 & 0 & 0 & 0 \\ 0 & 0 & 0 & 0 & 0 & 0 & 0 & 0 \\ 0 & 0 & 0 & 0 & 0 & 1 & 0 & 1 \\ 0 & 0 & 0 & 0 & -1 & -\gamma_1 & 0 & 0 \\ 0 & 0 & 0 & 0 & 0 & 0 & -2\gamma_2 & 2k \\ k & 0 & 0 & 0 & -1-k & 0 & 0 & -\gamma_2 \\ 0 & 0 & k & 0 & 0 & -1-k & 0 & -1 \\ 0 & 0 & 0 & -1-k & k & 0 & 1 & 0 \\ 0 & 0 & 0 & 0 & 0 & 0 & 0 & 0 \\ 0 & 0 & 0 & 0 & 0 & 0 & 0 & 0 \\ 0 & 0 & 0 & 0 & 0 & 0 & 0 & 0 \\ 0 & 0 & 0 & 0 & 0 & 0 & 0 & 0 \\ 0 & 0 & 0 & 0 & 0 & 0 & 0 & 0 \end{Bmatrix} \quad \ldots\ldots$$

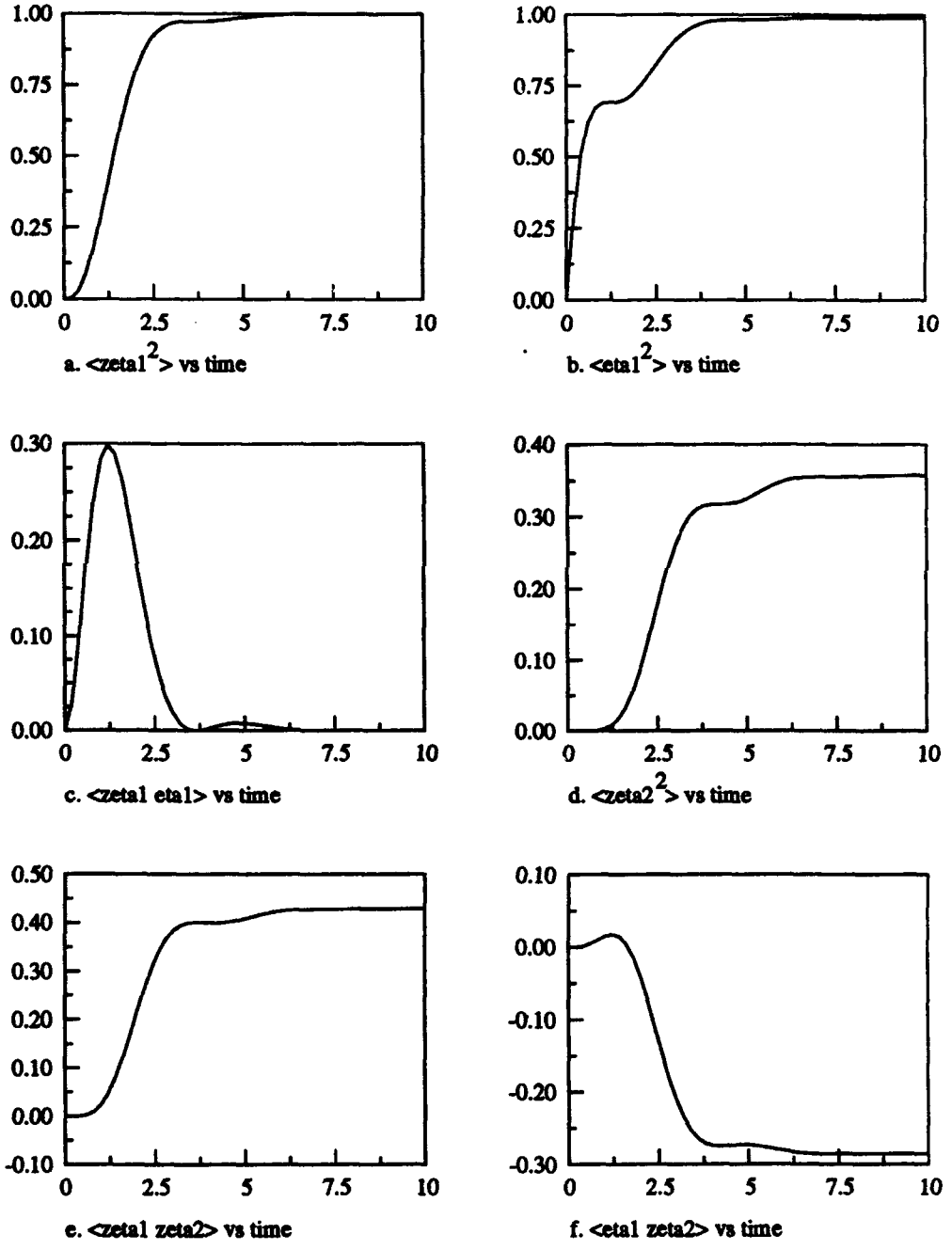

Figure 1: Response of coupled oscillators, $\gamma_1 = 1.0$, $\gamma_2 = 1.0$, $\tau_c = 0.01$, $k = 1.0$, calculated analytically.

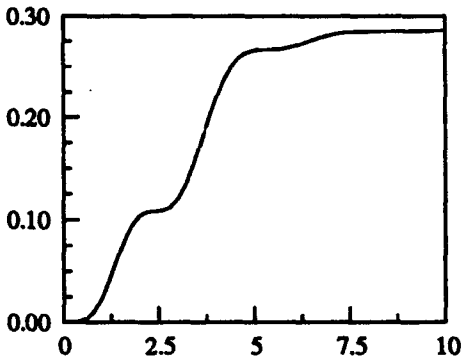

g. <eta2^2> vs time

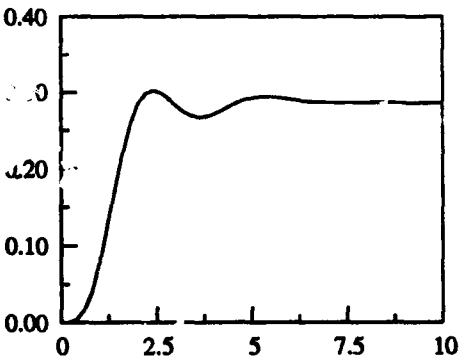

h. <zeta1 eta2> vs time

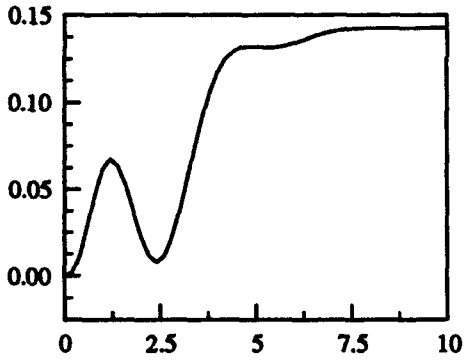

i. <eta1 eta2> vs time

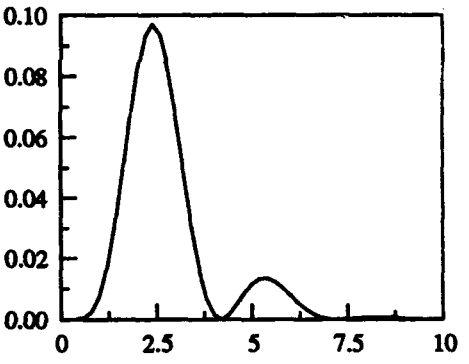

j. <zeta2 eta2> vs time

Key:

gamma1=1.0

gamma2=1.0

τ_c =0.01

k=1.0

Figure 1 (Continued): Response of coupled oscillators, $\gamma_1 = 1.0$, $\gamma_2 = 1.0$, $\tau_c = 0.01$, $k = 1.0$, calculated analytically.

$$
\begin{array}{cccccccc}
 & 0 & 0 & 0 & 0 & 0 & 0 & 0 \\
 & 0 & 0 & 0 & 0 & 2 & 0 & 0 \\
 & 0 & 0 & 0 & 1 & 0 & 0 & 0 \\
 & 0 & 2 & 0 & 0 & 0 & 0 & 0 \\
 & 0 & 0 & 0 & 0 & 0 & 0 & 0 \\
 & 1 & 0 & 0 & 0 & 0 & 1 & 0 \\
 & 0 & -2-2k & 0 & 0 & 0 & 0 & 0 \\
\ldots\ldots & 1 & 0 & 0 & 0 & 0 & 0 & 0 \\
 & -\gamma_1-\gamma_2 & 0 & 0 & 0 & 0 & 0 & 1 \\
 & 0 & -\gamma_2 & 0 & 0 & 0 & 0 & 0 \\
 & 0 & 0 & -2\mu & 0 & 0 & 0 & 0 \\
 & 0 & 0 & 0 & -\mu & 1 & 0 & 0 \\
 & 0 & 0 & 1 & -1 & -\mu-\gamma_1 & 0 & 0 \\
 & 0 & 0 & 0 & 0 & 0 & -\mu & 1 \\
 & 0 & 0 & 0 & k & 0 & -1-k & -\mu-\gamma_2
\end{array}
$$

Equation 55 can be solved by standard techniques to yield all the time evolving second order moments of the system.

3 Results and Figures

Figure 1 shows the result of the analysis for the case of $\gamma_1 = 1.0$, $\gamma_2 = 1.0$, $\tau_c = 0.01$, and coupling spring constant $k = 1.0$. Figure 2 shows the Monte Carlo results for the same system.

Agreement between the two sets of results is generally very good with no major points of difference. In general, the analytical results show slightly deemphasized local maxima and minima as compared to the Monte Carlo results. This effect is most pronounced in the cross correlation curves, such as $< \zeta_1 \eta_1 >$, Figures 1(c,e,f,j) and 2(c,e,f,j) that have a local maximum at about 5 seconds. Comparison of Figures 1(c), and 2(c) shows this effect most clearly. It is also seen that, in general, the steady state values of the Monte Carlo results are somewhat lower than those of the analytical results. This is consistent with the results of the previous two papers [2, 3].

Four studies on the effects of varying the several parameters, while keeping all others constant, are performed: 1) γ_1 is varied from 0.7 to 10, 2) γ_2 is varied from 0.7 to 10.0, 3) k, the constant of the coupling spring, is varied from 0.1 to 10.0, and 4) τ_c is increased from 0.001 to 10.0.

The results of the first of these studies are shown in Figures 3 and 4. The results are as would be expected from [2, 3]. The responses of the linear oscillator do not change shape significantly with changing values of γ_1; however, the magnitude does decrease with increasing values of γ_1. This is a direct result of the physics of the problem: increased damping of an oscillator should decrease the excursions. The decrease in the magnitude of the response of the Duffing oscillator is a direct result of the decreased magnitude of the response of the linear oscillator. The Duffing oscillator is excited by the displacement of the linear oscillator; it is reasonable that a decrease in the magnitude of the displacement of the linear oscillator will be reflected in a decrease in the response of the Duffing oscillator. The agreement between the analytical and numerical data is good. The analytical data show slightly deemphasized local maxima and minima, although the difference is not marked. The largest difference is seen in Figures 3(j) and 4(j). Comparison of these two figures shows the Monte Carlo traces becoming

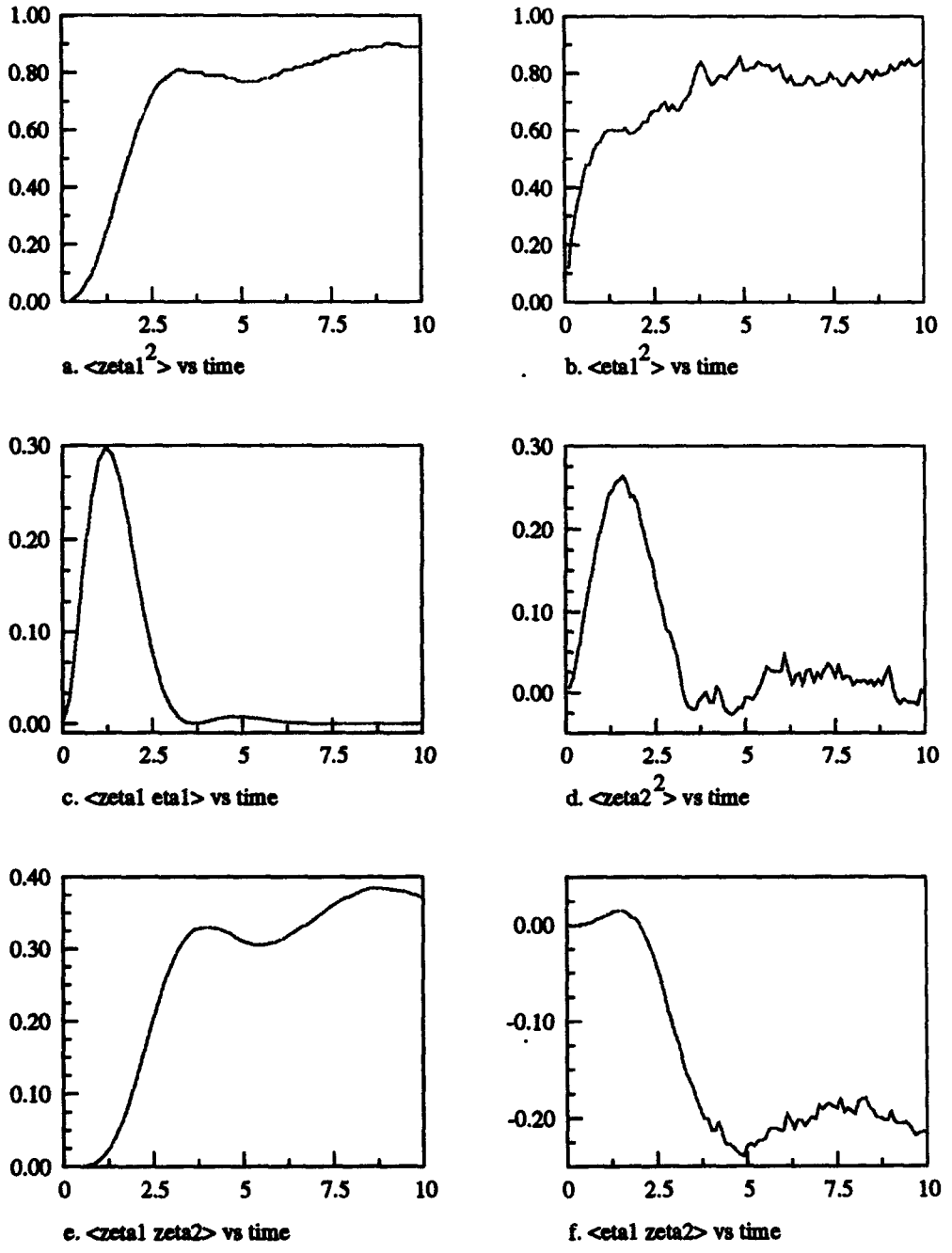

Figure 2: Response of coupled oscillators, $\gamma_1 = 1.0$, $\gamma_2 = 1.0$, $\tau_c = 0.01$, $k = 1.0$, calculated via a Monte Carlo experiment.

negative at five and ten seconds while the analytical traces merely reach local minima of about zero.

The results of the study of the effect of varying γ_2 is shown in Figures 5 and 6. These figures show no change in the response of the linear oscillator with changing γ_2. This is because, while the Duffing oscillator is excited by the displacement of the linear oscillator, the linear oscillator is independent of the Duffing oscillator; i.e., neither x_2 nor v_2 appear in the equations of motion of the linear oscillator. Therefore, one would not expect any variation of the Duffing oscillator to affect the linear oscillator. However, the effect on the Duffing oscillator of varying γ_2 is quite pronounced and similar to the effect on the linear oscillator of varying γ_1. All response curves of the Duffing oscillator decrease in magnitude as γ_2 increases. This is for the reasons stated above. Comparison of the Figures 5 and 6 shows the same similarities and contrasts as for the γ_1 study.

Figures 7 and 8 show the results of varying the spring constant, k, of the coupling spring. Again it is seen that varying the nature of the coupling has no effect on the linear oscillator: there is no change in the moments of the linear oscillator, $< \zeta_1^2 >$, $< \zeta_1 \eta_1 >$, and $< \eta_1^2 >$. The moments of the Duffing oscillator, $< \zeta_2^2 >$, $< \zeta_2 \eta_2 >$, and $< \eta_2^2 >$, do increase with increasing values of k. This is again because the driving force of the Duffing oscillator is $k(\zeta_1 - \zeta_2)$. Therefore, the larger values of k will lead to larger values of the forcing function, and so larger values of the moments. The cross correlations, $< \eta_1 \zeta_2 > < \zeta_1 \eta_2 >$, Figures 7(f,h) and 8(f,h) show a change in the phase angle between the two oscillators. Looking at the progression of traces as k is varied shows markedly different results than any other presented in this chapter. In all other figures presented, as a parameter is varied, the curves change monotonically in magnitude, but do not change significantly in shape. In these figures, the trace corresponding to $k = 10.0$, the largest value of the parameter, has the median value. Also, the traces corresponding to the two lowest values of the parameter, $k = 0.1$ and $k = 0.3$, do not show any discernible local maxima in the first 2.5 seconds; they increase monotonically from zero to their maxima. The other three traces show increasing local maxima with the local maximum of the $k = 10.0$ trace of roughly three times as great as the steady state value. The decrease in the magnitude of these traces, after each reaches its local maximum, represents a shift in the phase angle between the two oscillators. Comparison of the two methods of solution once again shows very good agreement with the same qualitative differences discussed above.

Figures 9 and 10 show the effects on the response of the oscillators of varying the correlation time of the noise. As in the previous papers, it is seen that there is negligible effect in varying τ_c from 0.001 to 0.01, and very small effect in changing τ_c to 0.1. For this oscillator, noise of correlation time $\tau_c < 0.01$ can be considered as white without any loss of information. For many systems, the white noise approximation is acceptable for the case of colored noise with correlation time $\tau_c = 0.1$. As in the other studies, the agreement between the analytical and experimental results was quite good.

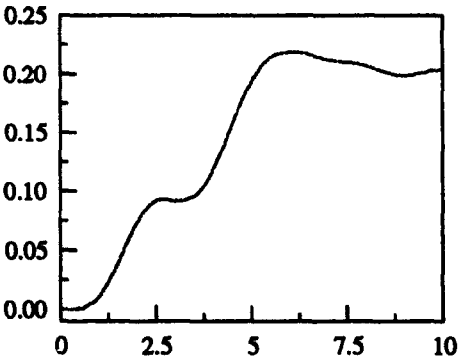

g. <eta2^2> vs time

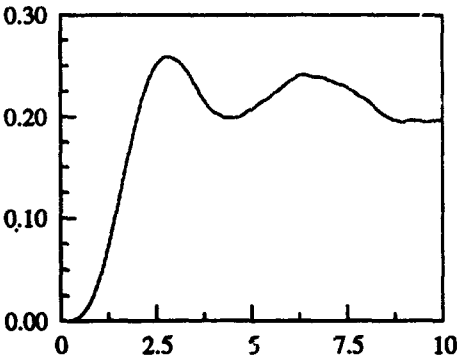

h. <zeta1 eta2> vs time

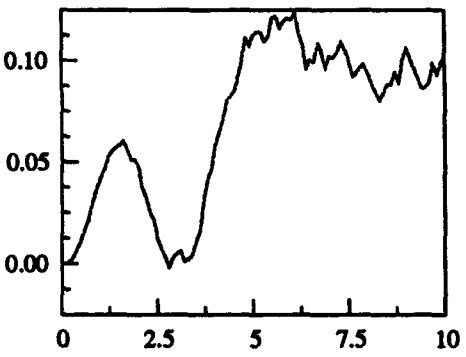

i. <eta1 eta2> vs time

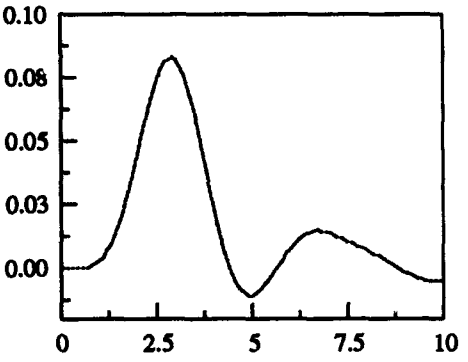

j. <zeta2 eta2> vs time

Key:

gamma1=1.0
gamma2=1.0
tau_C=0.01
k=1.0

Figure 2 (Continued): Response of coupled oscillators, $\gamma_1 = 1.0$, $\gamma_2 = 1.0$, $\tau_c = 0.01$, $k = 1.0$, calculated via a Monte Carlo experiment.

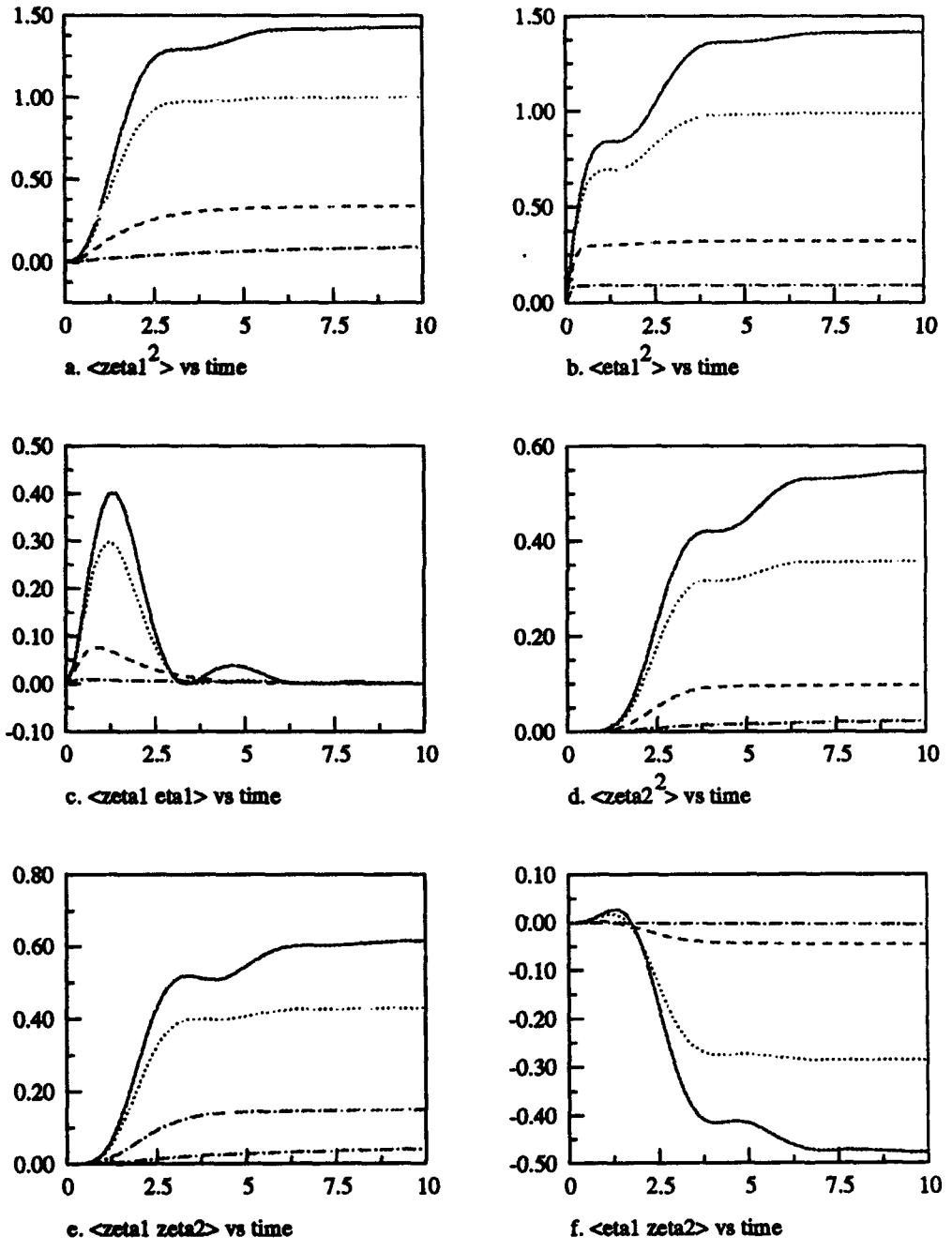

Figure 3: Effect of increasing γ_1 on the response of coupled oscillators, $\gamma_2 = 1.0$, $k = 1.0$, $\tau_c = 0.01$, calculated analytically.

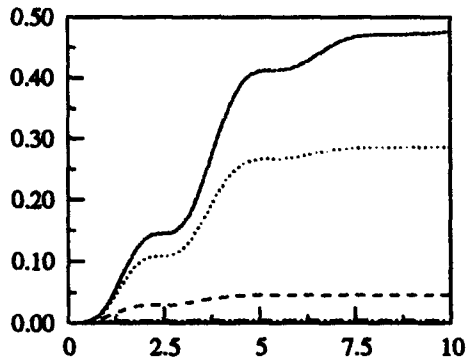

g. <eta2^2> vs time

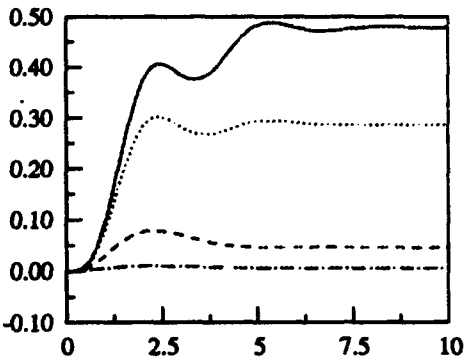

h. <zeta1 eta2> vs time

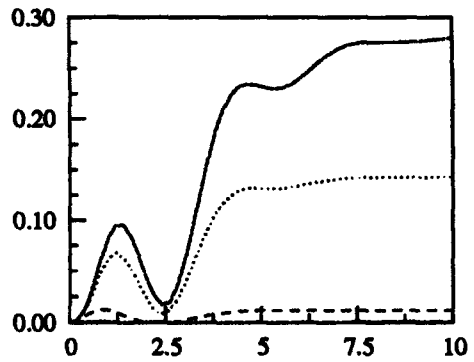

i. <eta1 eta2> vs time

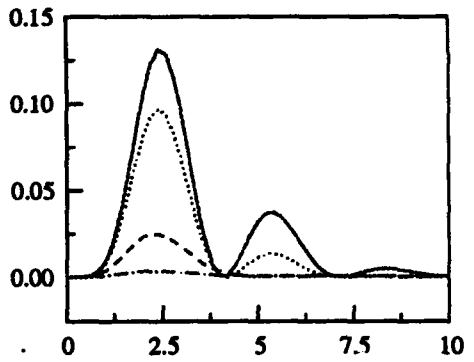

j. <zeta2 eta2> vs time

Key:

———	gamma1 = 0.7
.....	gamma1=1.0
- - - - - - - -	gamma1=3.0
—·—·—·—	gamma1=10.0

gamma2=1.0
tau=0.01
k=1.0

Figure 3 (Continued): Effect of increasing γ_1 on the response of coupled oscillators, $\gamma_2 = 1.0$, $k = 1.0$, $\tau_c = 0.01$, calculated analytically.

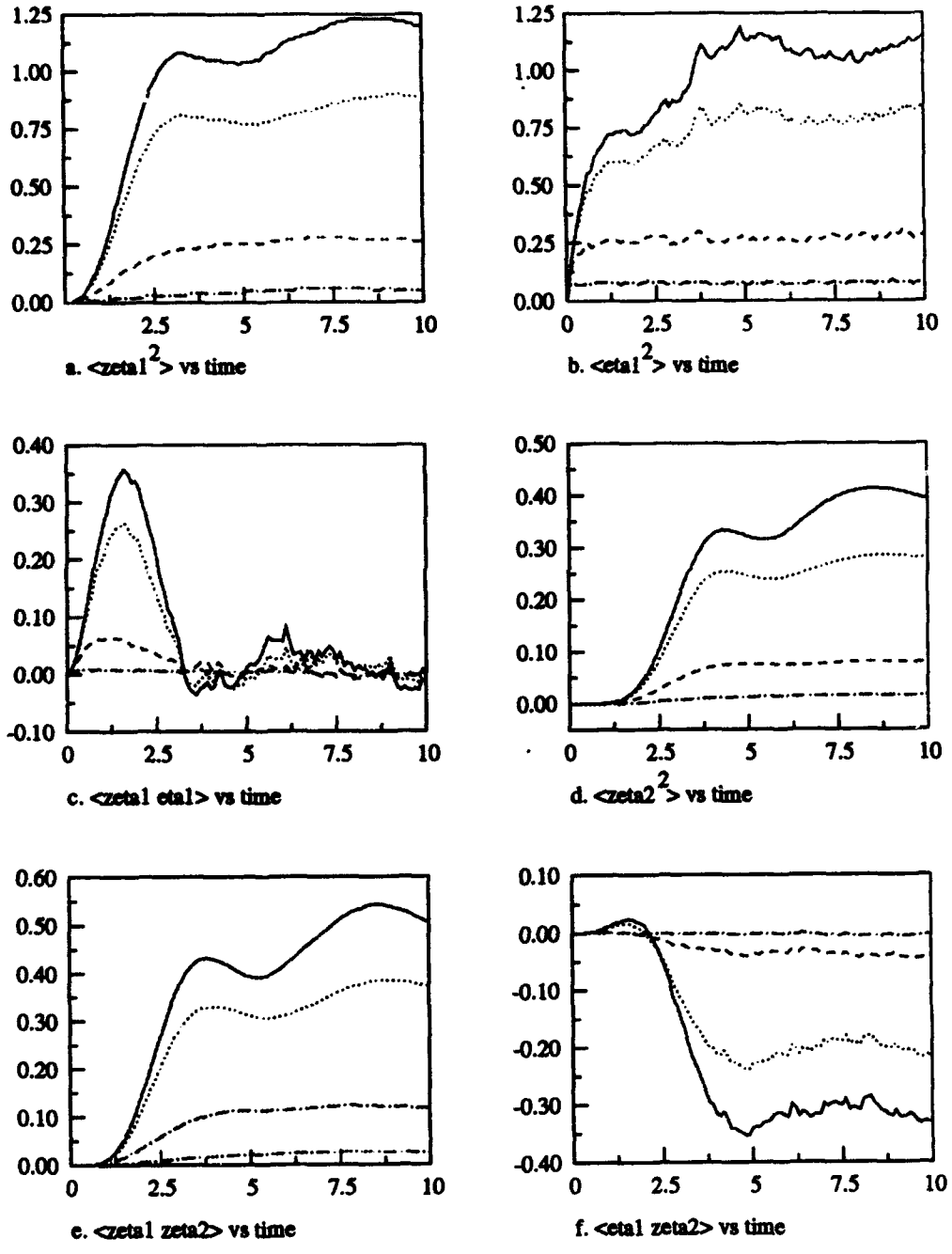

Figure 4: Effect of increasing γ_1 on the response of coupled oscillators, $\gamma_2 = 1.0$, $k = 1.0$, $\tau_c = 0.01$, calculated via a Monte Carlo experiment.

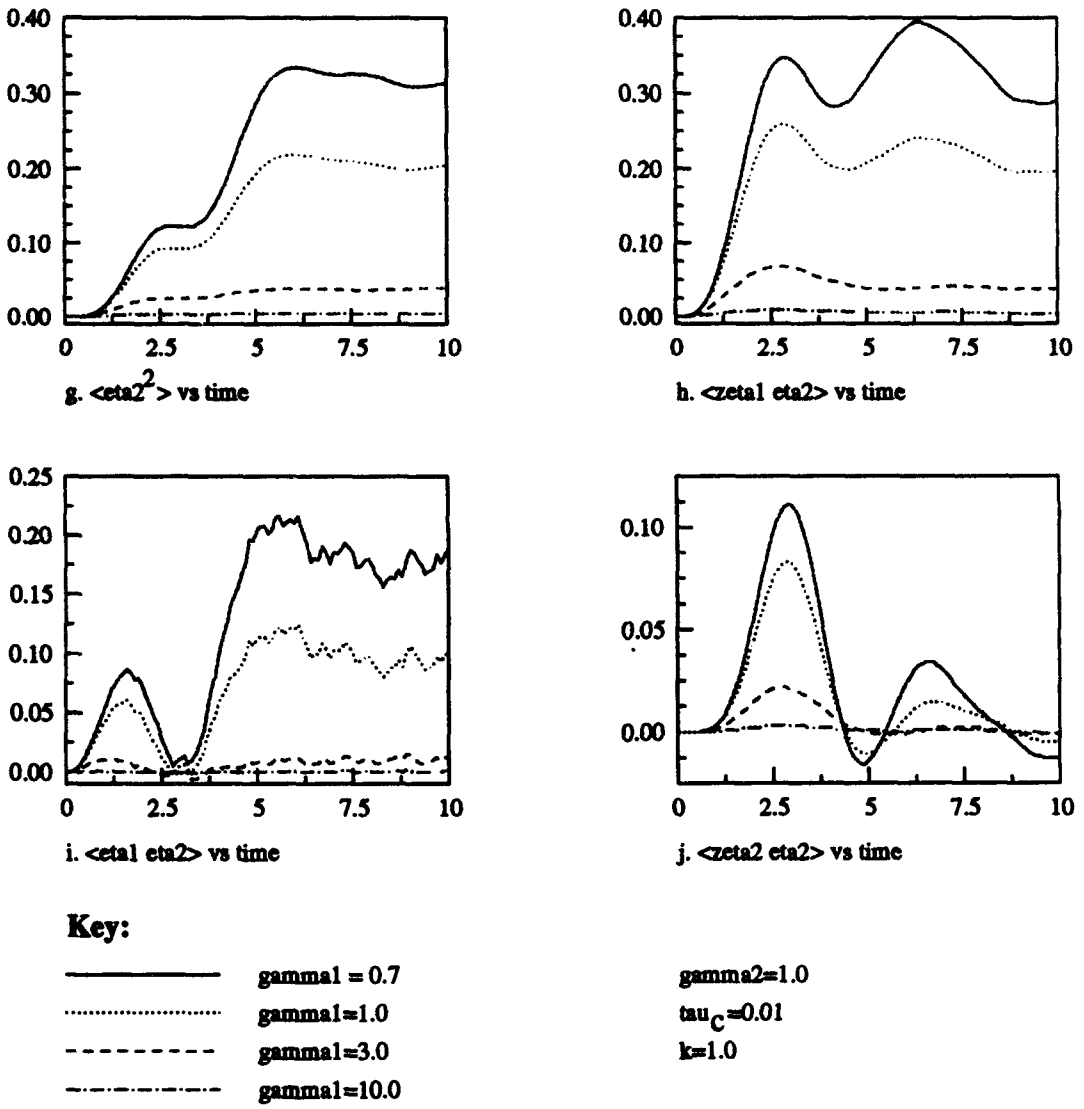

Figure 4 (Continued): Effect of increasing γ_1 on the response of coupled oscillators, $\gamma_2 = 1.0$, $k = 1.0$, $\tau_c = 0.01$, calculated via a Monte Carlo experiment.

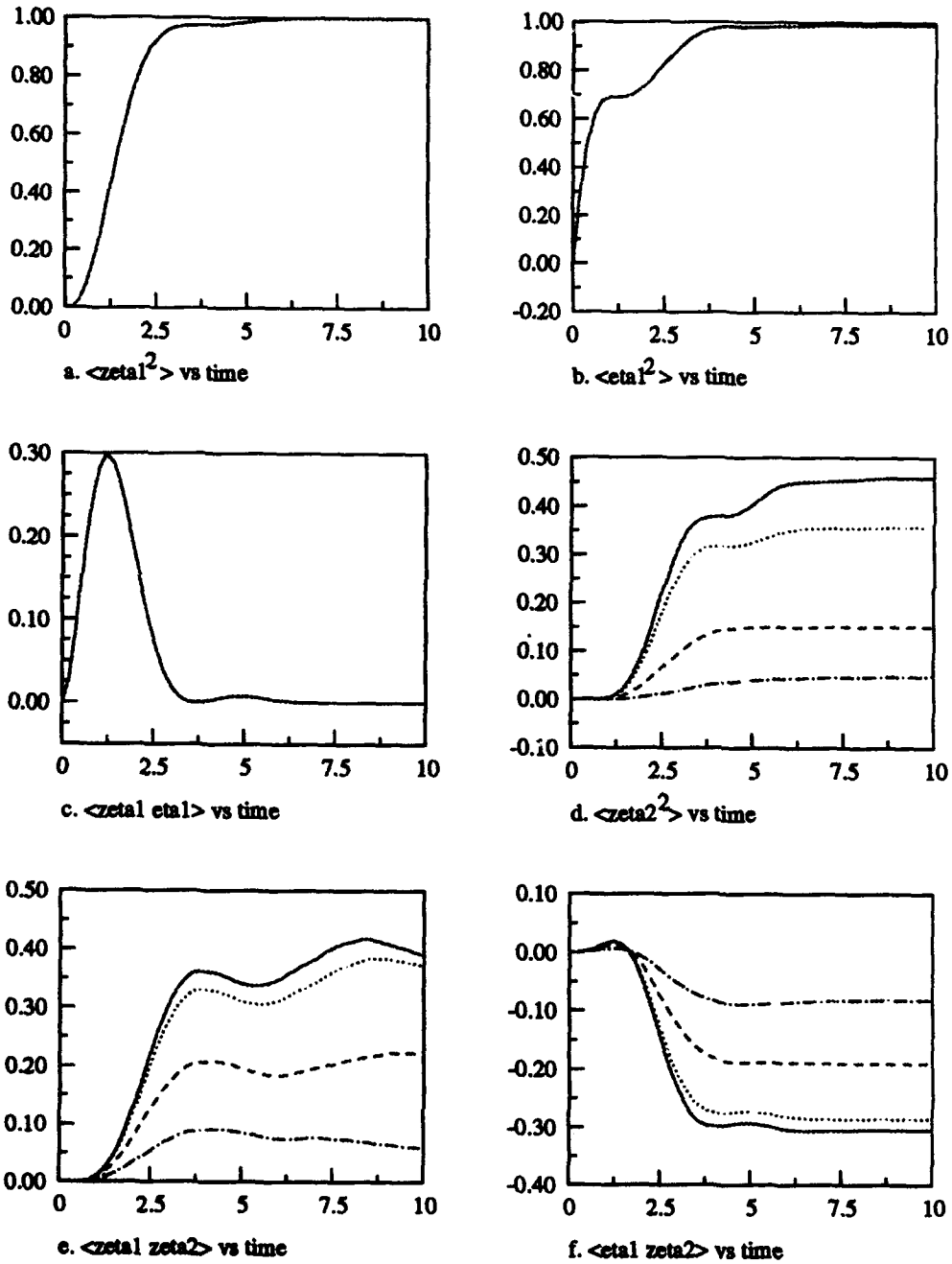

Figure 5: Effect of increasing γ_2 on the response of coupled oscillators, $\gamma_1 = 1.0$, $k = 1.0$, $\tau_c = 0.01$, calculated analytically.

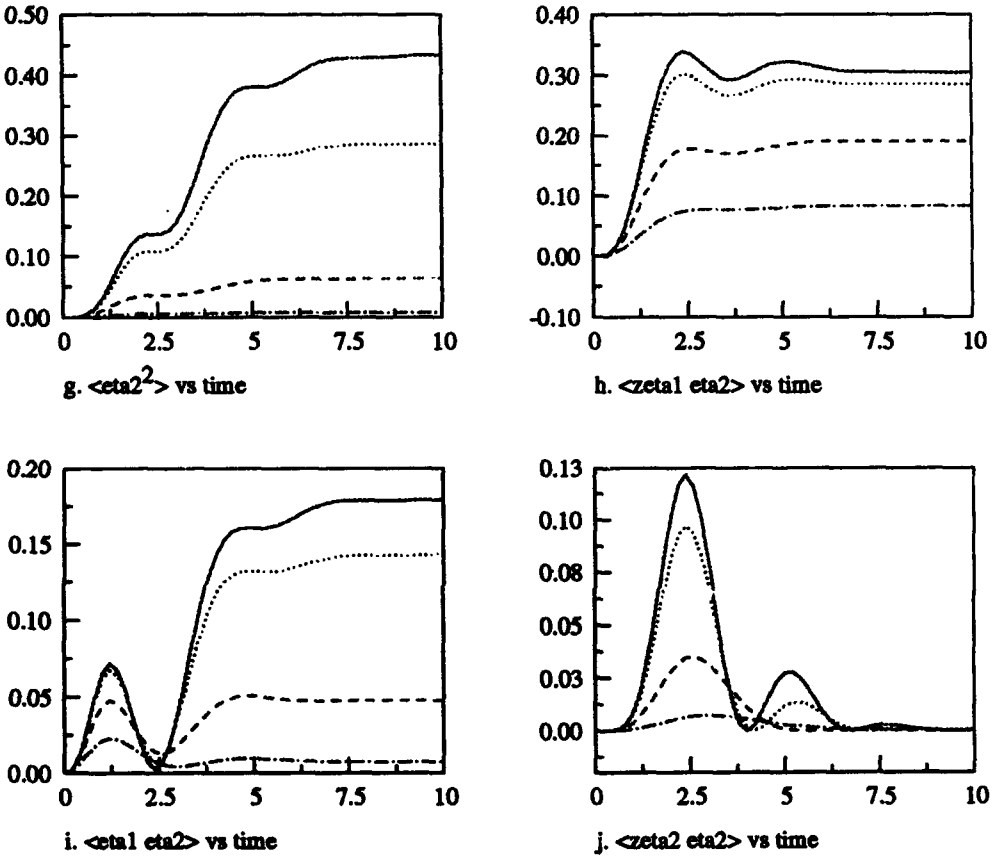

Figure 5 (Continued): Effect of increasing γ_2 on the response of coupled oscillators, $\gamma_1 = 1.0$, $k = 1.0$, $\tau_c = 0.01$, calculated analytically.

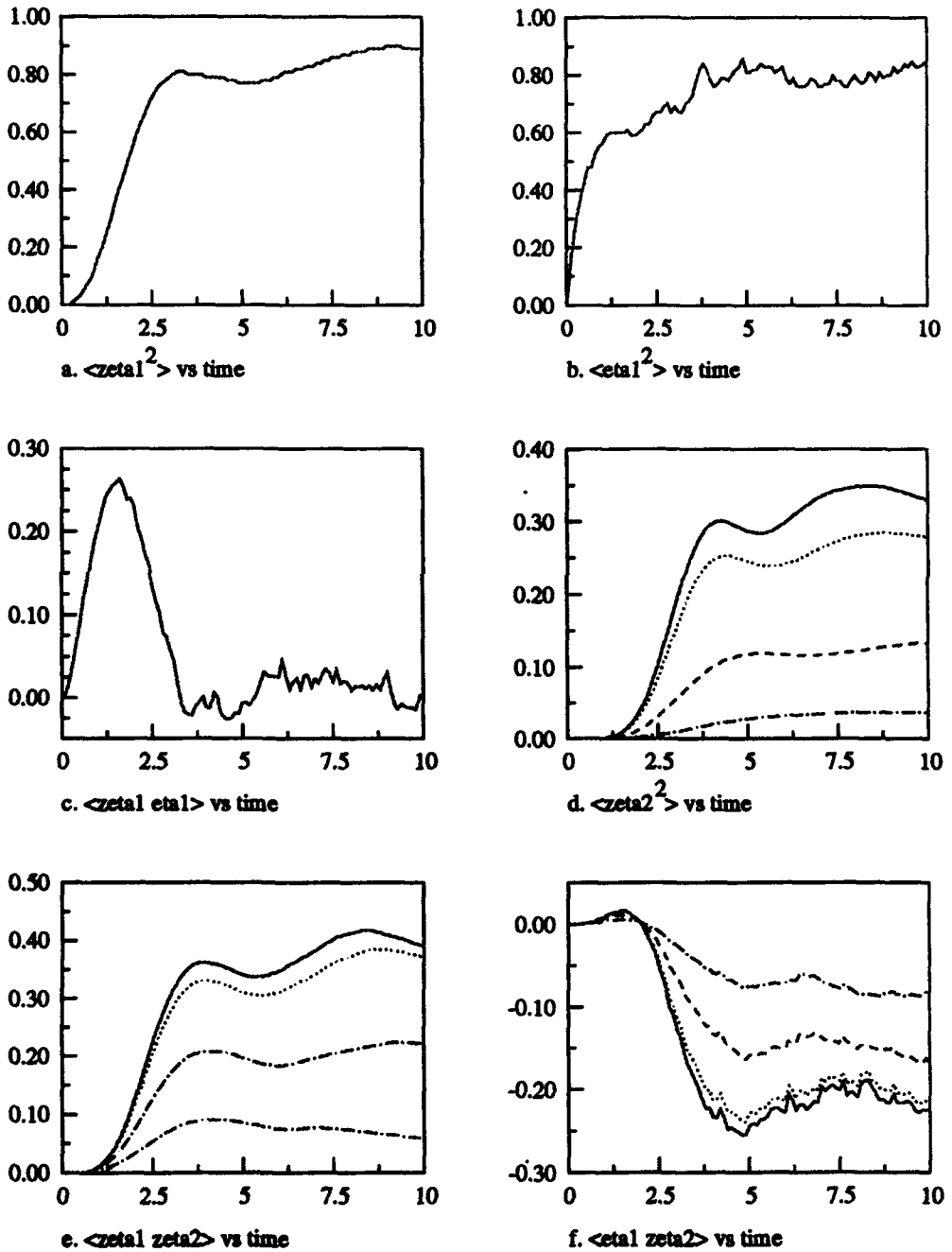

Figure 6: Effect of increasing γ_2 on the response of coupled oscillators, $\gamma_1 = 1.0$, $k = 1.0$, $\tau_c = 0.01$, calculated via a Monte Carlo experiment.

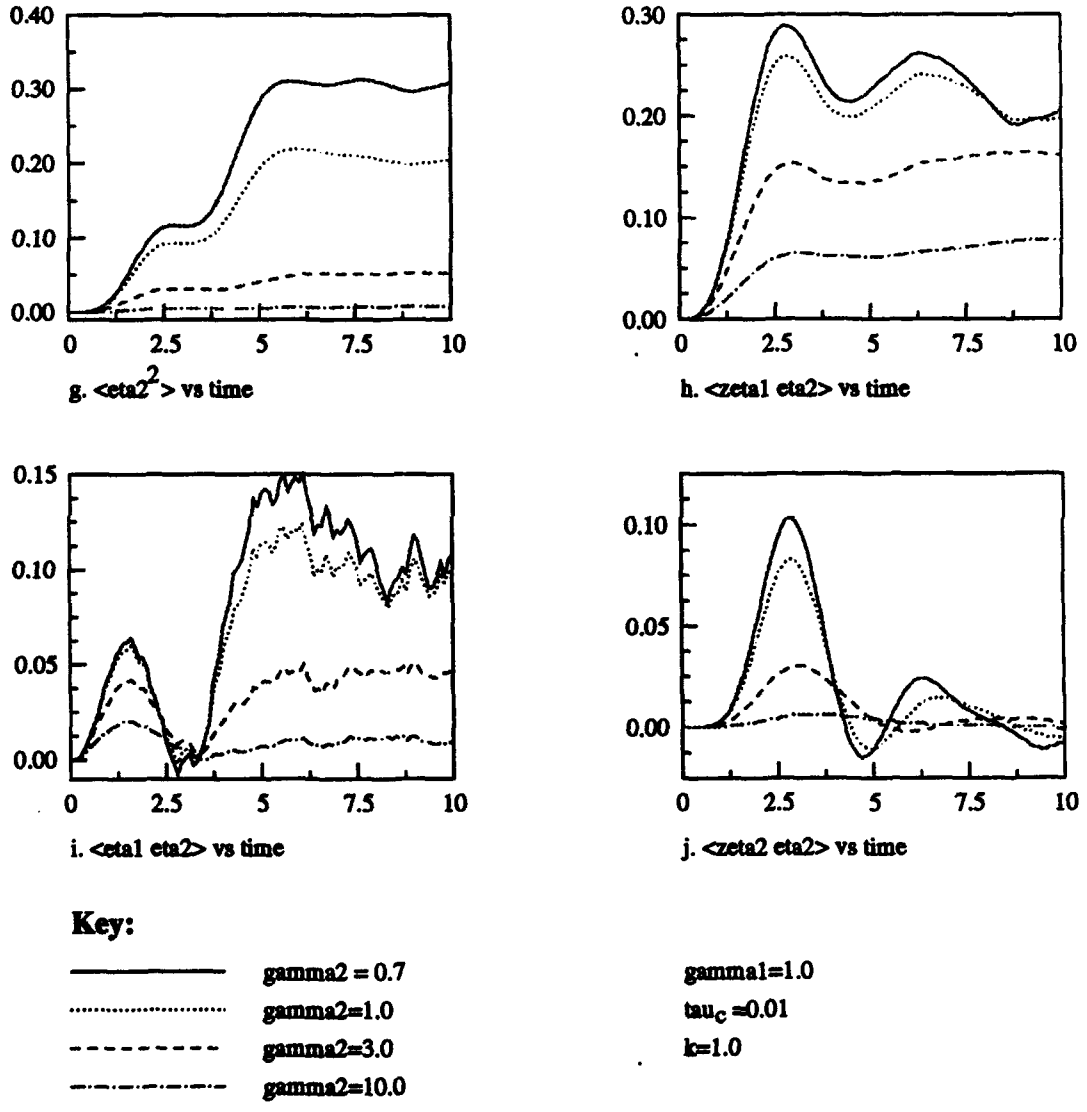

Figure 6 (Continued): Effect of increasing γ_2 on the response of coupled oscillators, $\gamma_1 = 1.0$, $k = 1.0$, $\tau_c = 0.01$, calculated via a Monte Carlo experiment.

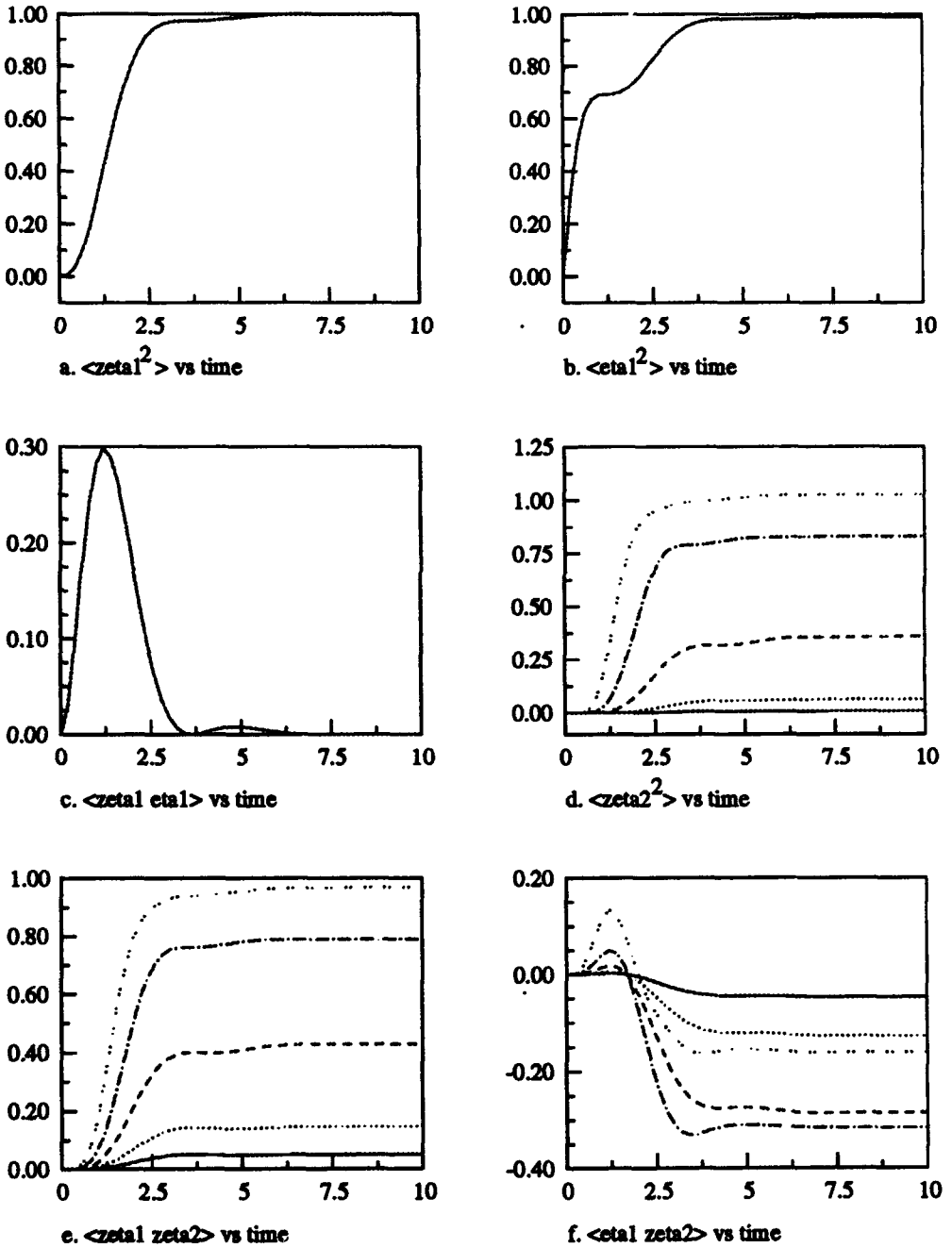

Figure 7: Effect of varying k on the response of coupled oscillators, $\gamma_1 = 1.0$, $\gamma_2 = 1.0$, $\tau_c = 0.01$, calculated analytically.

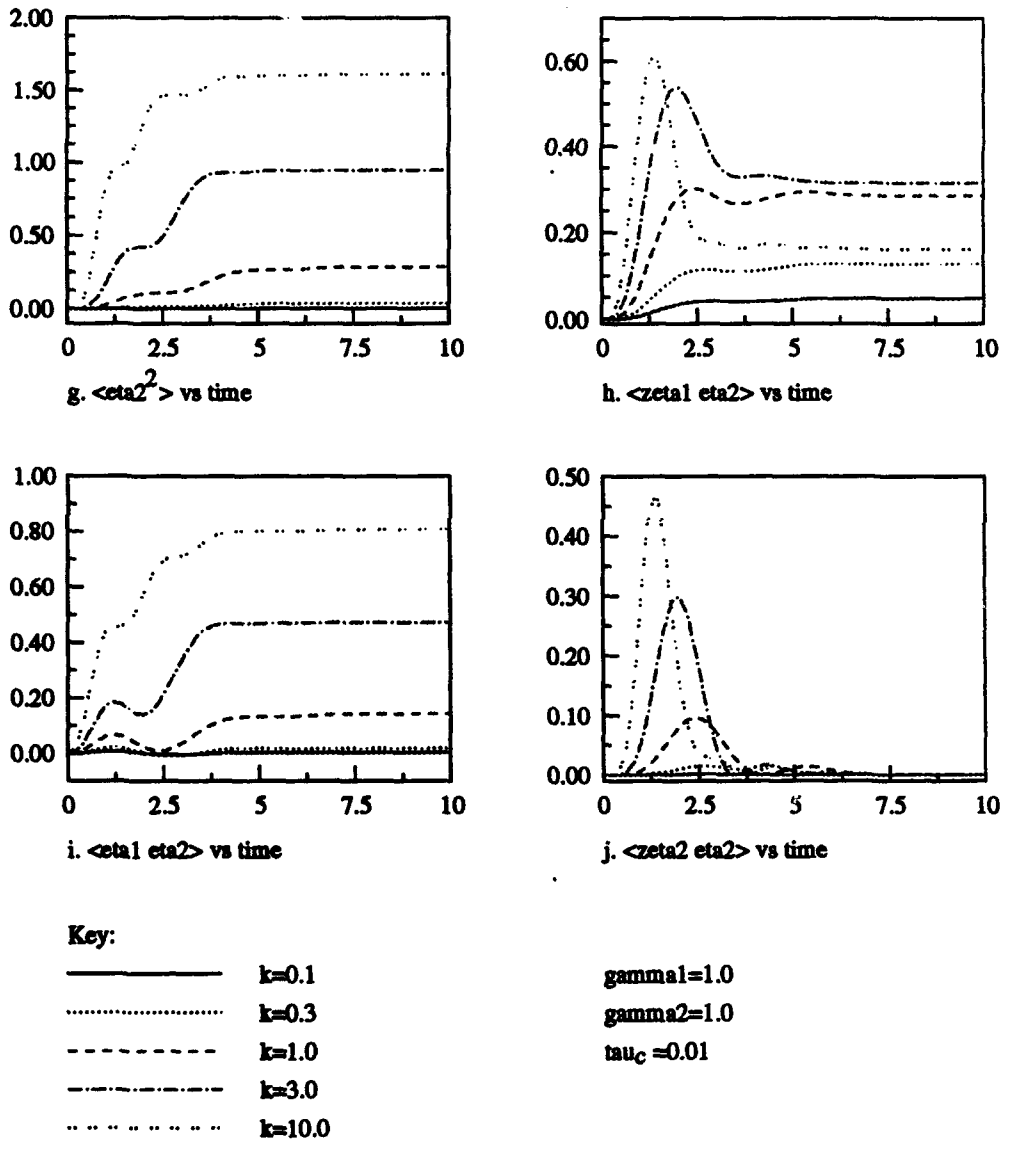

Figure 7 (Continued): Effect of varying k on the response of coupled oscillators, $\gamma_1 = 1.0$, $\gamma_2 = 1.0$, $\tau_c = 0.01$, calculated analytically.

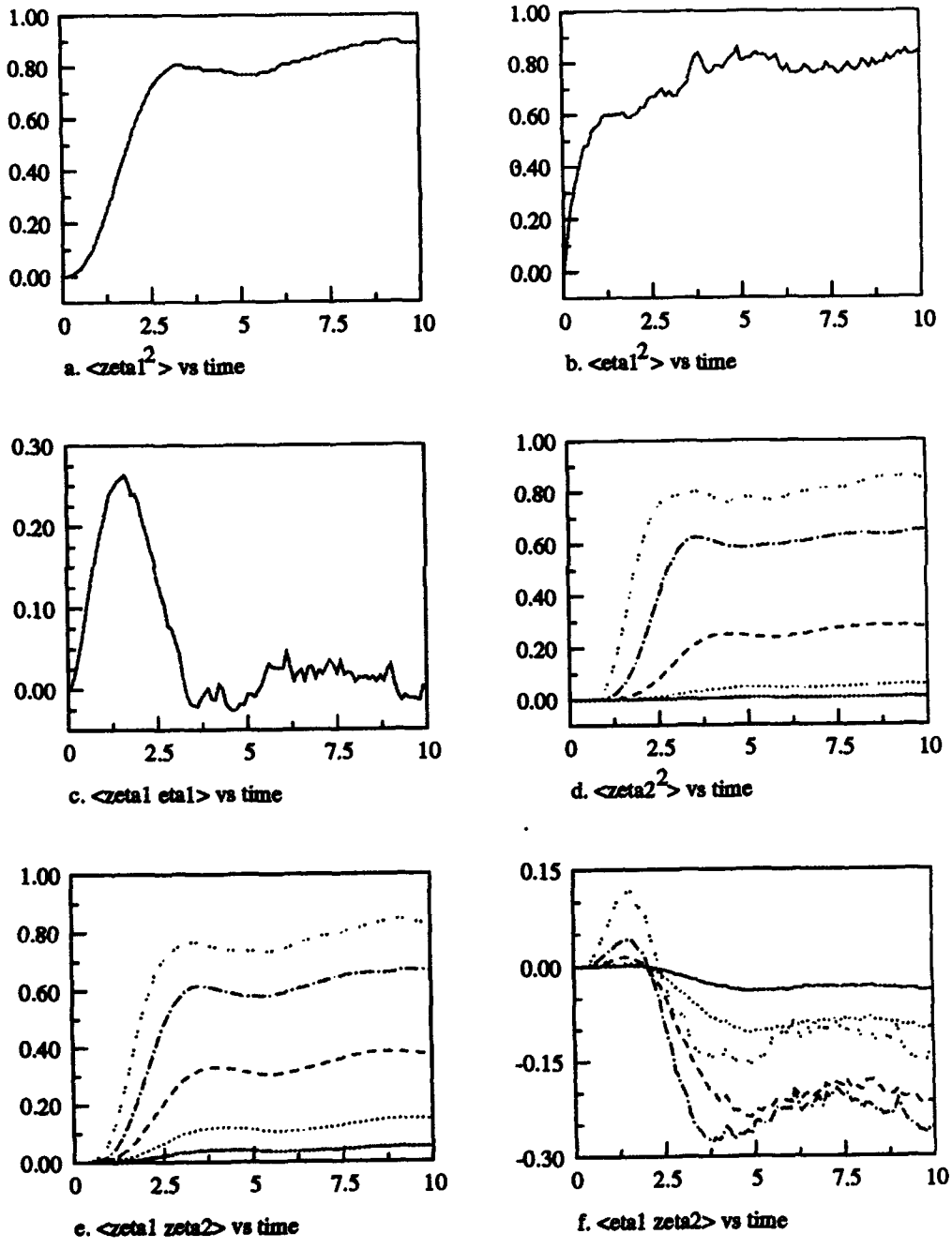

Figure 8: Effect of varying k on the response of coupled oscillators, $\gamma_1 = 1.0$, $\gamma_2 = 1.0$, $\tau_c = 0.01$, calculated via a Monte Carlo experiment.

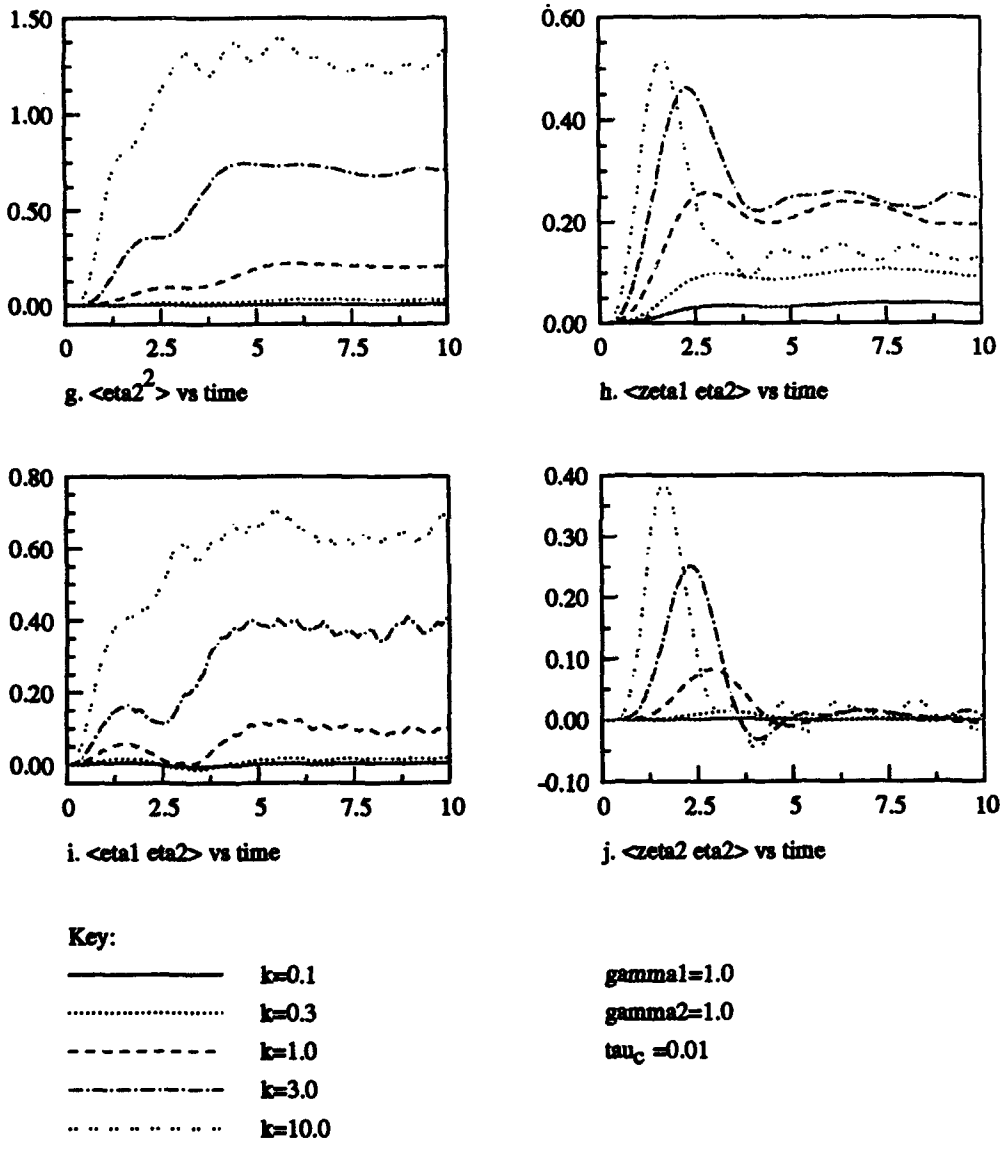

Figure 8 (Continued): Effect of varying k on the response of coupled oscillators, $\gamma_1 = 1.0$, $\gamma_2 = 1.0$, $\tau_c = 0.01$, calculated via a Monte Carlo experiment.

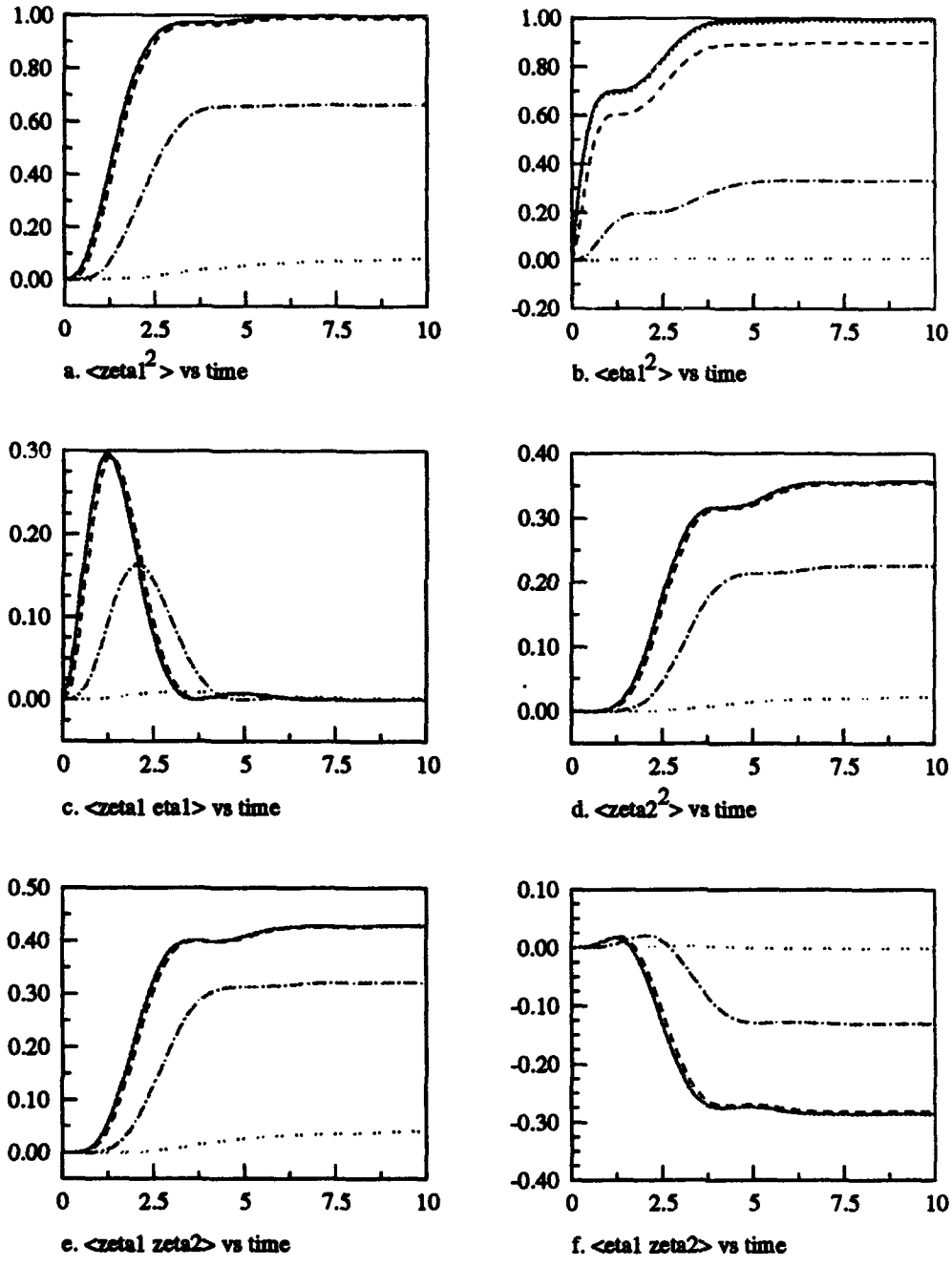

Figure 9: Effect of varying τ_c on the response of coupled oscillators, $\gamma_1 = 1.0$, $\gamma_2 = 1.0$, $k = 1.0$, calculated analytically.

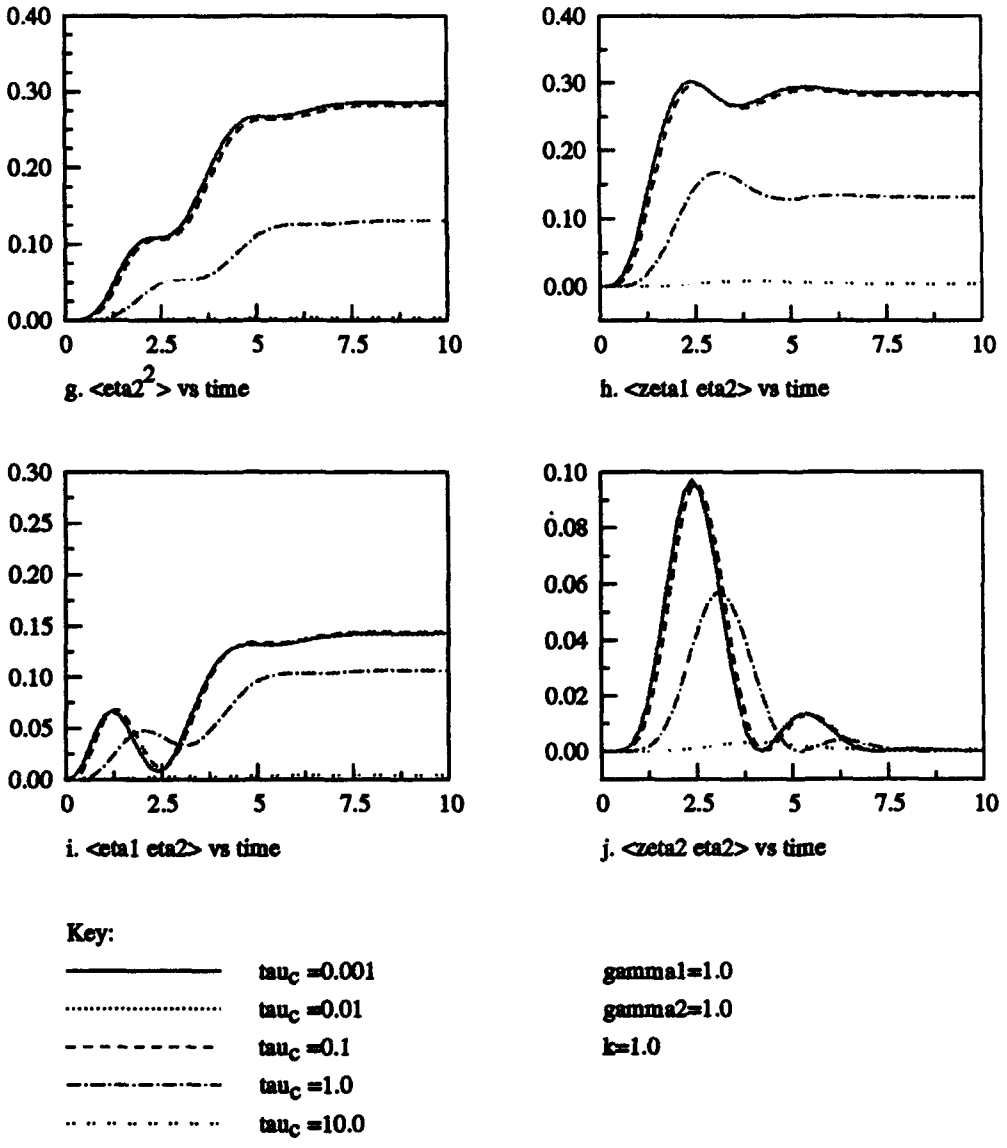

Figure 9 (Continued): Effect of varying τ_c on the response of coupled oscillators, $\gamma_1 = 1.0$, $\gamma_2 = 1.0$, $k = 1.0$, calculated analytically.

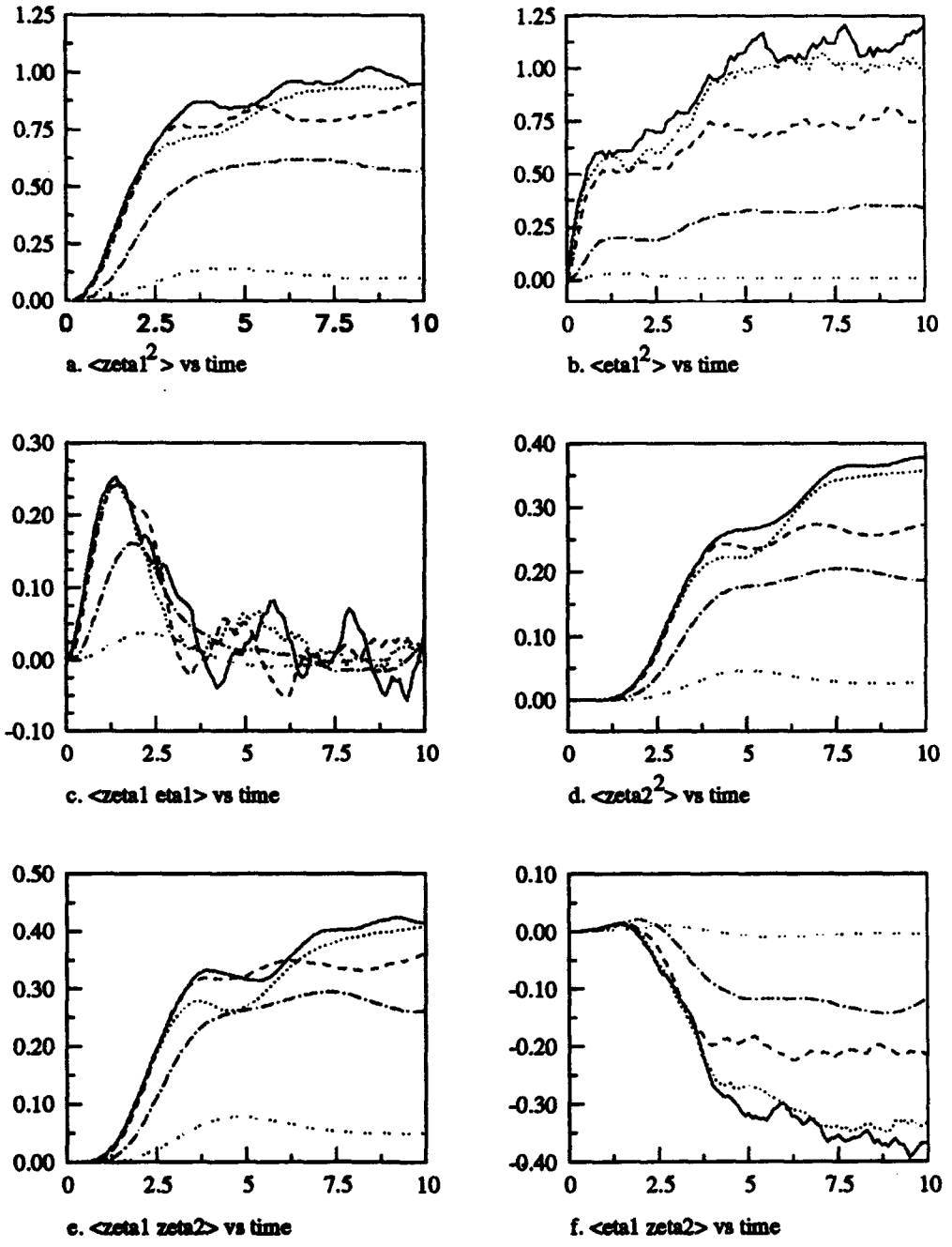

Figure 10: Effect of varying τ_c on the response of coupled oscillators, $\gamma_1 = 1.0$, $\gamma_2 = 1.0$, $k = 1.0$, calculated via a Monte Carlo experiment.

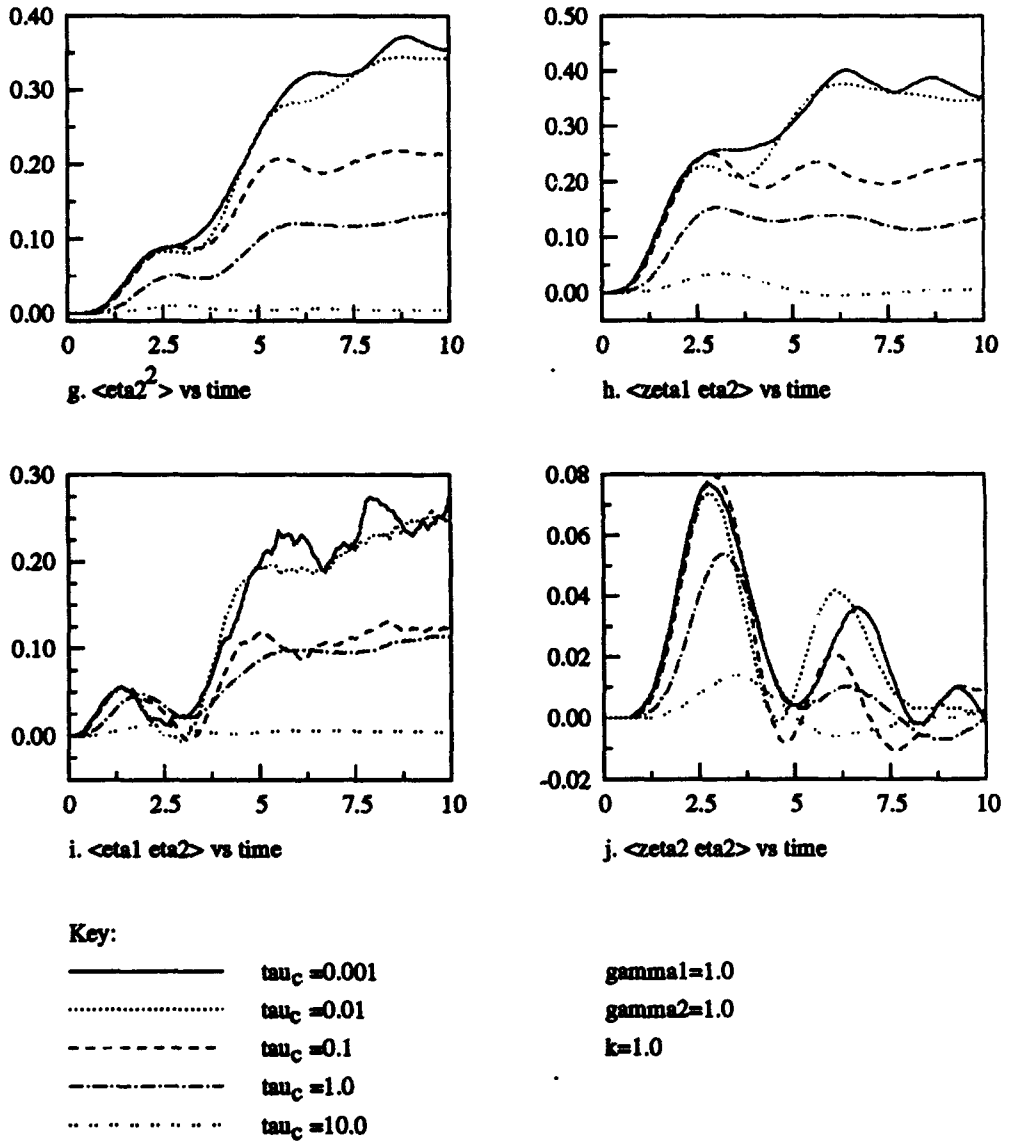

Figure 10 (Continued): Effect of varying τ_c on the response of coupled oscillators, $\gamma_1 = 1.0$, $\gamma_2 = 1.0$, $k = 1.0$, calculated via a Monte Carlo experiment.

4 Conclusions

The overwhelming similarity between the results given by the two methods implies that this adaptation of the van Kampen expansion is an accurate tool for predicting the statistics of the response of a coupled Duffing-linear oscillator excited by colored noise. Although not directly shown here, it seems reasonable to assume that this method would give good results for an arbitrary combination of linear and Duffing oscillators. It was also seen that, depending on the magnitude of the correlation time as compared to the natural period of the oscillator, simplifying assumptions can be made that obviate the need for this adaptation.

5 Acknowledgments

This work is prepared in partial fulfillment of the requirements for the degree of Doctor of Philosophy of the first author. The work was performed under the support of the Federal Aviation Administration Technical Center. The authors would like to thank Lawrence Neri of the Technical Center for his interest and support, Harry Kemp, also of the Technical Center for his support and expertise, and also the Department of Mechanical and Aerospace Engineering at Rutgers, the State University of New Jersey. The second author would also like to thank the Office of Naval Research and scientific officer Thomas F. Swean for support under grant number N00014-93-1-0763.

References

[1] R. Rodríguez and N.G. van Kampen. Systematic treatment of fluctuations in a nonlinear oscillator. *Physica*, 1976.

[2] Edward Weinstein and H. Benaroya. The van Kampen expansion for the Fokker-Planck equation of a Duffing oscillator. *Journal of Statistical Physics, Forthcomming* Nov, 1994.

[3] Edward Weinstein and H. Benaroya. The van Kampen expansion for the Fokker-Planck equation of a Duffing oscillator excited by colored noise. *Journal of Statistical Physics, Forthcomming* Nov, 1994.

[4] J.F. Wilson. *Dynamics of Offshore Structures.* John Wiley and Sons, New York, 1984.

[5] T. Oda, H. Ozaki and Y. Yanamouchi. A nonlinear system identification in the analysis of offshore structure dynamics in random waves. In F. Ziegler and G.I. Shuëller, editors, *Nonlinear Stochastic Dynamics Engineering systems*, pages 87–100, New York, 1987. IUTAM, Springer-Verlag.

[6] K.Y.R. Billah and M. Shinozuka. Numerical method for colored noise generation and its application to a bistable system. *Physical Review*, 12(42), Dec 1990.